A thesis submitted in partial fulfilment of the requirements for
the degree of Master of Science

Mass cytometry analysis of the tumour-immune landscape: The role of Axl receptor kinase

Sturla Magnus Grøndal

Supervisor: Prof. James Bradley Lorens, Dept. of Biomedicine

Co-supervisor: Assoc. Prof. Niels Aarsæther, Dept. of Biomedicine

Bergen, November, 2018

Abstract

Cancer is one of the leading causes of death in Norway (2016) and worldwide. Despite the advent of new immunotherapies, malignant cancer demonstrates an intrinsic plasticity and is able to evade, adapt and suppress the immune system. An important driver for this malignant phenotype is the epithelial-to-mesenchymal transition (EMT) program, characteristic of stem cells. Previous research showed a link between the AXL receptor tyrosine kinase (Axl) and EMT. The Axl receptor is further involved in immune suppression and could therefore serve as a potential target in immunotherapy and in combination with other cancer treatments. Chemotherapeutic treatment also shows evidence of immune involvement, and the immune system plays a vital role in all forms of cancer treatment. In this study, we evaluated current immunotherapy in combination the Axl kinase inhibitor, bemcentinib. Using single cell mass cytometry we conducted 30 parameter mapping of the immune system in an experimental murine tumour model. The data was analysed using dimensionality reduction and unsupervised clustering. By studying how the immune landscape changes during tumour development and immunotherapy treatment, important insights into how the immune system responds to tumour development and treatment was measured and a new treatment regime was evaluated.

Acknowledgements

Abbreviations

BSA	Bovine serum albumin
CTL	Cytotoxic T lymphocyte
CTLA-4	Cytotoxic T-lymphocyte-associated protein 4
CVD	Cardiovascular diseases
CWB	Cell washing buffer
CyTOF	Cytometry by time-of-flight
DNA	Deoxyribonucleic acid
DOTA	1,4,7,10-tetraazacyclododecane-1,4,7,10-tetraacetic acid
DPBS	Dulbecco's PBS
DTPA	Polymeric pentetic acid
EMP	Epithelial-to-mesenchymal plasticity
EMT	Epithelial to mesenchymal transition
ICB	Immune checkpoint blockade
MDSC	Myeloid derived suppressor cell
MHC	Major histocompatibility complex
NaAz	Sodium Azide
NK	Natural Killer
PBS	Phosphate buffered saline
PD-1	Programmed cell death protein 1
PP	Polypropylene
RCF	Relative centrifugal force
RF	Radio frequency
RT	Room temperature
TAM	Tumour associated macrophage
TCEP	tris(2-carboxyethyl)phosphine
TCR	T cell receptor
T_h	Helper T cell
TIL	Tumour infiltrating lymphocyte
T_{reg}	T regulatory

Glossary

Angiogenesis	Formation of new blood vessels from existing ones
Anoikis	Avoiding detachment-induced apoptosis
Antigens	A molecule that can be bound by an antibody and initiate an immune response.
Apoptosis	A form of nonimmunogenic controlled cell death.
Cell differentiation	When a cell goes from one cell type to another and quires different traits.
Immunogenic	A process capable of initiating an immune response.
Immunotherapy	The use of the immune system to treat cancer
Intercalator	A molecule that can be inserted between base pairs in DNA.
Leukocytes	White blood cells comprising the immune system.
Mahalanobis distance	A type of distance used in multivariate space to find the distance from the centroid to a given point. The centroid is the point where the means of all variables intersect.
MilliQ	A type of purified water.
Mutation	Permanent change in nucleotide sequence, either by insertion, deletion or substitution of a single nucleotide.
Neoantigens	New antigens.
Push	A single slice of the gas stream in the TOF chamber.
Reading	The integrated intensity of several pushes.
Torr	A unit of pressure that corresponds to 1/760 standard atmospheres.

Contents

List of Figures

1 Introduction

1.1 Tumours on a population level

Cancer is one of the leading causes of death in Norway (2016) [1] and one of the leading causes worldwide [2]. In addition, tumour-related deaths have been steadily increasing and will continue to rise (see Figure 1.1). Tumour incidence is also increasing in Norway and in 2017 almost 34'000 new cases were registered [3]. In 2014, the total costs, including treatment and loss of production, was estimated to be 40 billion NOK [4]. The treatment and care alone were estimated to cost 20 billion NOK, while the loss of production due to sick leave and death was estimated to be 18 billion NOK. Further, the accumulated risk of a cancer diagnosis during a lifetime of 75 years is about 30% for women and 36% for men [3]. Cancer therefore represents a significant economical and emotional burden to the society.
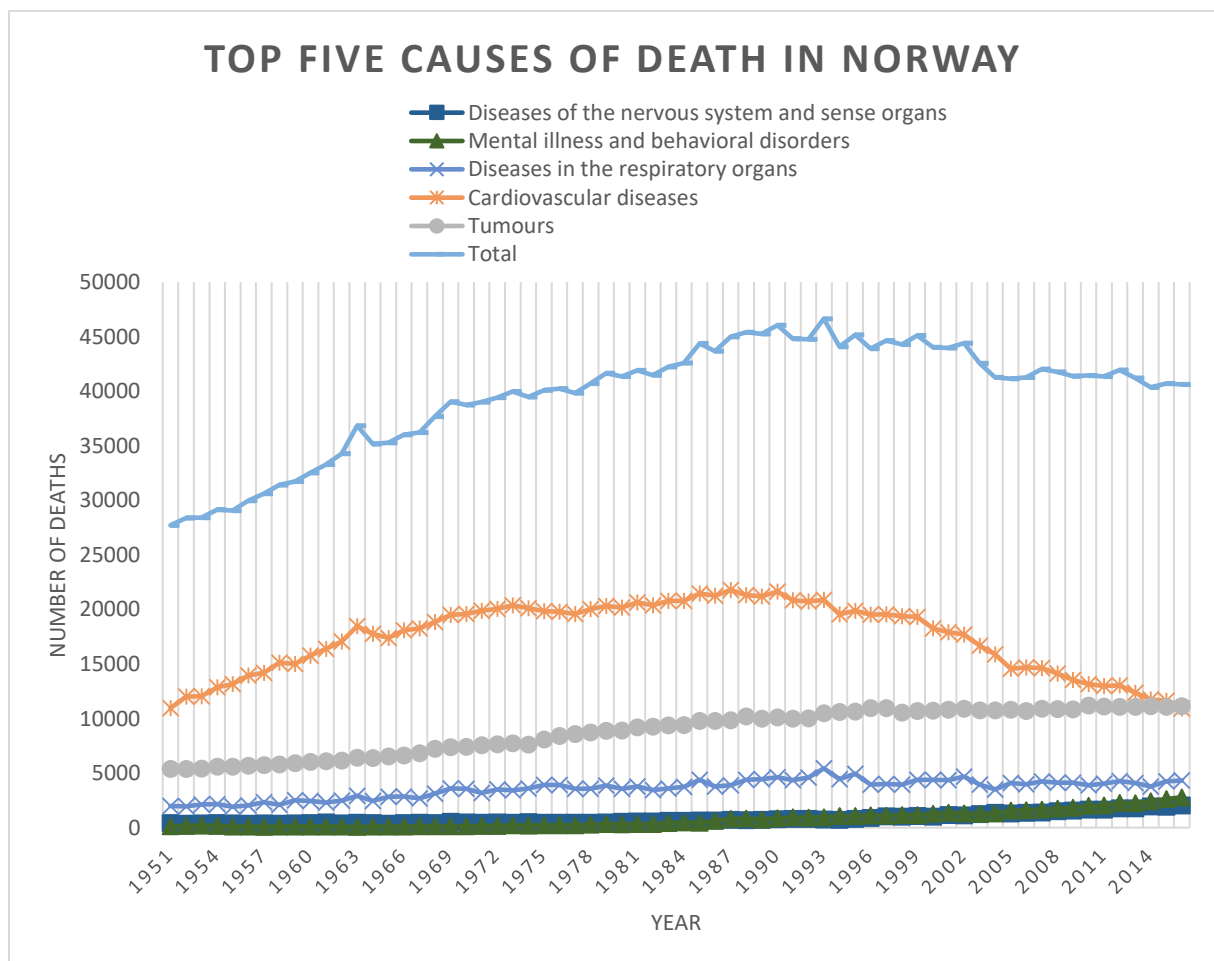
*Figure 1.1: **Top five causes of death in Norway.** In 2016 tumours passed cardiovascular diseases and became the number one cause of death in Norway [1].*

One of the main risk factors for cancer is age; 3 out of 4 new cancer cases are attributed to adults over 60 years old. Thus, it is expected that cancer incidence will increase as life expectancy increases. The inherent heterogeneity and plasticity of cancer complicates treatment. After an initial therapy efficacy, tumours inevitably develop resistance, after which treatment options are limited or non-existent [5].

1.2 Cancer development

Cancer is a genetic disease caused by gene mutations. Mutations occur naturally during DNA replication and as a result of exposure to carcinogens. The role of replication errors is evident from the correlation between cancer risk and number of stem cell divisions in the tissues [6]. Tomasetti et al. estimated that three mutations occur every time a human stem cell divides. Although apparently negligible within a human genome of three billion base pairs [7], the accumulated risk of mutating an important gene significantly increases by taking into considerations the number of divisions required to create the trillions of cells that make up a human body. Mutations arising due to environmental factors have also been extensively shown; the correlation between melanomas and sunburns, and smoking and lung cancer are well characterised [8, 9].

Mutations can affect proteins in several ways; it can alter protein expression, structure, and function. Mutations in oncogenes, such as growth factor receptors, promote cell survival and immortality. Oncogenic mutations drive uncontrolled cellular growth creating in situ tumours consisting of cellular clones from the original transformed cell. New mutations that further increase tumour cell fitness lead to evolution of the tumour. This selection process favours genomic instability that increases mutational rates. As a tumour develops it can therefore consist of several different cell populations (heterogeneity), all originating from the cancer cell-of-origin. Tumour growth also results in a modified microenvironment comprising altered blood vessels, connective tissue, extracellular matrix and immune infiltrate. Malignant tumour cells can invade adjacent tissues and spread throughout the body (metastasis) [10].

1.2.1 Malignancy and EMT

According to Hanahan and Weinberg six traits (hallmarks) of cancer cells exist [11]. These traits are: growth signal independence, insensitivity to anti-growth signals, evasion of programmed cell death (apoptosis), limitless replicative potential, sustained formation of new blood vessels

(angiogenesis), and tissue invasion and metastasis. In 2011 Hanahan and Weinberg added two new emerging hallmarks; deregulating cellular energetics and avoiding immune detection, and two new enabling characteristics; genome instability and mutation, and tumour promoting inflammation [12]. These hallmarks are further used as targets for cancer treatment.

Epithelial-to-mesenchymal plasticity (EMP), consisting of both the epithelial-to-mesenchymal transition (EMT) and mesenchymal-to-epithelial transition (MET), is regulated by a highly coordinated complex network of transcription factors and epigenetics [13]. Best known for formation of the mesoderm during early development, this cellular plasticity supports changes in cell phenotype, providing cells with new characteristics and functions. EMT-like processes are important in a number of physiological processes in addition to embryonic development, including wound healing, fibrosis, and organ formation [14]. In cancer cells EMT has been associated with invasion, avoiding detachment-induced apoptosis (anoikis), resistance to chemotherapy, immune escape, dissemination and resistance to apoptosis (see Figure 1.2)[14-20]. It is therefore considered a major player in enabling cancer progression and a target for therapies.
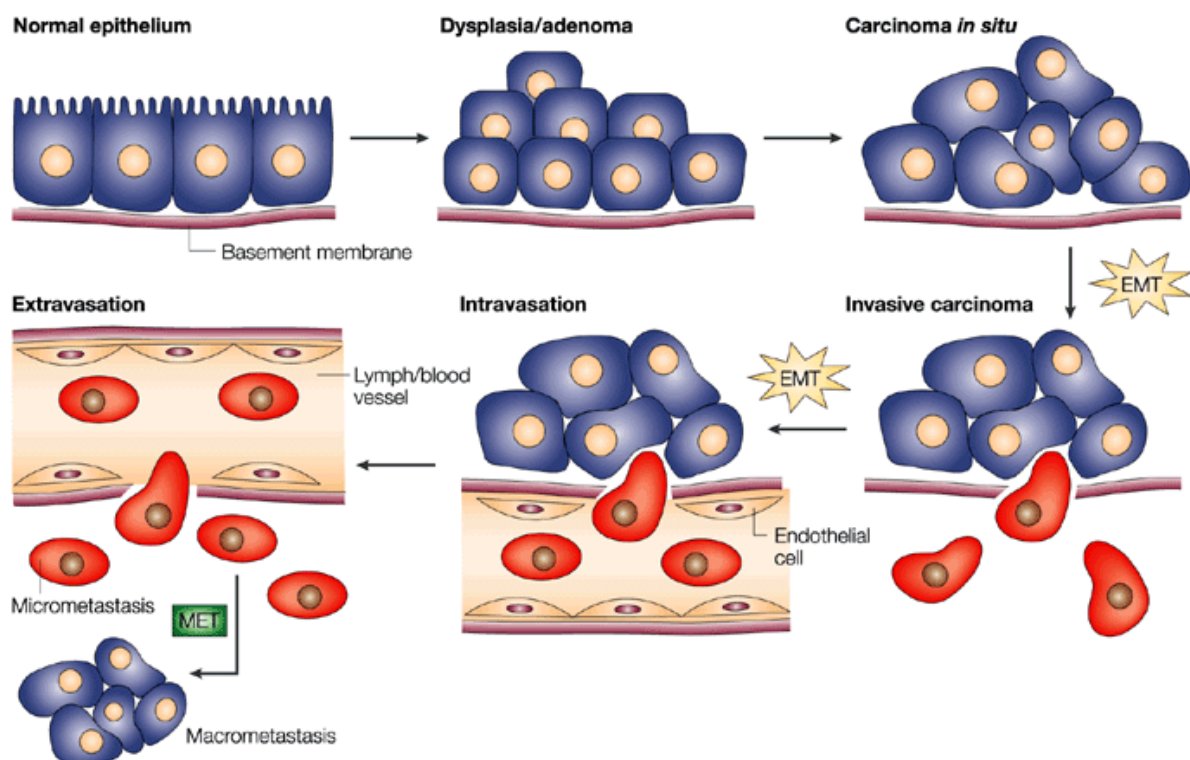
*Figure 1.2: **Process of metastasis.** Normal epithelium sits regularly on a basement membrane. Abnormal differentiation and growth, known as dysplasia, then develops. After further accumulation of epigenetic and genetic mutations, a carcinoma in situ is formed. The cells have still not broken through the basement membrane, but the carcinoma in situ cells have the potential to engender this ability. One way for cells to acquire this ability is through the epithelial–mesenchymal transition (EMT). The carcinoma in situ is then referred to as invasive carcinoma. The invasive cells enter the lymph or blood vessels and may use these to travel to distant parts of the body. By using the transformation opposite to EMT, the mesenchymal–epithelial transition (MET), the cells can form micro metastases and create a new tumour environment. Upon further differentiation, macro metastases may form. Picture is reprinted from Thiery's review "Epithelial–mesenchymal transitions in tumour progression" [21].*

The expression of AXL receptor tyrosine kinase, is induced by transcription factors important in EMT [22]. Studies show that Axl regulates tumour growth, proliferation, invasiveness and drug resistance and immune evasion [23-25]. In human mammary epithelial cells, EMT transcription factors induce expression of Axl [22]. Gjerdrum, C., et al., showed that breast cancer cells generate an autocrine loop with the ligand for Axl, Gas6. The same study showed that knockdown of Axl blocked dissemination of the cancer cells to several organs. This link between Axl and EMT was subsequently demonstrated in several other cancer cell types. Hence, Axl has emerged as an important drug target to prevent metastasis and reverse drug resistance. Down regulation of Axl expression by knocking out the Axl regulator vimentin demonstrated that Axl plays an important role in migration of breast cancer lines [24]. Treatment with the Axl inhibitor, bemcentinib (BGB324/R428), blocked breast cancer cell metastasis in breast cancer models. Inhibition of Axl has also been shown to revert EMT in different cancer models [26, 27].

1.2.2   Immunosuppression

In all nucleated cells, proteins are continuously degraded to peptides by the proteasome. The major histocompatibility complex type I (MHC I) protein has a binding site "groove" that will bind one of these peptides, called antigens, and present it at the cell surface. This allows cytotoxic T lymphocytes (CTLs) to probe each cell for the presence of non-self antigens (e.g. produced by a virus), by binding the MHC I with their T cell receptors (TCRs). If the CTL is mature and the TCR recognises the peptide antigen as non-native on the MHC I groove it can initiate an attack on the cell and kill it.

Several prerequisites are necessary for the CTLs to be able to kill tumour cells. These steps are known as the tumour immunity cycle and is summarised in Figure 1.3. Firstly, tumour cells with must have non-native "neoantigens"- mutated proteins- that are released and phagocytosed by a professional antigen presenting cells (pAPC) and degraded in its proteasome or phagosome. This pAPC must then travel to a lymph node and present this

neoantigen to naïve T and B cells using both MHC II molecules and in MHC I molecules. During antigen presentation, helper T cells (T_h) and CTLs will bind the MHC II and MHC I molecules respectively with their cell receptors. If the binding affinity is high enough and the pAPC in addition expresses co-stimulatory proteins, such as CD80 and CD86, T cells can mature and become active.

CD80 and CD86 bind CD28, expressed on naïve T cells, and is necessary for their activation. Post-activation, CD28 expression is decreased and cytotoxic T-lymphocyte-associated protein 4 (CTLA-4; CD152) expression is increased. CTLA-4 binds the same proteins as CD28, but with higher affinity and avidity, and, as opposed to CD28, CTLA-4 is a suppressive molecule inhibiting CTLs and T_hs. This creates the basis for anti-CTLA-4 immunotherapy where the suppression through CTLA-4 is mitigated [28, 29].

After T_hs have been activated they can proceed to activate B cells or home to the inflamed tissue along with CTLs. Activated B cells can secrete antibodies that bind surface antigens on the tumour cells. These antibodies can subsequently allow granulocytes, NK cells and macrophages to attack cancer cells. For the T cells to be able to infiltrate the tumour, the endothelial cells lining blood vessels must express adhesion molecules that allow T cell infiltration. These adhesion molecules are tissue and inflammation dependent. Thus, if the tumour prevents proper maturation blood vessels or expression of adhesion molecules, T cell infiltration is impaired [30]. If the lymphocytes are able to infiltrate the tumour tissue, they must then find tumour cells presenting the same specific neoantigen, as used for their activation, before an attack can commence. An attack of the CTLs on tumour cells will result in lysis of the tumour cell and release of more antigens. These antigens can then be digested and presented by DCs.
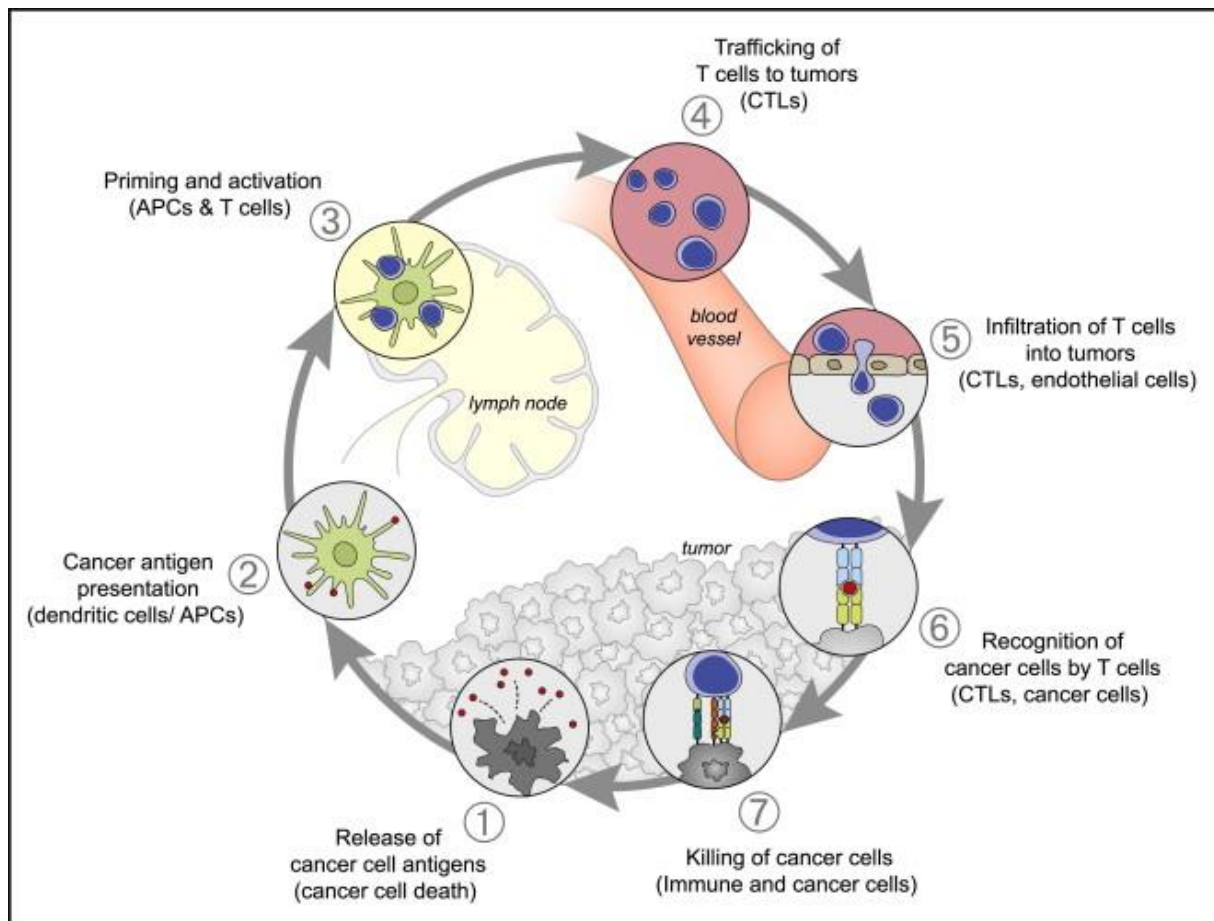
*Figure 1.3: **The tumour immunity cycle.** A cyclic process of digestion of tumour cell antigens, T cell activation and cancer cell killing. The term antigen presenting cells (APCs) is in this case used to refer to professional antigen presenting cells. Reproduced from [31].*

Even if tumour cells are discovered, the attack can be suppressed by activating suppressive molecules on the T cells, such as programmed cell death protein 1 (PD-1; CD279), by expressing one of its ligands PD-L1 or PD-L2 (programmed death-ligand 1 and 2; CD274, CD273). This creates the basis for anti-PD-1 immunotherapy where the suppression through PD-1 is mitigated [29, 32].

In addition, tumours can recruit regulatory T cells, regulatory B cells, myeloid derived suppressor cells (MDSCs) and suppressive tumour associated macrophages type 2 (TAM2) to aid in tumour growth and immune suppression. Of note, the polarisation of macrophages to the TAM2 phenotype has been related to AXL [33]. TAM2 cells have been shown to promote angiogenesis, secrete growth factors and suppress the adaptive immune response [34]. Blocking the TAM2s through AXL-inhibition can potentially improve existing immune therapies. Indeed, such an effect has already been shown (see Figure 1.4) [35].
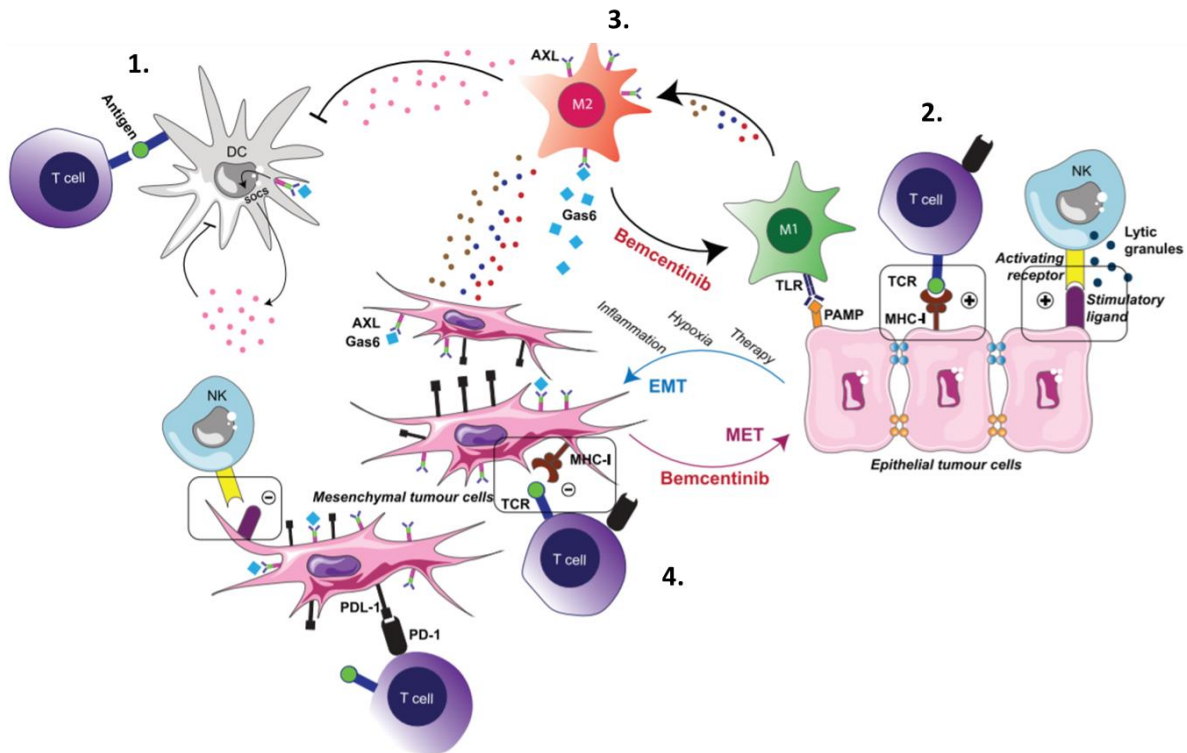
*Figure 1.4: **Overview of AXL's involvementin immune evasion.** Dots represent various stimulatory or inhibitory cytokines. **1.** Dendritic cells can present neoantigens from ingested tumour cells and activate T cells. **2.** Activated T cells can aid in killing tumour cells presenting the same neoantigen as used for their activation. NK cells and tumour associated macrophages type 1 (M1) do not need neoantigens for activation, but instead need stimulatory molecules. **3.** Tumour associated macrophages type 2 (M2) can suppress the immune response through activation of AXL and secretion of its ligand, Gas6. bemcentinib should inhibit this suppression. **4.** Tumour cells can switch from an epithelial phenotype to a mesenchymal-like phenotype through activation of AXL. Bemcentinib can inhibit and reverse this transition. Tumour cells can also express inhibitory molecules such as PD-L1 and prevent CTLs from attacking them. Adapted from BerGenBio poster [35].*

The immune system is, however, not solely dependent on the display of neoantigens. Often, tumour cells downregulate the display MHC I molecules by dysregulating parts of the antigen presentation cycle. Despite not displaying antigens, natural killer (NK) cells use the MHC I molecules as a negative regulator and cell stress markers as positive regulators to decide whether to eliminate a cell. Cancer cells that present stress induced ligands and have low amounts of MHC I are therefore targeted and killed by NK cells [36].

1.3   Treatment of Breast Cancer

Treatment of breast cancer in Norway is based on guidelines developed by Norwegian Breast Cancer Group. Every year new guidelines are published. As of 2018, first line treatment for curative patients is surgical removal of the tumour and nearby affected tissue as well affected ipsilateral axillary lymph nodes. Depending on tumour and patient characteristics, patients receive adjuvant conventional cytotoxic chemotherapy, radiation therapy and/or targeted

therapy for hormone receptor positive tumours and Her2 overexpressing tumours. Patients with distant metastasis or inoperable tumours at diagnosis can be treated with several lines of palliative chemo-radiation and targeted therapy [37].

1.3.1   Anti-PD-1 and Anti-CTLA-4

Immunotherapy aids the immune system in attacking tumour cells. Two common immunotherapies are the anti-PD-1 and the anti-CTLA-4 immunotherapies (comprising the immune checkpoint blockade), as noted in section 1.2.2 [29]. These therapies are given as antibodies that bind the functional domains and prevent activation. Anti-PD-1 and anti-CTLA-4 have both been proven effective in treatment of melanoma and lung cancer[38, 39]. In addition, an increased effect is seen during combination [40]. In breast cancer, anti-PD-1 shows some effect in advanced patients with triple negative disease, while anti-CTLA-4 shows minimal effect [41].

CTLA-4 is a suppressive molecule expressed on CTLs and T_hs, while PD-1 is a suppressive molecule upregulated on activated CTLs and T_hs. In addition, CTLA-4 and PD-1 tends to be upregulated on T_{reg}s, where it may enhance suppressive function and proliferation respectively [29]. With the use of antibodies inhibiting activation of these proteins it is expected an increase of the CTL and the T_h population.

1.3.2   Bemcentinib

Bemcentinib (Figure 1.5) is a small molecule that binds the ATP pocket of the Axl kinase, inhibiting autophosphorylation and thus receptor activation [27]. As noted in section 1.2.1, AXL expression is associated with EMT, immune evasion and poor patient survival. In addition, the TAM2 immune suppressive phenotype has been related to Axl. Bemcentinib can thus potentially function as an anti-immune suppressive drug.
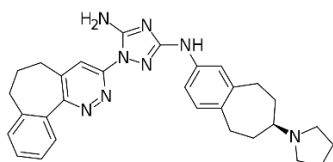
*Figure 1.5: **Molecular structure of bemcentinib.** Bemcentinib works by blocking autophosphorylation and selectively inhibiting the phosphorylation site tyrosine kinase domain of the receptor tyrosine kinase AXL[27]. Structure is drawn by Wikipedia user Edgar181 and is part of public domain.*

1.3.3   Combination of Bemcentinib and Immunotherapy

Bemcentinib in combination with Keytruda (anti-PD-1) is currently in phase II trials on triple negative breast cancer patients [42]. The increased efficacy of immunotherapy-bemcentinib combination has also been shown in preclinical trials (see Figure 1.6) [35]. Mice harbouring mammary adenocarcinomas with a combination of bemcentinib and anti CTLA-4 and anti-PD-1, comprising the immune checkpoint blockade (ICB), resulted in a significantly increased survival.
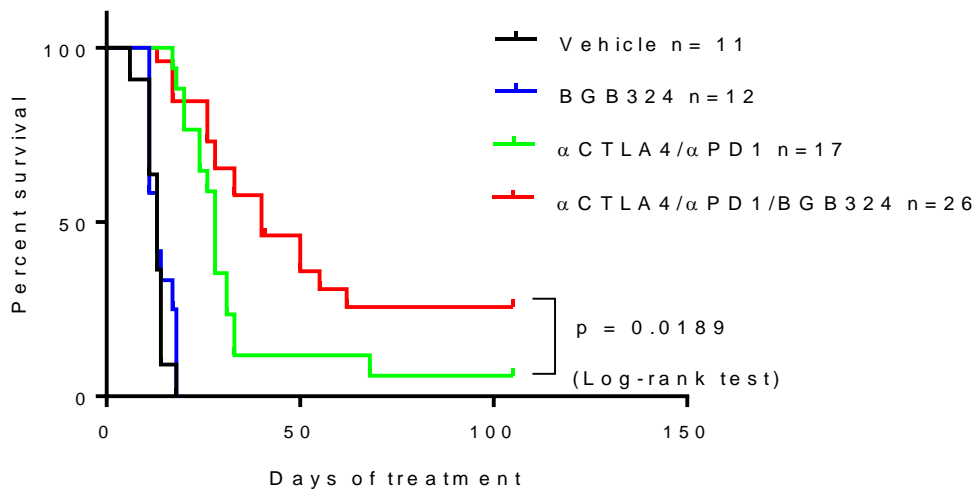
*Figure 1.6: **Preclinical survival study studying a combined treatment of bemcentinib and immunotherapy.**Pooled data from two independent survival analyses of BALB/C mice implanted with 4T1 breast cancer cells. Upon reaching a tumour volume of 500 mm³ the mice were registered as non-survivors. The mice were given treatments with control (vehicle), bemcentinib (BGB324), anti CTLA-4 and anti-PD-1 combination (ICB), or a combination of bemcentinib and ICB. Figure is reprinted from [35]*

The mechanism behind this result is, however, poorly characterized.

1.4   Aims and Objectives

As discussed in the previous sections, cancer is one of the leading causes of death in Norway and one of the leading causes of deaths worldwide. Malignant cancer has an intrinsic plasticity driving therapy resistance, and immune system suppression. An important driver for this malignant phenotype is the EMT program. Earlier research indicates a link between AXL, EMT and immune suppression in tumours. Combined immune checkpoint and AXL-inhibitor therapy bemcentinib demonstrated a synergistic effect. We therefore endeavoured to determine the mechanism behind this therapeutic effect.

9
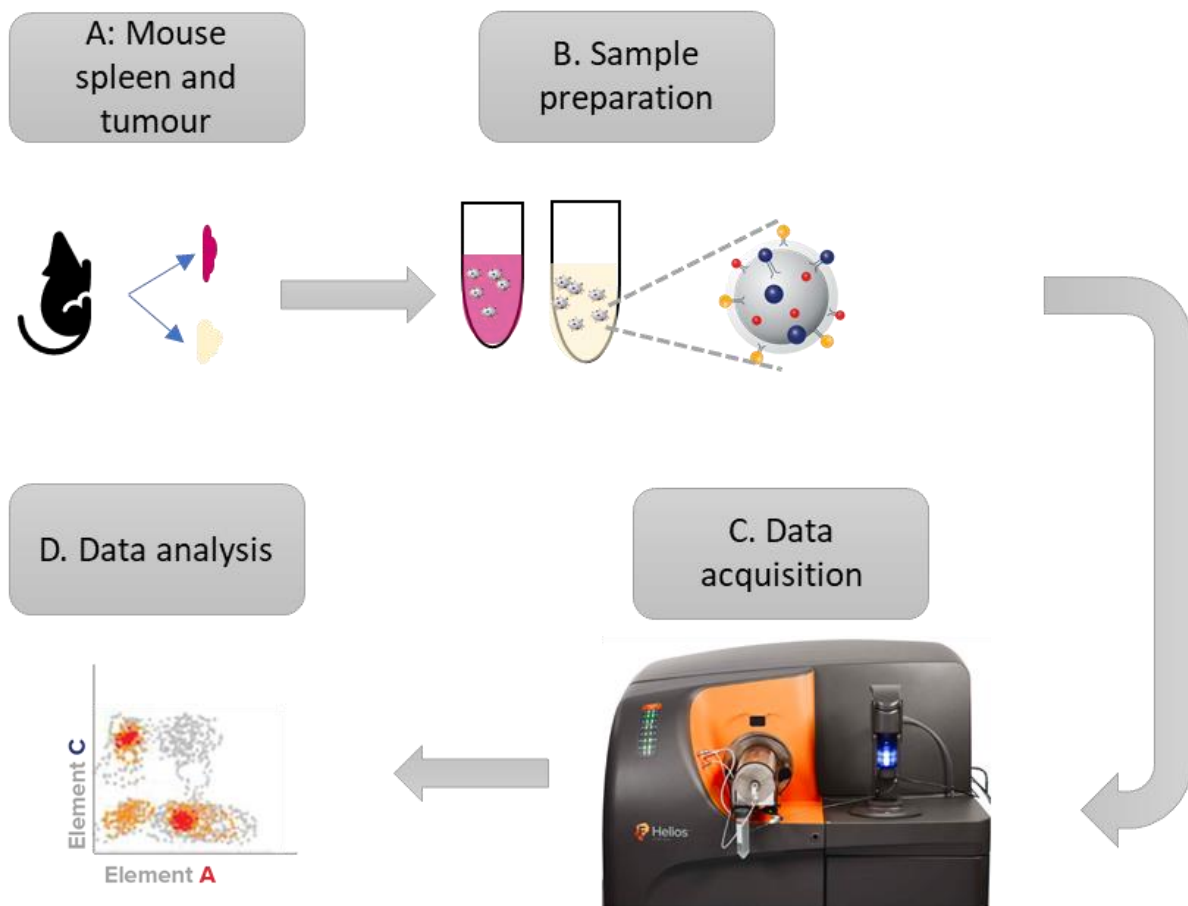
*Figure 1.7: **Methods summary. A**: Spleen and tumours were collected at two different timepoints from mice in four different treatment groups. **B**: The tissues were dissociated to single cells, fixed and frozen for storage. The samples were later stained and **C**: run on the mass cytometer. **D**: After data acquisition the data was analysed with regular gating, high dimensional analyses and statistics. The depicted stained single cell is adapted from [43] and the mass cytometer is reproduced from [44].*

To investigate how this combination affects the tumour immune response we harvested tumour and spleen tissue from tumour bearing mice at different timepoints treated with vehicle, bemcentinib, immune checkpoint blockade, or a combination of bemcentinib and immune checkpoint blockade. These tissues were dissociated to single cells and analysed by mass cytometry, an approach that allows for measurement of multiple proteins on single cells. High dimensional analyses were used to map the immune landscape across tissues, treatments, and timepoints. By studying how the immune landscape changes during tumour development and treatment, important insight into effects of the combined treatment could be made.

2 Methodological considerations

2.1 Mass cytometry

Mass cytometry is a novel method for analysing multiple parameters in single cells [45]. These parameters include, but are not limited to, proteins, lipids, and nucleic acids. The targets on the cells are labelled directly or indirectly with heavy metal isotopes before running the sample through a mass spectrometer and measuring the metal content single cells.

A typical chronological staining procedure for mass cytometry is to: 1) use a reagent to distinguish between live and dead cells; 2) identify cells or proteins of interest by staining for specific proteins with antibodies, and 3) to identify whole cells by staining with a DNA intercalator. Depending on the type of experiment and proteins of interest, cells are fixed and permeabilised before or after staining with antibodies.

2.1.1.1 Instrument

Before data acquisition, the mass cytometer is tuned, a procedure entailing estimation of dual count coefficients, calibration of gas flows, and electric voltages over the cones and the detector. At the end of the tuning is a quality control is normally required to be passed in order to run any experiments.

The mass cytometer consists of a mass spectrometer coupled with a system to deliver a cloud of singly positively charged atoms from a single cell [46, 47]. A schematic of the prototype is shown in Figure 2.1.
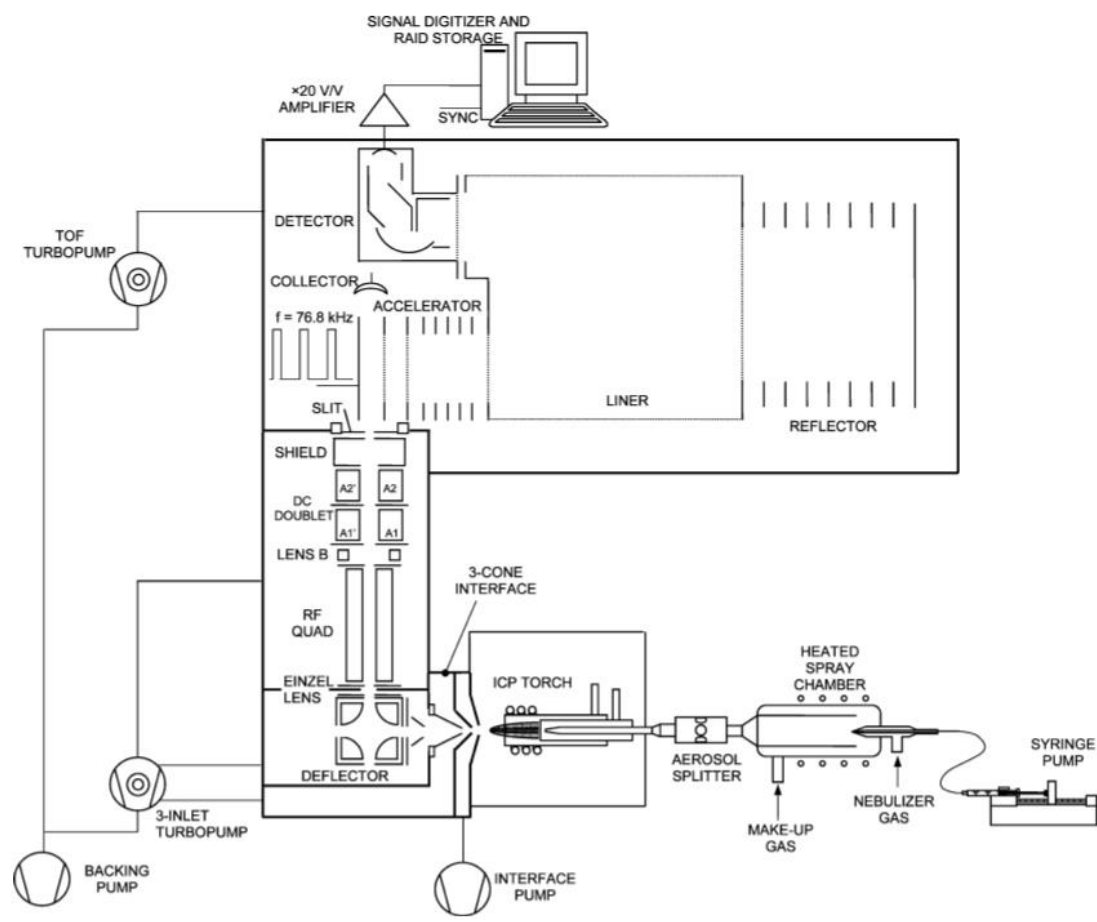
*Figure 2.1: **"Schematics of the prototype CyTOF mass cytometer".** The sample enters the machine in the lower right corner and is made into a mist by the nebuliser. The mist with single cell droplets is heated leading to single cells suspended in gas. The cells are then ionised and fully burned in the induction coupled plasma before being filtered by the deflector and the quadrupole. The filtered cloud lastly enters the time-of-flight (TOF) chamber where sequential slices of the cloud are launched into a parabolic path separating the singly charged atoms based on mass prior to hitting the detector. Reproduced from [46].*

2.1.1.2   Sample Introduction and Ionisation

A test tube containing a fixed, stained sample of single cells is placed into the autosampler chamber (see Figure 2.2) and a small sample line is inserted into the test tube. Argon gas is released into the closed chamber and the increased pressure pushes the sample up the sample line and through a nebuliser.

*Figure 2.2: **Fluidigm's mass cytometer model Helios.** The Helios differs from other mass cytometer systems by having the autosampler instead of a syringe pump to inject the sample. The autosampler can be seen standing on the shelf on the right side of the machine. Reproduced from [44].*

The nebuliser combines the sample with argon and pushes it through a nozzle, creating a mist of small droplets, each optimally containing only a single cell. The mist is mixed with more argon gas and heated in the spray chamber to evaporate fluid from the droplets, leaving only single cells suspended in argon gas. Each cell is then transferred, in a stream of argon, through a plasma [44].

The plasma is generated by an induction coupled plasma torch. The torch functions by applying a spark to the argon gas in an alternating electromagnetic field, created by a coil connected to a radio frequency (RF) generator. The oscillating field amplifies the movement of the electrons from the spark, increasing the electron collision rate with other atoms and molecules and establishes the plasma. The continuously oscillating electromagnetic field stabilises the plasma in the flowing argon gas. The temperature of the plasma is about 5000 kelvin in the core of the stream and 7000 kelvin around the edges [48]. This is comparable to the temperature of the surface of the sun. Despite the high temperature, without the nebuliser and the heating chamber the cells would not be fully atomised and ionised. Because they are already dry and suspended as single cells almost all the molecules in the cells travelling through the plasma are atomised and ionised resulting in clouds of singly positively

charged ions. If the plasma is relatively cool or the argon flow rate is too high, oxides can form and lead to +16 dalton spill. This means that a 150Nd tag can be registered as a 166Er tag.

Electrostatic repulsion and heat from the plasma leads expansion of the atomised cloud. The expansion of the cloud dominates over cell size, so that regardless of the cell's size, the cloud expands to approximately 1-2 mm [49]. To prevent cloud expansion, vacuum is needed to cool the gas. The vacuum is created by a set four vacuum pumps evacuating the interfaces between three cones and the rest of the machine. The first cone extracts 10% of the plasma and decreases the pressure from 760 torr to about 2 torr. The second cone only extracts 1% of the gas passing the first cone and further decreases the pressure. The last cone transmits 100% of the gas from the second cone and has a voltage applied to improve ion transmission before being focussed by a lens prior to entering the deflector.

2.1.1.3 Ion Optics

The deflector consists of four pillars assembled in the corners of a square. Each pillar has the opposite charge of its lateral and vertical neighbour and the same charge as its diagonal neighbour. The ions enter from the side, between the front positive and negative pillars. The positive ions are pulled toward the negative pillar, but due to their velocity, they travel in a curved path and exit 90 degrees to the left (or right depending on the charge of the pillars) of where they entered. Neutral particles and photons travel straight through. The removal of photons is vital because it is impossible to differentiate a photon from an ion hitting the detector. The positive ions are then focused by lenses before entering the quadrupole. In the quadrupole, low mass ions (such as argon) are removed and ejected from the stream, leaving only atoms with a single positive charge and around 80 daltons. The now filtered cloud of singly positive atoms move towards the time of flight (TOF) chamber [46].

2.1.1.4 Ion Separation and Detection

In the TOF chamber sequential vertical slices of the ion stream are launched into a reflector creating a parabolic path. The slice of ions ejected from the stream is referred to as a push. During the push the force applied to each ion is the same, since they all have the same single positive charge, however, the speed they gain is different because the mass of the ions is different. The lightest ions will therefore travel faster than the heavier ones and arrive earlier at the detector. This separation of mass packets allows a mass windows for each mass to be

estimated based on the time of flight. Due to variability in initial speed and position of the ions prior to the push, the ions in each mass packet will spread out and some ions might enter a neighbouring mass window. This is referred to as abundance sensitivity and is less than 0.3% for 159Tb [50]. Thus if 1000 ions are registered in the 140Ce channel, 3 ions are estimated to enter each of the neighbouring mass windows 139La and 141Pr.

At the end of the parabolic path, a cathode serves as the start of an electron multiplier tube. Upon hitting the cathode, electrons are released, but too few are released to be able to register, hence the electron multiplier tube is needed. The electrons released from the first cathode are accelerated towards the next plate, called dynode, by an electric field. For each dynode the electrons hit, the number of released electrons multiplies. At the end of the tube an amplifier amplifies the voltage created by the electrons. Since not every electron hits the final anode at the same time, the signal is manifested as a pulse. The voltage from the anode is amplified and converted to digital signals by an analogue-to-digital converter (ADC) at 1 GHz.
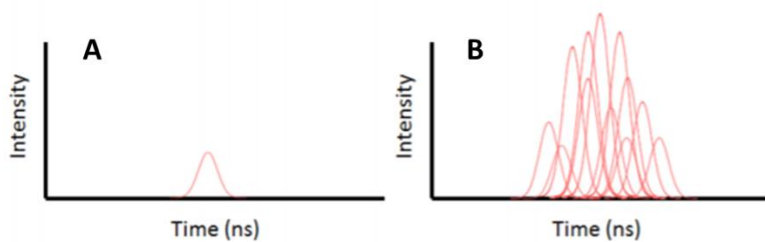
*Figure 2.3: **Signal pulse overlap** Electron pulses are generated when ions hits the detector. **A**: When few ions hit the detector in the same push, the pulses are not overlapping. The ion counts can therefore be found by counting the pulses. **B**: When more ions hit the detector, the pulses can overlap, and the integrated intensity is instead used. The integrated intensity is calculated by multiplying the maximum intensity with the width at half maximum. Later on, the integrated intensity is multiplied with the dual count coefficient to estimate the true number of ions hitting the detector. Reproduced from [44].*

When multiple ions hit the detector at the same time or are sufficiently close, the generated voltage pulses overlap (see Figure 2.3). This means that the number of ions hitting the detector must be approximated based on the generated voltage. Each electron pulse generates a voltage pulse lasting a few nanoseconds. To estimate the intensity, the maximum voltage of the electron pulse is multiplied by the width of the pulse at half max. Since each ion hitting the cathode should release the same number of electrons, a linear relationship between the true count and the intensity should exist.
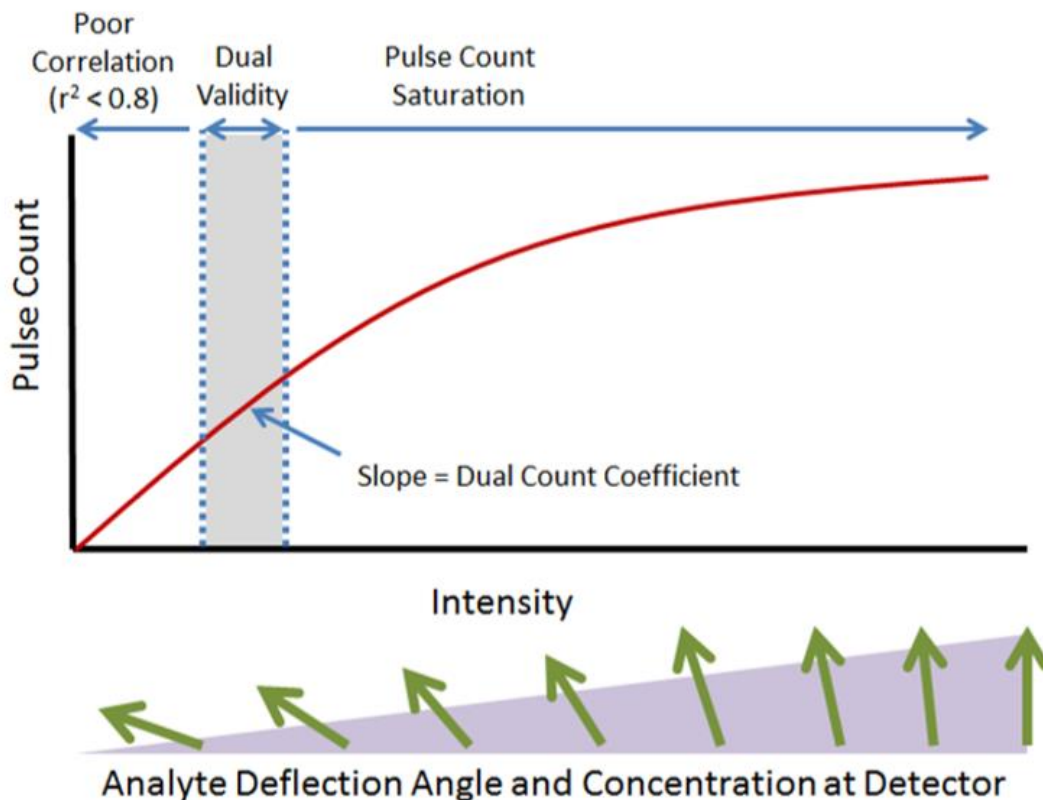
*Figure 2.4: **Analyte deflection during tuning.** As the deflector voltage is altered during tuning the number of ions entering the TOF chamber changes. When number of pulses per push is between 0.1 and 1 a linear relationship between true count and intensity exists. The slope of the linear fit is called the dual count coefficient. By using this coefficient, the true counts of ions hitting the detector can be estimated by multiplying it with the integrated intensity. Reproduced from [51].*

During tuning the linear correlation between intensity and true count is estimated. This is done by running a "tuning solution", containing the specific heavy metal isotopes 133Cs, 139La, 155Gd, 159Tb, 169Tm 191Ir, and 193Ir, through the machine. To gradually increase the number of ions entering the TOF chamber, the voltage on the deflector (before entering the quadrupole) is adjusted. When very few ions hit the detector there is a linear relationship between the intensity and the pulse count. This zone is referred to as the zone of dual validity. Several readings, each consisting of one or more pushes, are taken and used to plot a curve between the pulse counts and the intensity. The zone of dual validity is valid only when pulses per push is between 0.1 and 1. In this zone the relationship between intensity and pulse counts is linear and a regression is performed to find a dual count coefficient which allows for calculation of true counts based on intensity alone (see Figure 2.4). The dual counts are named after the dual values it returns. If the number of pulses created in a push is below 0.1 (default threshold), pulses are returned, while if the number of pulses per push is above 0.1 the

estimation of true counts based on intensity is returned. At the end of the tuning is a quality control where the final signal intensity and oxide generation is checked. If the signal intensity is too low or the oxide generation is too high the tuning will not pass.

2.1.1.5   Data Processing

Upon starting data collection on the mass cytometer, the masses to record have to be manually selected. Even though a mass is not selected for recording, it will still hit the detector if it is in the sample. Having determined the dual count coefficient during tuning, dual counts for every selected mass in every push is calculated. For each push the dual counts are summed over the selected masses. This sum is referred to as total ion current and is used to filter out non-single cloud events. The filtering process works by applying a convolutional threshold that the total ion current must exceed for at least 10, but not more than 150 pushes. This threshold has a standard value of 400, but it can be changed manually. In addition, noise reduction can be applied. The noise reduction calculates the mean total ion current between cell events and subtracts this value from total ion current measured during a proximal event [49]. If the number of pushes in an event, referred to as event length, is between 10 and 150, then a gaussian fit will be performed on the total ion current. From this fit, the gaussian parameters width, centre, residual, and offset are returned. The event length, width, centre and residual can later be used to find single cell events. The offset, however, is poorly described and is not commonly used in further analysis. Having characterised an event, the dual count for each selected mass is summed over the pushes in the event and saved in a flow cytometry standard (fcs) file along with the gaussian parameters. For visualisation and analysis purposes the calculated dual counts are often randomised to a gaussian or uniform distribution and assigned new values.

2.1.2   Sample Preparation

To label desired targets a staining procedure must be performed. Often several are needed to label all targets. Tagging of specific proteins can be done by conjugating antibodies that will bind the target proteins[52-54]. Nucleic acids can be tagged by using rhodium or iridium chelated intercalators [55]. Lipids can also be stained by using osmium or ruthenium tetroxide[56] and DNA synthesis can be measured by adding 5-iodo-2-deoxyuridine to the cell medium [57]. By using an approach similar to RNA-scope specific RNAs can be stained [58, 59].

Proteins can also be stained non-specifically by using nonspecific tags such as cisplatin or isothiocyanobenzyl-EDTA chelated with different isotopes of palladium [60-62].

2.1.2.1   Live Dead Staining

To differentiate between live and dead cells we use the fact that the membrane of dead cells is more permeable. By using non-specific markers dead cells can be labelled and later excluded from analysis. Typical live dead markers are cisplatin and the intercalators mentioned above[55, 62]. Both of these markers stain dead cells strongly, but they might also stain live cells to a lesser degree. This applies especially if the cells tend to have a high turnover of pinocytosis (common in tumour cells) and the staining is performed over an extended period.

2.1.2.2   Barcoding

To ensure equal staining conditions among different samples a barcoding procedure can be performed. This also allows collection of data from multiple samples simultaneously. The barcoding procedure entails staining each sample with a specific pattern of mass tags before combining the samples together for simultaneous antibody staining. The most common procedure for barcoding is by the use of palladium tags, however, other tags, such as CD45 conjugated antibodies, can also be used [63]. A common staining scheme used during barcoding is the doublet filtering scheme Zunder et al [61] illustrated in Figure 2.5.

	102Pd	104Pd	105Pd	106Pd	108Pd	110Pd
Sample 1	■	■	■			
Sample 2	■	■		■		
Sample 3	■	■			■	
Sample 4	■	■				■
Sample 5	■		■	■		
Sample 6	■		■		■	
Sample 7	■		■			■
Sample 8	■			■	■	
Sample 9	■			■		■
Sample 10	■				■	■
Sample 11		■	■	■		
Sample 12		■	■		■	
Sample 13		■	■			■
Sample 14		■		■	■	
Sample 15		■		■		■
Sample 16		■			■	■
Sample 17			■	■	■	
Sample 18			■	■		■
Sample 19			■		■	■
Sample 20				■	■	■

This scheme allows for easy detection of doublets or aggregates from separate samples, since they would be positive for more than three isotopes. Doublets of the same sample can still occur and would need to be gated out separately. If it's desired to stain even more samples at once, the scheme can be expanded to allow all permutations, but it is important to note that this entails some drawbacks. Using all permutations negates doublet filtering and if the samples are not washed thoroughly before mixing, remnant staining solution can stain the wrong sample and lead to wrongful debarcoding during pre-gating.

2.1.2.3 Antibody Conjugation

Before staining with antibodies, they must be tagged with metal isotopes. Several procedures exist, but the most common one is to use the MAXPAR polymer from Fluidigm. Other procedures may use cadmium nanoparticles, cisplatin, and palladium or indium chelated to monomers of DOTA (1,4,7,10-tetraazacyclododecane-1,4,7,10-tetraacetic acid) or DTPA (polymeric pentetic acid) [64]. The MAXPAR polymer, DOTA, and DTPA all have chelation sites that bind heavy metals strongly. After having bound metals to the polymer or monomer, hereafter referred to as polymer, the polymer can be conjugated to antibodies. Antibodies have several functional groups that can be used for conjugation, but only conjugation kits using disulphide bridges (see Figure 2.6) are offered by Fluidigm as of November,2018.

By reducing antibodies with TCEP, disulphide bridges are converted to thiols, which readily react with the maleimide group on the polymers. During reduction, the antibodies are partially denatured. The denaturing is crucial to successful conjugation, but if the antibodies are overly denatured they might become unusable. Each antibody should therefore be tested after conjugation. The thiol-maleimide reaction creates a covalent bond, effectively bonding the metal loaded polymers to the antibody. This method has been proven effective on IgG isotype antibodies without changing the antibody specificity [54]. However, due to differences in locations of disulphide bonds among the isotypes other isotypes may not work. The IgM isotype for example is not recommended when using this procedure. After the conjugation, the antibody should always be titrated.
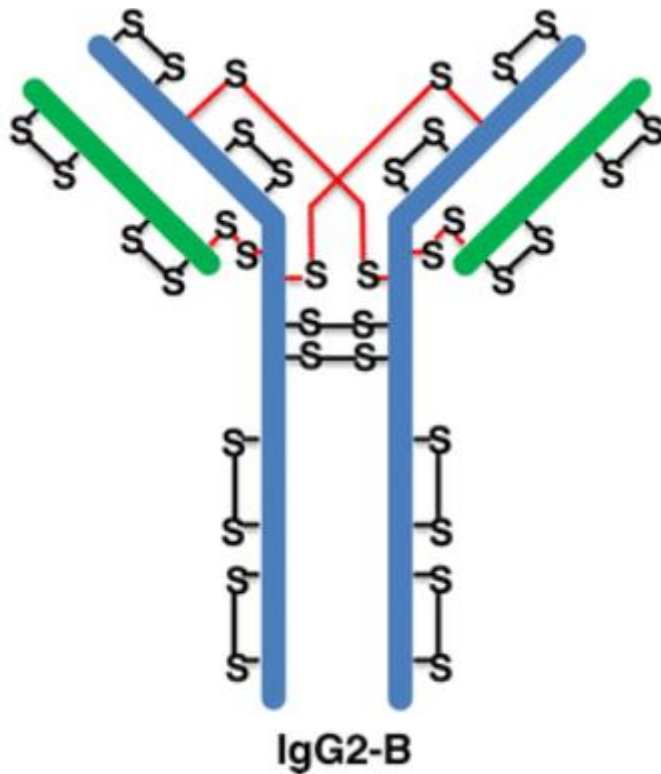
*Figure 2.6: **General antibody structure.** The structure of a human IgG2-B antibody. Heavy chains of the antibody are coloured blue and light chains are coloured green. During reduction of the antibody using TCEP, disulphide bridges are reduced to thiols. The thiols can bind maleimide. By using polymers with maleimide groups, reduced antibodies can be conjugated to the polymers. If the antibodies are overly reduced it can result in a loss of function. The antibodies bind one antigen in each of the two upper edges. Adapted from [65]*

2.1.2.4   DNA Staining

The last part of sample preparation is usually to stain the DNA. The DNA stain is used to differentiate cells from beads (for normalisation) and debris. This is often done using one of the intercalators mentioned in section 2.1.2 along with formaldehyde and a permeabilization solution. The formaldehyde is important for preventing cell loss during water washes and data collection.

2.1.2.5   Water Washes

The last part of the sample prep is washing the sample in pure Milli-Q grade water. This is to reduce build-up of salts in the machine and in the nebuliser. Salt build up can cause clogs and lead to ion transmission loss due to accumulation on the cones. The water washes are, however, damaging for the cells. The hypotonic solution leads to cell disintegration and can create puzzling artefacts. Proper fixation is therefore vital. Recently Fluidigm has released a new solution to replace the water to use during data acquisition. This new solution is called

cell acquisition solution (CAS). To use this solution however, the injector that transfers cells from the heating chamber to the plasma must be switched with one having a wider bore.

2.1.3   Flow Cytometry as an Alternative

Most current studies use flow cytometry to study immune cell populations. While flow cytometry can analyse tens of thousands of cells per second, it is often limited to only ten simultaneous measurements [46]. In research laboratories the use of 17 fluorescent labels in flow cytometry has been utilised, but it demands extensive customisation [66]. Mass cytometry has a disadvantage in terms of cell throughput, reaching a theoretical maximum at 3000 cells per second [46]. The advantage is, however, the potential of measuring 135 different isotope tags, as the mass cytometer has a mass range covering 75 through 209 daltons [44]. This high dimensional single cell analysis can allow for characterisation of never seen before cell types. A comparison of mass cytometry and flow cytometry is summarised in Table 2.1.

Table 2.1: Comparison of flow cytometry and mass cytometry.

	Flow cytometry	Mass cytometry
Throughput	>10,000 cells/s	>3,000 cells/s
Number of parameters	Typically, 8+2 (physical)	47 commercially available
Physical parameters	Forward scatter and side scatter	Osmium tetroxide can be used as surrogate marker for forward scatter.
Background	Significant spectral overlap with increased number of markers.	Abundance sensitivity (>0.3%), oxide formation (>3%), and isotopic impurity (<2%)
Cell endpoints	Cell can be kept alive and sorted after analysis.	Cells are incinerated during analysis.
Autofluorescence	Significant autofluorescence	Minimal autofluorescence (depending on sample origin and treatment).

2.2   Data analysis

The data analysis is generally divided into two parts; the pre-gating and the high dimensional analyses. During pre-gating machine dependent sensitivity decline is corrected for and barcoded samples are debarcoded.

2.2.1   Normalisation

During running, loss of detector sensitivity leads to a decline in registered signal intensity. This means that two identical cells with identical staining will yield two different signal intensities depending on when they were run. To correct for the decline, beads are mixed with the sample before acquisition. The beads contain a mix of different heavy metal covering a part of the mass spectrum registered by the machine and are highly similar to each other. By using these beads, the decline in sensitivity can be corrected for using normalisation procedures. In addition, cleaning of the instrument can affect ion throughput, and thus the intensity registered. This again means that identical samples run on separate days can yield different results. By using the beads as a reference however, the difference can be normalised. Two procedures exist for normalisation and differ in the reference used during normalisation. The Fluidigm method uses a lot specific dual count mean from the bead production to correct for the differences across different runs on different machines (of the same model). The MATLAB method, however, uses the median intensity across the samples as a reference [67]. This means that the samples have to be normalised as a group for them to be comparable, as opposed to the Fluidigm method where they can be normalised one by one [68].

The sample acquisitions are often interrupted. Since each run gives one file, the same sample can end up being in spread over multiple different files. To make data handling more manageable the files are typically concatenated after normalisation.

2.2.2   Debarcoding

If several samples were barcoded as previously described and combined before staining, it is necessary to debarcode them again to extract the individual samples. This is done by stratifying the events based on the three barcoding isotopes with highest intensity. The barcode intensities are normalised so the highest in the sample gets a value of 1 and the lowest a value of 0. The separation between the 3rd and 4th strongest barcode isotopes after

normalisation are then used as a threshold to remove doublet and debris. A Mahalanobis distance threshold can also be applied to remove outliers.

It is important to note that the barcode staining intensity is highly dependent on the cell number during staining and cell type [61]. This means adjusting the barcode separation or applying a minimum intensity threshold can select for specific samples or cell types.

2.2.3   Gating

To filter out singlets of the sample a combination of event length and intercalator intensity is typically used. A drawback using the intensity of intercalator is however that different cell types stain differently [69]. Thus, using this as a primary gate could potentially be biasing the data. As mentioned in the last paragraph of section 2.1.1.5, the gaussian parameters can be used to identify singlets. Several types of doublets exist. The doublets can be caused by a single cell cloud overlapping with debris or another single cell cloud or by cells sticking to each other due to poor mixing during fixation. If the clouds are overlapping the singlet filtering can be based on the gaussian parameters alone (see Figure 2.7). However, if cells are sticking to each other, the intercalator, or another marker, must be used in addition. It is therefore best to use all of the mentioned parameters.
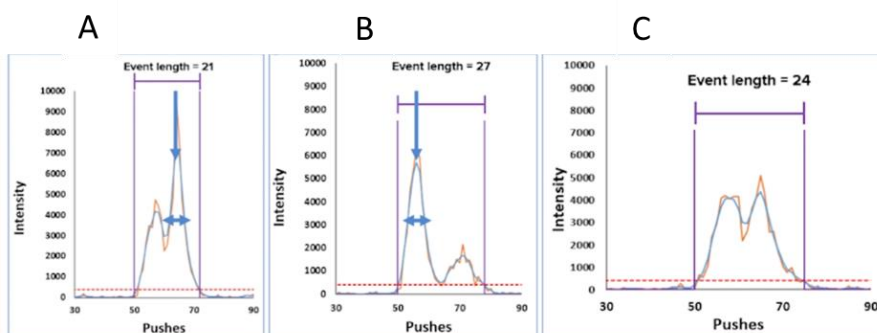
Figure 2.7: ***Three different types of doublets due to overlapping clouds.*** *The doublets affect the gaussian parameters, making them easy to identify. All doublets yield a high residual due to the non-gaussian shape and a high event length.* ***A****: The high second peak gives a high centre and a low width.* ***B****: The high first peak gives a low centre and a low width.* ***C****: The centre and width values can vary. Reproduced from [69].*

2.2.4   Dimensionality Reduction

In mass cytometry over 30 different parameters can be measured per single cell. Due to the high dimensionality of the data, creating a 2D projection showing all differences between each cell is impossible (except if all but two parameters are 0 in every event). By using an algorithm

known as t-distributed stochastic neighbour embedding (tSNE) [70], similar cells can be placed close to each other in an iterative process where short distances in the high dimensional space cause an attractive force between the cells and long distances in the high dimensional space cause a repelling force. To calculate the similarity between the 2-dimensional space and the high-dimensional one a Kullback-Leibler (KL) divergence is calculated and used as a cost function. The gradient of the cost function is calculated to know how to move each cell to reduce the KL divergence [71]. The KL divergence is a useful tool to determine if enough iterations have been performed on the tSNE.

2.2.5   Clustering

Traditionally cells have been divided into separate cell types. Since all cells originate from the same embryo, however, every cell type must have an intermediate. This leads to a fundamental problem: how do you decide where the line separating two cell types is? Traditionally, samples have been gated using subjective knowledge and established norms, but with the increase of measured parameters the traditional gating procedure can become very laborious. If 30 parameters are measured, a total of $\frac{30*29}{2} = 435$ unique scatter plots can be made. All of the scatterplots might not make sense to analyse given prior knowledge. But, using only prior knowledge can lead to loss of cell phenotype discovery. Automatic clustering algorithms therefore represent a way to cluster a sample fast and less biased. In addition, high dimensional clustering algorithms are not restricted to analysing only two parameters at a time when deciding cluster.

Phenograph [72] is a common clustering algorithm applied to mass cytometry data. Briefly, the algorithm works by creating a network connecting each cell to its k (a user chosen value) nearest neighbours and then weights each connection by the calculating the number of shared neighbours for each cell-cell pair. Communities (i.e. clusters) are then found by applying an approximation, known as the Louvain Method, on the weighted network. This approximation gradually assigns cells to communities based on the increase of modularity (an estimate of network density in a community). The Louvain Method is run several times and the communities from the run with the highest overall modularity is returned as clusters.

2.2.6   Cluster Characterisation

Since the clustering algorithm often finds several clusters, an easy way of characterising each cluster is needed. Marker Enrichment Modelling is a useful tool developed by Diggins et. al [73] and works by calculating a MEM-value for each marker in each cluster.

The equation used is:

$$MEM = \left|median_{cluster} - median_{reference}\right| + \left(\frac{IQR_{reference}}{IQR_{cluster}}\right) - 1$$

$$if\ \left(median_{cluster} < median_{reference}\right)\colon MEM = -MEM$$

Thus, if there is a large difference between the median of the cluster and the population, or if the interquartile range (IQR) is smaller in the cluster than in the reference, then the MEM-value increases.

The reference used is often the rest of the clusters, but a selected reference sample can also be used.

2.3   Reasons for the Approach

The immune system is complex and consists of several different phenotypes, each serving specific functions. To determine how the immune system is affected by tumour development and therapy, the immune landscape must be mapped and compared across timepoints and treatments. Since the cell phenotype is determined by protein expression, it is vital to detect these proteins. Mass cytometry allows measuring of over 40 tags simultaneously on single cells and is commercially available. Thus, this method is fit to determine cell phenotypes in heterogenous single cell samples. The high dimensional data would earlier be a problem, but due to recent developments in data processing and machine learning the data can be analysed unbiased and efficiently. An alternative to mass cytometry is flow cytometry. However, flow cytometry is limited by the number of tags that can be used simultaneously and the significant compensation needed to be done after acquisition.

3 Materials and Methods

3.1 General Overview

The methods can be divided into four parts as depicted in Figure 1.7. The first part entails tumour injection, treatment and tissue harvesting. The second part continues with tissue treatment and its treatment until being run on the mass cytometer. The data acquisition has gotten its own section to separate it from the analysis and the sample preparation. Lastly, the data analysis is explained, starting with normalisation and ending with calculation of statistics from cell clusters. Animals, chemicals, antibodies, and equipment

Table 3.1: Materials used for cell culturing, mouse treatment, and tissue dissociation.

Description	Source	Product number	Details
4T1	ATCC		CRL-2539
Anti-mCTLA-4	BioXCell	BE0131	Syrian Hamster IgG, clone 9H10
Anti-mPD-1	BioXCell	BE0146	rat IgG2a, clone RMP1-14
BALB/c mice	Taconic Laboratories		50 females
Bemcentinib	BerGenBio		
Cisplatin-194	Fluidigm	201194	5mM stock
C-tubes	Miltenyi Biotec	130-096-334	
Fetal bovine serum	Sigma	F7524	
gentleMACS Dissociator	Miltenyi Biotec	130-093-235	
L-Glutamine solution	Sigma	G7513-100ML	
MACS SmartStrainers (70 μm)	Miltenyi Biotec	130-110-916	
MACS Tissue Storage Solution	Miltenyi Biotec	130-100-008	
Matrigel Basement Membrane Matrix Growth Factor Reduced	BDBioscience	354230	
Penecillin-Streptomycin	Sigma	P0781-100ML	
Polyclonal Armenian Hamster IgG	BioXCell	BE0091	BE0091
Pre-Separation Filters (30 μm)	Miltenyi Biotec	130-041-407	
Red Blood Cell Lysis Solution (10×)	Miltenyi Biotec	130-094-183	
RPMI -1640 Medium	Sigma	R8758-500ML	
Spleen Dissociation Kit, mouse	Miltenyi Biotec	130-095-926	

Sterile Cell Strainner 40 µm	Fischer Scientific	22363547
Trypsin - EDTA Solution	Sigma	T4047-100ML
Tumor Dissociation Kit, mouse	Miltenyi Biotec	130-096-730

Table 3.2: Materials needed for antibody conjugation.

Description	Source	Product numbe	Lot number
Antibody stabilizer	CANDOR	131 050	131D324v
C-buffer	Fluidigm	S00004	0071601
L-buffer	Fluidigm	S00008	2781505
R-buffer	Fluidigm	S00002	3271511
TCEP	Thermo Scientific	77720	QH220380B
W-buffer	Fluidigm	S00006	2751520
X8 polymers	Fluidigm	S00009	P17G1002-P02, P18D0201-P09, P15J0201-P03
Lanthanide solutions	Fluidigm		
Centrifugal Filter Unit: 3 kDa Amicon Ultra 500 µL V bottom	Millipore	UFC500396	
Centrifugal Filter Unit: 50 kDa Amicon Ultra 500 µL V bottom	Millipore	UFC505096	

Table 3.3: Chemicals used during sample preparation.

Description	Source	Product number	Lot number
Antibody stabilizer	CANDOR	131 050	131D324v
Barcode perm (10x)	Fluidigm	201057	1381803
Barcodes	Fluidigm	S00114	2461603
Bovine serum albumin (BSA)	Sigma Aldrich	A9647-100G	SLBV4996
C-buffer	Fluidigm	S00004	0071601
Cell staining buffer	Fluidigm	201068	3001610
DNase I	Sigma Aldrich	DN25-1G	SLBV1446
Dulbecco's phosphate buffered saline (DPBS)	Gibco	14040-133	1941466
EDTA	Sigma Aldrich	E5134-250G	BCBV7014
Filter 0.2 µm	GE Healthcare Life Sciences	10462200	

Paraformaldehyde 16% solution, EM grade	Electron Microscopy Sciences	15710	
Phosphate buffered saline (PBS)	Sigma Aldrich	P4417-100TAB	SLBW3999
Sodium azide	Merck	106688	
Syringe 30 ml	BD Plastipak		
Tube 15 ml	Sarstedt	62.554.502	
Tube 5 ml	Sarstedt	55.1578	
Tube 50 ml	Sarstedt	62.547.254	

Table 3.4: List of mass cytometry panel and antibodies used for staining. *Antibodies used during intracellular staining. †Antibodies used during surface staining. All antibodies from companies other than Fluidigm were conjugated to the given mass tag. Superscripted numbers indicate backbone number.

Product	Mass tag	Clone	Source	Product number	Lot
Intercalator (Rh)	103Rh	None	Fluidigm	201103A	1801702
CD11c†[1]	142Nd	N418	Fluidigm	3142003B	2431705
CD69†[3]	143Nd	H1.2F3	Fluidigm	3143004B	1171706
CD115†[2]	144Nd	AFS98	Fluidigm	3144012B	1111704
CD4†[2]	145Nd	RM4-5	Fluidigm	3145002B	0901505
CD8a†[2]	146Nd	53-6.7	Fluidigm	3146003B	0351301
CD45†[1]	147Sm	30-F11	Fluidigm	3147003B	0901705
PD-1 (CD279)†[2]	148Nd	RMP1-30	eBiosciences	14-9981-82	4311070
CD83†[3]	149Sm	Michel-17	eBiosciences	14-0831-82	4274058
CD24†[3]	150Nd	M1/69	Fluidigm	3150009B	0901508
CD64†[1]	151Eu	X54-5/7.1	Fluidigm	3151012B	2601611
CD3e†[1]	152Sm	145-2C11	Fluidigm	3152004B	3181714
PD-L1 (CD274)†[1]	153Eu	10F.9G2	Fluidigm	3153016B	1711724
CD11b†[1]	154Sm	M1/70	Fluidigm	3154006B	2341710
CD114†[2]	155Gd	723806	R&D	MAB60391	CFZR0117071
CD103†[3]	156Gd	2E7	eBiosciences	14-1031-85	4318103
FOXP3*[3]	158Gd	FJK-16s	Fluidigm	3158003A	3461707
FOXP3*[3]	158Gd	FJK-16s	Fluidigm	3158003A	1841813
F4/80†[2]	159Tb	BM8	Fluidigm	3159009B	0541707
ARGINASE 1*[3]	160Gd	Polyclonal	Novus Biologicals	NBP1-32731	42893
iNOS*[3]	161Dy	CXNFT	Fluidigm	3161011B	1171714
Ly-6C†[2]	162Dy	HK1.4	Fluidigm	3162014B	2341706
CD40†[3]	163Dy	1C10	R&D	MAB440	AHY1717071
CD49b†[1]	164Dy	HMα2	Fluidigm	3164011B	1531401
CD25†[3]	165Ho	280406	R&D	MAB2438	VDI0113021
CD19†[1]	166Er	6D5	Fluidigm	3166015B	3181409

CD335 (NKp46) †[1]	167Er	29A1.4	Fluidigm	3167008B	3131704
CTLA-4 (CD152) †[2]	168Er	UC10-4B9	invitrogen	14-1522-82	1953873
CD206†[3]	169Tm	C068C2	Fluidigm	3169021B	1881729
MER†[1]	170Er	2B10C42	BioLegend	151502	13233030
CD80†[3]	171Yb	16-10A1	Fluidigm	3171008B	3001404
CD86†[3]	172Yb	GL1	Fluidigm	3172016B	3331708
CD116 (GM-CSF R) †[2]	173Yb	698423	R&D	MAB6130	CFEE0217121
Ly-6G/C (Gr-1) †[2]	174Yb	RB6-8C5	Fluidigm	3174008B	3181408
AXL†[3]	176Yb	MAB854	R&D	MAB854	JMT0218061
AXL†[3]	176Yb	MAB8541	R&D	MAB8541	HFY0118011
Intercalator (Ir)	191/193Ir	None	Fluidigm	201192B	2301702
Cisplatin	194Pt	None	Fluidigm	201194	
I-A/I-E†[2]	209Bi[3]	M5/114.15.2	Fluidigm	3209006B	2851707
CD16/32*†	None	93	eBiosciences	16-0161-85	4316711

3.1.1 Preparation of stock solutions

3.1.1.1 Cell Culture Medium

50 ml FBS, 5 ml L-glutamine, and 5 ml Penicillin-Streptomycin was diluted in 500 ml RPMI1640 in a sterile laminar airflow hood. The cell medium was stored at 4°C.

3.1.1.2 100x DNase I

10 ml DPBS was transferred to a 15 ml tube. 250 mg DNase I was transferred to the tube and dissolved. The 10 ml were aliquoted to and stored at -20°C.

3.1.1.3 10x PBS

2 PBS-tablets were dissolved in 40 ml MilliQ in a 50 ml tube. The solution was stored at 4 °C.

3.1.1.4 10x PBS (20 mM EDTA)

2 PBS-tablets and 297.8 mg EDTA was dissolved in 40 ml MilliQ in a 50 ml tube. The solution was stored at 4°C.

3.1.1.5   25x stock sodium azide (NaAz)

250 mg sodium azide was diluted in 50 ml MilliQ in a 50 ml tube and stored at 4°C.

3.1.1.6   Cell Washing Buffer (CWB)

5 g BSA, 48 ml DPBS, and 2 ml 25x NaAz was transferred to a 50 ml tube. After the BSA had dissolved the solution was passed through a 2 μm filter using a 30 ml syringe and stored at 4°C. At the day of use, thawed 100x DNase I was added in the ratio of 1:99.

3.1.1.1   2% PFA

1 ml 10x PBS (20mM EDTA) and 1.25 ml 16% PFA were diluted in 7.75 ml MilliQ in a 50 ml tube. The solution was passed through a 2 μm filter using a 30 ml syringe.

3.2   Mice

The following mouse experiment was approved by the Norwegian Food Safety Authority (Mattilsynet) and performed in accordance with Regulation on the use of animals in research. Mice were checked every 2-3 days before treatment start and daily thereafter.

BALB/c mice (n=50) were implanted with 4T1 breast cancer cells and treated with a control, bemcentinib, anti-CTLA-4 and anti-PD-1 (ICB), or a combination of bemcentinib and ICB. 40 of the 50 animals were divided into 8 equal sized groups by treatment and treatment duration. The 10 extra animals were needed to ensure the 8 groups were in similar stages of tumour growth, i.e. that the tumour volumes were similar, to be used as test samples for titration of antibodies, and to make a control sample to compare results across mass cytometry runs. Each cage contained 5 animals and was assigned a letter and a number based on treatment and treatment duration, as shown in Table 3.5. The extra animals were placed in cages E1 and E2. A timeline for the treatments and euthanasia is shown in Figure 3.1.

Table 3.5: Treatment and day of euthanasia for the different groups. Tissues were harvested immediately after euthanasia. Each group contains 5 animals.

Group	Oral gavage	Intraperitoneal injection	Euthanasia
A1	Vehicle	IgG	Day 15
A2	Vehicle	IgG	Day 22
B1	Bemcentinib	IgG	Day 15

B2	Bemcentinib	IgG	Day 22
C1	Vehicle	Anti CTLA-4 and anti PD-1	Day 15
C2	Vehicle	Anti CTLA-4 and anti PD-1	Day 22
D1	Bemcentinib	Anti CTLA-4 and anti PD-1	Day 15
D2	Bemcentinib	Anti CTLA-4 and anti PD-1	Day 22
E1	Vehicle	IgG	Day 15
E2	Vehicle	IgG	Day 22
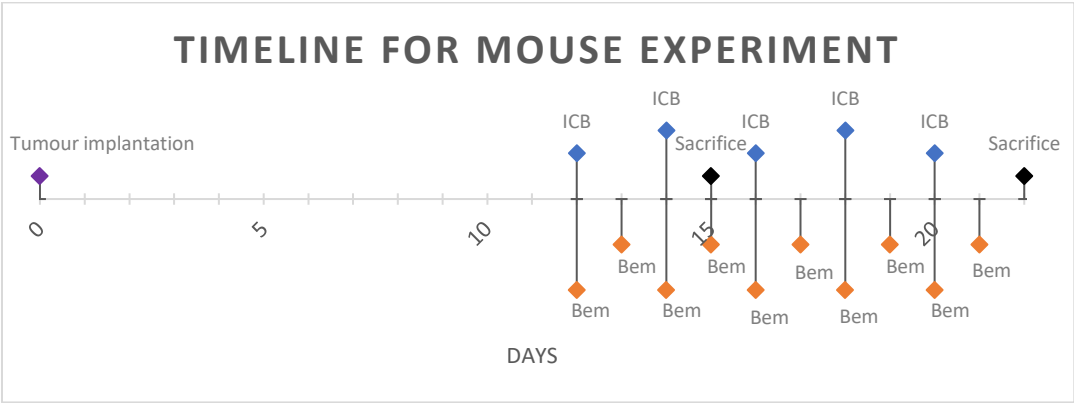
*Figure 3.1: **Timeline for mouse experiment.** Five groups were sacrificed 15 days after implantation (2 days of treatment) and five groups were sacrificed 22 days after implantation (10 days of treatment). Bem denotes treatment with bemcentinib and ICB (immune checkpoint blockade) denotes a combined treatment of anti-PD-1 and anti-CTLA-4. No treatments were given to the animals on the day they were euthanised.*

3.2.1 Cell Culture

Cells were always treated in a sterile laminar airflow hood with gloves and personal lab coat.

1 million 4T1 BALB/c breast cancer cells were seeded in a T75 flask (75 cm^2) and cultured in medium (10 ml, as made in 3.1.1.1) in an incubator (37°C, 5% CO_2, 21% O_2). Upon reaching 80-90% confluency, the cells were split into 2 T175 flasks with cell medium each containing 20 ml cell culture medium.

After reaching a final confluency of 80-90% in both flasks, medium was aspirated, and cells were washed with sterile PBS (10ml). The cells were thereafter trypsinised (5 ml, 5 min, 37°C)

for cell detachment, after which, medium (10ml) was added for quenching. The cells were then transferred to a 15 ml tube and centrifuged (290 g, 7 min, RT). Supernatant was aspirated, and the cells were resuspended in new medium and counted using the Countess Cell Counter. Medium was then discarded until only 12 million cells remained (200,000 cells per injection, thus 12 million cells equates to 60 injections). The cells were again centrifuged (290 g, 7 min, RT) and aspirated.

Cold serum-free RPMI1640 (2 ml) was mixed with Matrigel in a ratio of 1:1. The cells were resuspended in RPMI1640-Matrigel mix (3 ml) to a concentration of 4 million cells per ml. 1 ml syringes were drawn up with 0.3 ml each and left on ice until tumour implantation.

3.2.2 Tumour Implantation

Each animal was anaesthetised by Sevoflurane and after reaching sufficient unconsciousness, the mice were weighed and placed back in anaesthesia in a cuff and shaved. To remove residual hair, Veet Hair Removal Cream was applied to the shaven area and swiftly removed with a wet tissue paper RPMI1640-Matrigel mix (0.05 ml, 200,000 cells) was injected into the fourth mammary fat pad on right side of the mouse using a 1 ml syringe with a 30-gauge needle.

3.2.3 Preparation of Treatments

Vehicle (water with 0.1% w/w TWEEN 80 and 0.5% w/w hydroxypropyl methylcellulose) was prepared by BerGenBio. To make the stock bemcentinib solution, vehicle was mixed with bemcentinib powder (10 mg/ml), vortexed, and sonicated for 15 min. The stock was then diluted with vehicle (5 mg/ml) to a dosing suspension. The same dose volume of bemcentinib was used for the vehicle-only treatments.

The anti-mCTLA-4 and anti-mPD-1, comprising the Immune therapy blockade (ICB), were individually diluted with sterile PBS to a concentration of 2 mg/ml. A dose of 10 mg/kg was used for each mouse. For the control antibody, hamster IgG, a lower dose and a higher concentration was used to equalise the volume and amount of antibodies injected with the ICB treatment. The treatments with doses and volumes are summarized in Table 3.6.

Table 3.6: Concentrations and volumes used for drugging mice.

Treatment	Dose concentration [mg/kg]	Drug concentration [mg/ml]	Dose volume [µl/g]
Bemcentinib	50	5	10
Anti-mCTLA-4	10	2	5
Anti-mPD-1	10	2	5
Hamster IgG	20	1	10
Vehicle	NA	NA	10

Injection volumes were calculated as follows:

$$V = W_{mouse} * \frac{C_{dose}}{C_{drug}}$$

V is volume to be injected, W is the weight of the mouse, C_{dose} is the concentration of the dose [mg/kg], and C_{drug} is the concentration of the drug [mg/ml].

Below, a case of for mouse of 25 grams treated with bemcentinib is exemplified:

$$V_{Bemcentinib} = 0.025 \, kg * \frac{50 \frac{mg}{kg}}{5 \frac{mg}{ml}} = 0.250 \, ml$$

Thus, a total volume of 250 µl is to be injected by oral gavage.

3.2.4 Randomisation and Treatments

After the mice had developed tumours with volumes[1] ranging from 50 mm^3 to 100 mm^3 and aged beyond 8 weeks, they were randomised into ten cages (5 mice per cage) consisting of five treatment groups and two endpoints, by sorting by weight and using Latin Square design. At the day of randomisation, treatment was also initiated.

---

[1] The tumour volume is calculated using the formula $V = \frac{a*b^2}{2} \, mm^3$, where a and b are the long and short diameter of the tumour respectively.

Bemcentinib and ICB were prepared as stated in section 3.2.3. Prior to each injection the weight of the mouse was recorded and used to calculate injection volume, as stated also in section 3.2.3. The treatments for the groups are displayed in Table 3.5.

ICB treatment was given intraperitoneally every other day while bemcentinib and vehicle was given by oral gavage twice a day.

3.2.5   Tissue Collection

Mice were euthanised at two different timepoints as shown in Table 3.5 and Figure 3.1. The mice were first anesthetized with Sevoflurane before being euthanised with cardiac puncture followed by cervical dislocation. After euthanasia, tumour and spleen tissue was collected and temporarily stored on ice in a 15ml tube with MACS Tissue Storage Solution.

3.3   Sample Preparation

Samples were provided as written in section 3.2.5. Sample preparation has been divided into two parts: tissue dissociation to make single cell suspensions and the treatment of the single cells until running them on the mass cytometer.

All centrifugation steps were completed on a Centrifuge 5810 R (Eppendorf) with a Swing-Bucket rotor.

3.3.1   Tissue Dissociation

3.3.1.1   Tumour Dissociation

For tumour tissue dissociation the Tumor Dissociation Kit, mouse (Miltenyi) was used along with the supplied protocol. Briefly, for each tumour, a digestion enzyme mix was made by mixing RPMI1640 (2350 µl), Enzyme D (100 µl), Enzyme R (50 µl) and Enzyme A (12.5 µl) in a C-tube. The tumour was cut in small pieces, transferred to the C-tube and run on the gentleMACS Dissociator (Miltenyi) with the m_impTumor_02 program before being incubated on a tumble wheel in an incubator (40 min, 37°C). The C-tube was again run on the dissociator with the program m_impTumor_03 twice, followed by m_impTumor_01 once. The sample was then strained through a 70 µm filter on a 50 ml tube. The filter was washed with RPMI1640 (10 ml) before again straining the sample through a 40 µm filter into the same tube. The filter was washed with RPMI1640 (10 ml). The sample was then centrifuged (200 g, 7 min, RT) and supernatant was aspirated. The cells were resuspended in PBS, transferred to a PP-tube (15

ml) and centrifuged (200 g, 7 min, RT). Supernatant was again aspirated, and the cells were resuspended in PBS (500 µl) and 1x RBCL (5 ml), made from Red Blood Cell Lysis Solution (10×) diluted in MilliQ, and incubated (2 min, RT). The sample was centrifuged (200g, 10 min, RT) and supernatant aspirated.

3.3.1.2   Spleen Dissociation

For spleen tissue dissociation the Spleen Dissociation Kit, mouse (Miltenyi) was used along with the supplied protocol. Briefly, for each spleen, a digestion enzyme mix was made by mixing Buffer S (2.4 ml), Enzyme D (50 µl), and Enzyme A (15 µl) in a C-tube. The spleen was transferred whole to the C-tube and run on the gentleMACS Dissociator (Miltenyi) with the m_spleen_02 program before being incubated in a tumble wheel for 15 min at 37°C. The C-tube was then run on the dissociator with the program m_spleen_03, before being strained through a 30 µm filter on a 15 ml tube. The filter is washed with 1x Buffer S (2.5 ml). The sample was then centrifuged (200 g, 10 min, RT) and supernatant was aspirated. The cells were resuspended in PBS (500 µl) and 1x RBCL (5 ml), made from Red Blood Cell Lysis Solution (10×) diluted in MilliQ, and incubated (2 min, RT). The sample was centrifuged (200g, 10 min, RT) and supernatant aspirated.

3.3.1.3   Live Dead Staining

After having prepared the samples as stated in section 3.3.1, the cells were resuspended in RPMI1640 (5 ml, 10% FBS, 0.25 µM cisplatin) and mixed by inverting the tube. The sample was incubated (5 min, RT) before being quenched by the addition of RPMI1640 (5ml, 10% FBS). The sample was then centrifuged (200 g, 6 min, RT). Supernatant was aspirated, and cells transferred to a Cryotube (1.8 ml) with RPMI1640 (900 µl). The sample was fixed for 10 min by the addition of PFA (100µl, 16%) before centrifugation (900 g, 5 min, RT). Supernatant was aspirated, and the tube frozen to -80°C.

3.3.2   Antibody Conjugation and Titration

3.3.2.1   Antibody Conjugation

Antibody conjugation was performed using Maxpar Antibody Labeling Kit, containing all the necessary solutions except TCEP and Antibody stabiliser, with the supplied protocol. Briefly, the MAXPAR polymer was thawed and mixed with L-buffer (95 µl) and lanthanide ion solution (5 µl). The tube containing the polymer was placed in a heating block (30 min, 37 °C). The

concentration of the antibody to be conjugated was measured on a NanoDrop (2000/2000c , Thermo Scientific). A calculated volume (100 µg antibody) was transferred to the 50 kDa filter with additional R-buffer to get a total volume of 0.5 ml and centrifuged (12 000 g, 10 min, RT). A TCEP-R-buffer solution was prepared by diluting TCEP (8 µl, 0.5 M) in R-buffer (992 µl). Flow through from the antibody centrifugation was discarded and the antibody was resuspended in TCEP-R-buffer (100 µl) and incubated in a heating block (30 min, 37 °C). The lanthanide polymer was transferred to the 3 kDa filter and diluted in additional L-buffer (200 µl) and centrifuged (12 000 g, 25 min, RT). Flow through was discarded and the polymer was washed again in C-buffer (400 µl) and centrifuged (12 000 g, 30 min, RT). C- buffer (300 µl) was added to the 50 kDa filter with the antibody before the antibody was centrifuged (12 000 g, 10 min, RT). The flow through from the antibodies was discarded and the wash repeated with C-buffer (400 µl) and centrifugation (12 000 g, 10 min, RT). The flow through from both the polymer and the antibodies was discarded.

C-buffer (60 µl) was added to the 5 kDa filter with the polymer and used to transfer the polymer to the 50 kDa filter containing the antibodies. The 50 kDa filter now containing both the polymers and the antibodies was placed in a heating block (90 min, 37 °C).

W-buffer (200 µl) was added to the 50 kDa filter before being centrifuged (12 000 g, 10 min). Flow through was discarded and the wash repeated three times, for a total of four, with W-buffer (400 µl). After discarding the flow through, the antibody concentration was measured on the Nanodrop. The measured concentration was used to calculate the volume of Antibody Stabilizer needed for diluting the antibody to 0.5 mg/ml. The 50 kDa filter was centrifuged (12 000 g, 10 min, RT) and the calculated volume of Antibody Stabilizer was added to the filter. The filter was then transferred to a new tube and placed upside down for collection of the antibody during centrifugation (1 000 g, 2 min, RT). The conjugated antibody was then stored at 4 °C in the dark.

3.3.2.2 Antibody Titration

The complete antibody panel was divided into three backbones (see Table 3.4), so that the canonical markers were titrated first, and markers on subpopulations of the canonical markers were titrated next. For each backbone, about 3 million cells from a spleen sample was divided into six tubes and barcoded. The samples were then stained with a serial dilution of the antibody backbone cocktail, except for the last tube which was left unstained. All samples

were then combined in a tube. The samples were run on the mass cytometer and, ±1 spill, +16 spill, and separation between positive and negative populations were analysed and used to determine the best titration for each antibody.

3.3.3 Cell Staining

Each sample was divided into 6 groups as shown in Table 3.7. Each of the groups contains 20 samples and was stained and run at the mass cytometer at the same time. The extra test samples from the E-group were used for titrating antibodies and making a control spleen sample to be included in every run.

Table 3.7: All single cell suspension samples from section 3.3.1.3 were divided into five groups based on tissue, treatment group and treatment duration. Each cell designates an animal characterised by the treatment group (first letter), the treatment duration (first number before the dash) and mouse number in the given cage (the last number).

Tumour T1	Tumour T2	Spleen T1	Spleen T2	Test tumour	Test spleen
A1-1	A2-1	A1-1	A2-1	E1-1	E1-1
A1-2	A2-2	A1-2	A2-2	E1-2	E1-2
A1-3	A2-3	A1-3	A2-3	E1-3	E1-3
A1-4	A2-4	A1-4	A2-4	E1-4	E1-4
A1-5	A2-5	A1-5	A2-5	E1-5	E1-5
B1-1	B2-1	B1-1	B2-1	E2-1	E2-1
B1-2	B2-2	B1-2	B2-2	E2-2	E2-2
B1-3	B2-3	B1-3	B2-3	E2-3	E2-3
B1-4	B2-4	B1-4	B2-4	E2-4	E2-4
B1-5	B2-5	B1-5	B2-5	E2-5	E2-5
C1-1	C2-1	C1-1	C2-1		
C1-2	C2-2	C1-2	C2-2		
C1-3	C2-3	C1-3	C2-3		
C1-4	C2-4	C1-4	C2-4		
C1-5	C2-5	C1-5	C2-5		
D1-1	D2-1	D1-1	D2-1		
D1-2	D2-2	D1-2	D2-2		
D1-3	D2-3	D1-3	D2-3		
D1-4	D2-4	D1-4	D2-4		
D1-5	D2-5	D1-5	D2-5		
Control	Control	Control	Control		

3.3.3.1 Barcode Staining

All centrifugation steps were performed with swing-bucket rotor at 900 g for 5 min in RT.

The samples from section 3.3.1.3 were divided into four groups based on tissue and treatment endpoint. A sample control made from a mix of spleen samples from the E-group was included in each mass cytometry run.

Each sample was thawed and resuspended in DPBS (500 µl) with 1x DNase I. A small sample of about 10 µl was used the estimate cell count in the tube. Based on the cell count, at least 3 million cells were transferred to a new 5 ml tube. Additional cell washing buffer (CWB) was subsequently added to give a final volume of 1 ml. The sample was then vortexed, centrifuged, and subsequently decanted.

Perm buffer was prepared by diluting 10x perm buffer (5ml, Fluidigm) with 10x PBS (5 ml) and Milli-Q (40 ml). The sample was washed with perm buffer (1 ml), centrifuged, and subsequently decanted. This washing step was performed twice, except aspirating to remove supernatant the second time.

For the control sample: rhodium intercalator (1µl, 500µM) was mixed with perm buffer (200µl). The control sample cells were resuspended in the rhodium intercalator mix and incubated (30 min, RT).

For non-control samples: the samples were put on ice and when ice cold, ice cold perm buffer (195 µl) was mixed with barcode solution (5 µl, Fluidigm) and swiftly used to resuspend the cells by pipetting. The cells were incubated (30 min, RT).

After incubation, CWB (800 µl) was transferred to the tubes before being centrifuged and subsequently decanted. The cells were resuspended with CWB (1 ml), vortexed and incubated (10 min, RT) before being centrifuged and supernatant aspirated. Each sample was resuspended in CWB (100 µl) and grouped in a 5 ml tube. CWB (100 µl) was added to each sample tube to transfer any remaining cells to the grouped 5 ml tube. The grouped samples were centrifuged and subsequently decanted before being washed with CSM (4 ml, Cell staining medium). After centrifugation the tube was decanted and put on ice.

3.3.3.2   Marker Staining

All centrifugation steps were performed with swing-bucket rotor at 900 g for 5 min in RT., except where other settings are noted.

Fc-block (anti-CD16/32) was diluted in CSM in a ratio of 1:199. The cells from section 3.3.3.1 were resuspended in diluted Fc-block (35 µl per 3 million cells) and incubated (10 min, on ice). All antibodies (see Table 3.4) were vortexed, centrifuged (10,000 g, 5 min, RT) and put on ice. Titrated amounts of each surface antibody (see Table 10.1) were mixed with CSM to give a total volume of 40 µl per 3 million cells. The antibody cocktail was mixed with the sample and incubated (30 min, RT). After incubation, the sample was centrifuged, aspirated and resuspended and incubated in DPBS (4 ml) with 1x DNase I for 10 min. The sample was then centrifuged and subsequently resuspended in PBS (4ml, 2 mM EDTA), centrifuged, and decanted.

200 µl 2% PFA per 3 million cells was used to resuspend the sample. The sample was then incubated (30 min, RT, in the dark) before being centrifuged (900g, 5 min, RT), and supernatant aspirated. The sample was then resuspended in CSM/perm (2ml, 10% 10x perm buffer), centrifuged, and decanted. This washing procedure was repeated once for a total of two times. Fc-block (anti-CD16/32) was diluted in CSM/perm in a ratio of 1:199. The sampel was then resuspended in diluted Fc-block (35 µl per 3 million cells) and incubated (10 min, on ice).

Titrated amounts of each intracellular antibody (see Table 10.1) were mixed with CSM/perm to give a total volume of 40 µl per 3 million cells. The antibody cocktail was mixed with the sample and incubated (30 min, RT). After incubation, the sample was centrifuged, aspirated and resuspended and incubated in CWB (4 ml, 10 min, RT). The sample was then centrifuged and subsequently resuspended in PBS (4ml, 2 mM EDTA), centrifuged, and decanted.

3.3.3.3   DNA-Staining, Water Washes and Data Aquisition

Iridium intercalator (0.33 µl per 20,000,000 cells, 500 µM) was mixed with 2% PFA (1 ml per 20,000,000 cells). The cells were incubated at 4°C overnight.

The sample was centrifuged (900 g, 5 min, RT), and supernatant was aspirated. CWB (2 ml) was used to resuspend the cells. The sample was incubated (10 min, RT) then centrifuged (900 g, 5 min, RT). The sample was finally resuspended in PBS (2ml, 2 mM EDTA) and put on ice.

Before running the sample on the mass cytometer, the sample was washed in MilliQ. This was done by transferring 200 µl (roughly one million cells) of the sample to a new 5 ml tube and filling it with MilliQ (4 ml). The tube was inverted for mixing, centrifuged (400 g, 5 min, RT), and subsequently decanted. This washing step was repeated 3 times for a total of 4 washes.

Finally, the cells were resuspended in about 0.75 ml 1x bead solution to a final concentration of about 1-2 million cells per ml, pushed through a 40 µm filter and acquired on the mass cytometer. During acquisition a rain plot showing the amount of each isotope detected in each push can be studied to identify contaminations (see Figure 3.2).
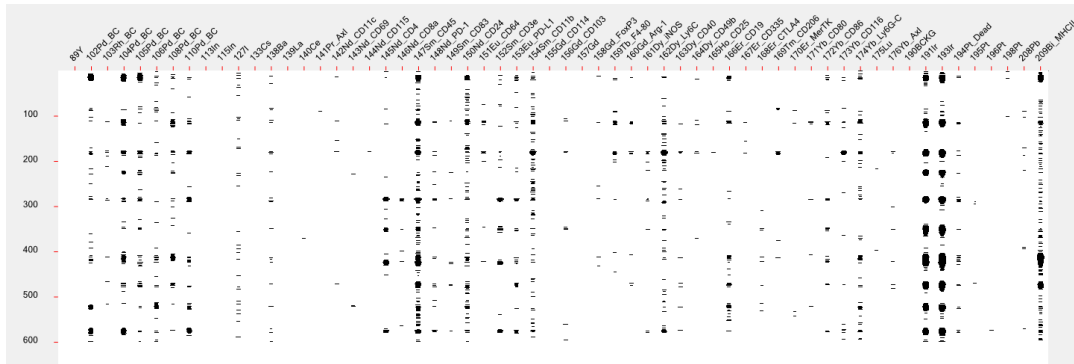
*Figure 3.2: **A mass cytometry rainplot.** A rain plot showing measured isotopes (columns) in each push (rows). Pushes containing cells can be identified by finding the pushes with high amounts of iridium 191 and 193. Some background of 147Sm and 209Bi can be identified by comparing the intensity between cells.*

For each timepoint, approximately 10 million events were collected from the spleen samples and 14-15 million events from the tumour samples.

The mass cytometry was performed using the Helios at the Flow Cytometry Core Facility, Department of Clinical Science, University of Bergen.

3.4   Data Analysis

3.4.1   Pre-gating

3.4.1.1   Normalisation

Samples were normalised with the Fluidigm CyTOF software (version 6.7.1014). The median bead intensity was used on a sliding window of 200 seconds. After normalisation, the files were concatenated and randomised. The values above 0 were randomised using a gaussian distribution with a sigma of 1, while zero-values were randomised with a sigma of 1 and a half-zero randomisation power parameter of -0.5.

3.4.1.2   Debarcoding

Normalised events were debarcoded using Fluidigm CyTOF software (version 6.7.1014). The separation cut-off and the Mahalanobis distance were manually adjusted for each mass

cytometry run. The signal intensity cut-off was used for the tumour sample, but not used for the spleen samples. A typical debarcoding result is shown in Figure 3.3.
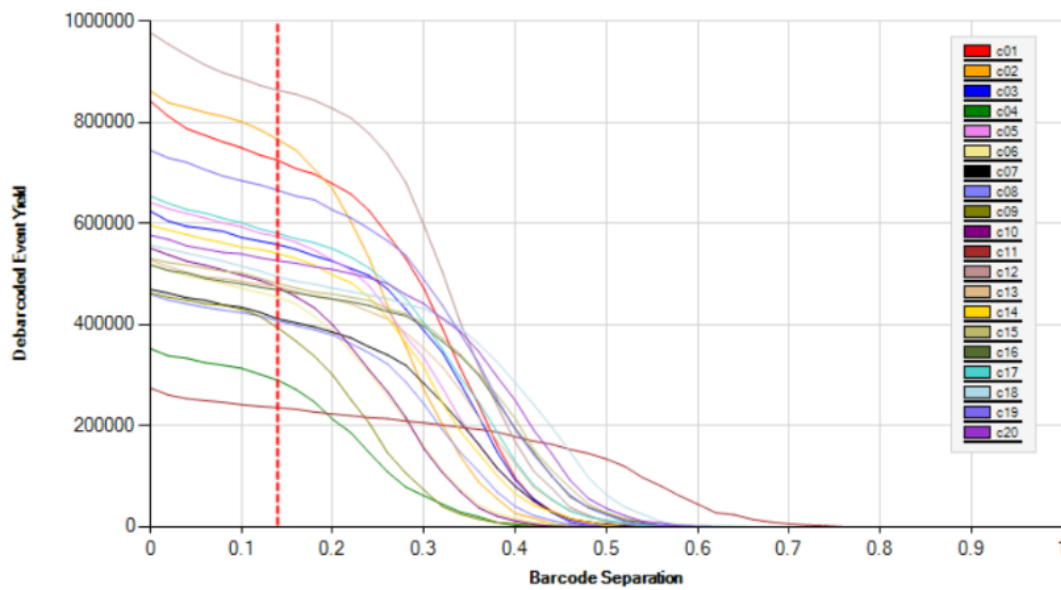
*Figure 3.3: **Debarcoding yields.** Debarcoding of the first tumour run, containing 20 sample and 1 control (unassigned). A separation threshold of 0.14 was used in this case for debarcoding. Due to differing amount of cells during barcoding, the optimal barcode separation threshold varies across sampels.*

3.4.1.3   Gating

Before gating, an arcsinh transformation with the argument of 2 was applied on all marker channels. The general gating strategy is summarised in Figure 3.4. The process starts with removal of 140Ce positive beads and then uses the gaussian parameters to select single ions clouds. Live single cloud events are then selected by excluding 194Pt high events. Single immune cells are selected by CD45 and based on 103Rh staining the cells are characterised as controls or normal samples.
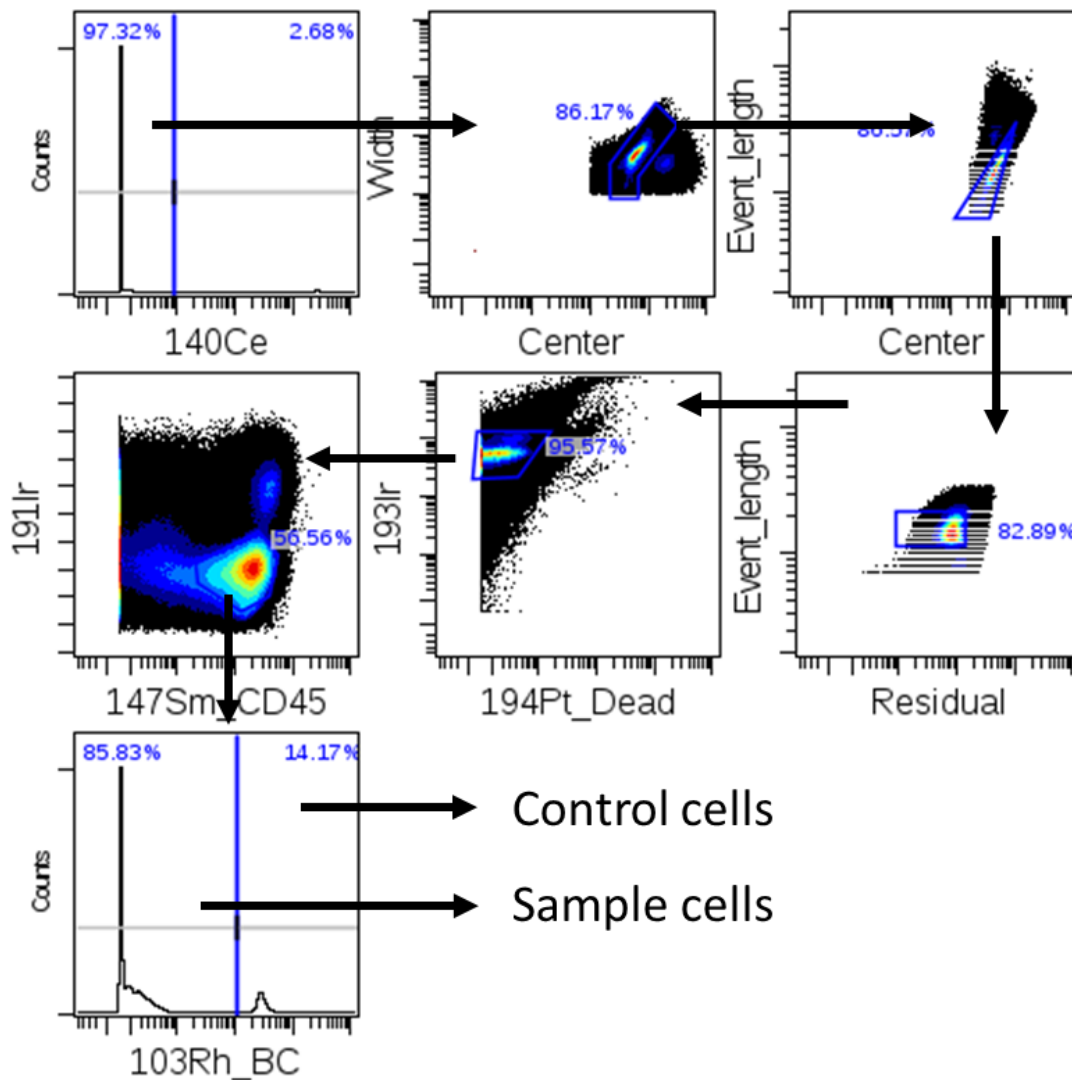
*Figure 3.4: **Manual gating strategy.** Gating strategy to select single immune cells for the samples and the control.*

3.4.2 Clustering and Dimensionality Reduction

After gating out single immune cells, each file in each mass cytometry run was subsampled equally. The spleen samples were randomly subsampled to 20 000 cells per file, and the tumour samples were subsampled to 23 809 cells per file. Phenograph clustering was run on tissue and timepoints separately with a k=30. The Phenograph algorithm was run on R (version 3.5.1) using the R implementation of Phenograph [72] and *flowCore* [74]. Phenograph plots were made using cytofkit [75].

The tSNE algorithm was run separately on each of the four phenograph clustering analyses using the viSNE implementation in Cytobank.

Markers used during clustering and dimensionality reduction are summarised in Table 3.8. FOXP3 was excluded from clustering and dimensionality reduction due to improper staining.

Table 3.8: Markers used during dimensionality reduction and clustering. FOXP3 was not used due to not staining any T cells.

Marker	Mass tag	tSNE	Clustering
Intercalator (Rh)	103Rh	No	No
CD11c†[1]	142Nd	Yes	Yes
CD69†[3]	143Nd	Yes	Yes
CD115†[2]	144Nd	Yes	Yes
CD4†[2]	145Nd	Yes	Yes
CD8a†[2]	146Nd	Yes	Yes
CD45†[1]	147Sm	Yes	Yes
PD-1 (CD279)†[2]	148Nd	Yes	Yes
CD83†[3]	149Sm	Yes	Yes
CD24†[3]	150Nd	Yes	Yes
CD64†[1]	151Eu	Yes	Yes
CD3e†[1]	152Sm	Yes	Yes
PD-L1 (CD274)†[1]	153Eu	Yes	Yes
CD11b†[1]	154Sm	Yes	Yes
CD114†[2]	155Gd	Yes	Yes
CD103†[3]	156Gd	Yes	Yes
FOXP3*[3]	158Gd	No	No
FOXP3*[3]	158Gd	No	No
F4/80†[2]	159Tb	Yes	Yes
ARGINASE 1*[3]	160Gd	Yes	Yes
iNOS*[3]	161Dy	Yes	Yes
Ly-6C†[2]	162Dy	Yes	Yes
CD40†[3]	163Dy	Yes	Yes
CD49b†[1]	164Dy	Yes	Yes
CD25†[3]	165Ho	Yes	Yes
CD19†[1]	166Er	Yes	Yes
CD335 (NKp46) †[1]	167Er	Yes	Yes
CTLA-4 (CD152) †[2]	168Er	Yes	Yes
CD206†[3]	169Tm	Yes	Yes
MER†[1]	170Er	Yes	Yes
CD80†[3]	171Yb	Yes	Yes
CD86†[3]	172Yb	Yes	Yes
CD116 (GM-CSF R) †[2]	173Yb	Yes	Yes
Ly-6G/C (Gr-1) †[2]	174Yb	Yes	Yes
AXL†[3]	176Yb	Yes	Yes
AXL†[3]	176Yb	Yes	Yes
Intercalator (Ir)	191/193Ir	No	No

Cisplatin	194Pt	No	No
I-A/I-E†[2]	209Bi[3]	Yes	Yes

3.4.3 Cluster Characterisation

To characterise each cluster and make heatplots, the R-package MEM [76] was used, with the remaining clusters acting as reference.

3.4.4 Statistical Analysis

Each of the four Phenograph clustering analyses were analysed separately by running a two-way factorial ANOVA, with bemcentinib and ICB as two-level factors, to compare each cluster across treatments. The false discovery rate was controlled for each Phenograph analysis at 5% using the Benjamini-Hochber method.

A two-way analysis of variance (ANOVA) was conducted on the influence of two independent variables (Bemcentinib treatment, ICB treatment) on the number of cells in each cluster. Both bemcentinib and ICB treatment included two levels, (yes, no). The ANOVA was conducted in R, using the manova function in "stats" (version 3.5.1) with the formula "clusters ~ bemcentinib*ICB". P-value correction and calculation of means for cluster sizes was performed in GraphPad Prism 8.0. Circle diagrams, representing number of cells in each cluster, was made using Excel.

The following analyses were also performed in GraphPad Prism 8.0. Cluster sizes were analysed with multiple linear regression against tumour and spleen weight. A three-way ANOVA was performed using tumour size across treatments and time as factors. The same analysis was also used on spleen size and tumour weight. Spleen weight and tumour weight was correlated using linear regression.

3.4.5 Phenotyping

The following scheme was used in phenotyping:

T helper cells	$CD3^+CD4^+$
Cytotoxic T cells	$CD3^+CD8^+$
B cells	$CD19^+I-A/I-E^+$
NK cells	$CD335^+$

Dendritic cells	I-A/I-E$^+$CD11c$^+$CD11b$^-$
Tumour associated macrophage type 1	iNOS$^+$CD11b$^+$
Tumour associated macrophage type 2	CD206$^+$CD11b$^+$
Myeloid derived suppressor cells	Ly6G/C$^+$CD11b$^+$

4 Results

4.1 Spleen and Tumour Weight

4.1.1 Tumour Volume

The study by Davidsen et al. shown in section 1.3.3 analysing the combination of ICB and bemcentinib used tumour volume of as endpoint. To analyse if the same effect was observed in this study, a three-way ANOVA was performed with the independent factors bemcentinib, ICB, and time (see Table 4.1) and tumour volume as the dependent variable. The ANOVA reported statistically significant main effects from ICB treatment and time. In addition, an interaction effect between ICB and time was statistically significant. By analysing the means for the different treatment groups (plotted in Figure 4.1 and shown in Table 10.2) it is evident that the time effect is associated with an increase of tumour volume, while ICB is associated with a decrease mainly in the second timepoint.

Table 4.1: ANOVA on tumour volume. A three-way ANOVA with time, bemcentinib-treatment, and ICB-treatment as factors. The P-values are not adjusted. Interactions are indicated with a colon.

Source of variation	% of total variation	P value	Statistically significant?
Time	43.83	<0.0001	Yes
ICBs	11.20	0.0016	Yes
Bem	0.004298	0.9466	No
Time:ICB	10.85	0.0019	Yes
Time:Bem	1.046	0.3000	No
ICB:Bem	1.741	0.1836	No
Time:ICB:Bem	1.173	0.2729	No
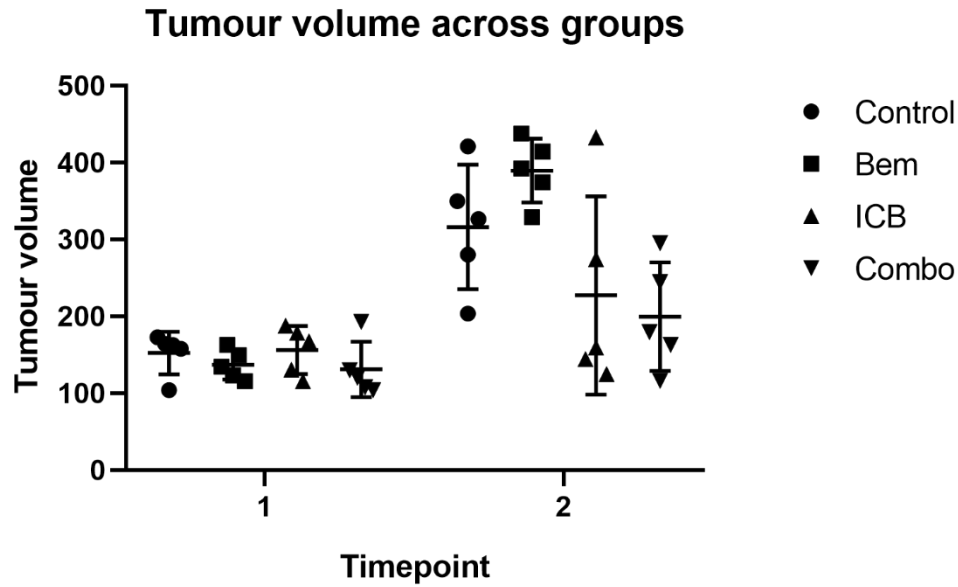
*Figure 4.1: **Tumour volume across treatment groups.** Tumour volume measured in [mm³] across groups. Error bars show standard deviation.*

4.1.2 Spleen and Tumour Weight

An interesting pathological development from the 4T1 breast cancer cell line is splenomegaly (enlarged spleen). A Pearson correlation performed on spleen and tumour weight resulted in a positive correlation (r = 0.8559, p<0.0001, n=40). A linear regression of spleen and tumour weight is shown in Figure 4.2.
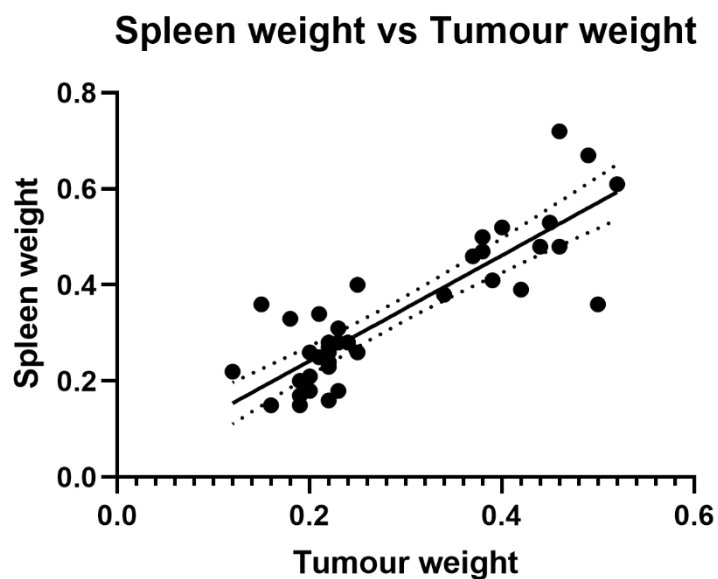
Figure 4.2: **Spleen weight vs tumour weight correlation plot.** Spleen weight [gram] is plotted against tumour weight [gram] with a fitted line and a 95% confidence interval (dotted lines).

A three-way ANOVA conducted on the influence of three independent variables (Bemcentinib treatment, ICB treatment, and time) on spleen weight resulted in statistically significant main effects from bemcentinib treatment and statistically significant interaction effects between time and ICB, and time and bemcentinib (see Table 4.2). The interaction effect between bemcentinib and ICB is nonsignificant. This indicates that the combination group should see the greatest effect on spleen weight. Indeed, this is the case as shown in Figure 4.3.

Table 4.2: ANOVA on spleen weight. Results from running a three-way ANOVA with time, bemcentinib-treatment, and ICB-treatment as factors. The P-values are not adjusted. Interactions are indicated with a colon.

Source of Variation	% of total variation	P value	Statistically significant?
Time	62.34	<0.0001	Yes
ICB	1.563	0.0511	No
Bemcentinib	3.234	0.0065	Yes
Time:ICB	15.92	<0.0001	Yes
Time: bemcentinib	4.015	0.0027	Yes
ICB: bemcentinib	0.2467	0.4268	No
Time:ICB: bemcentinib	0.4931	0.2636	No

A one-tailed t-test resulted in a statistically significant difference (p=0.0481) between group treated with ICB only and the group treated with a combination of bemcentinib and ICB.
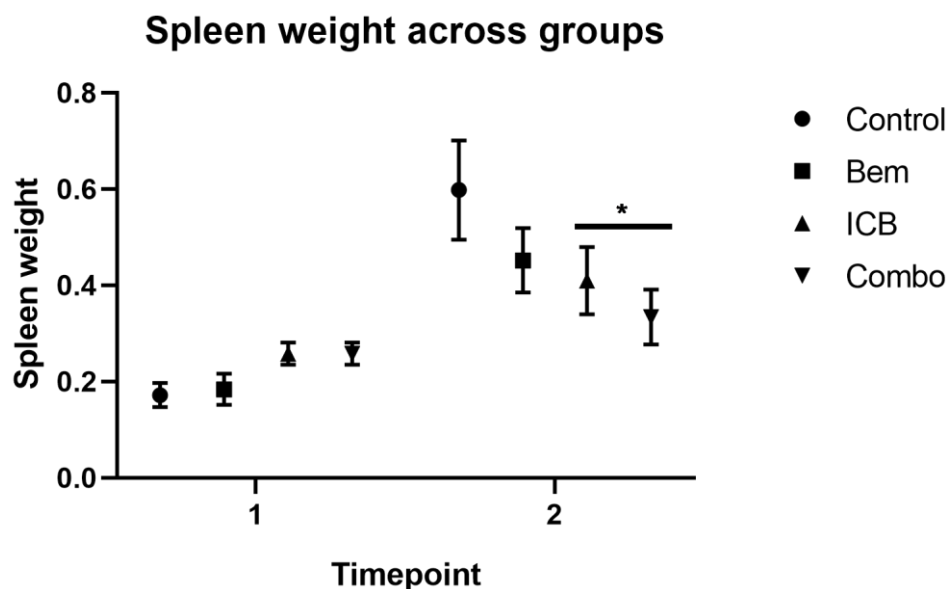
*Figure 4.3: **Spleen weight across treatment groups.** Spleen weight measured in [gram] across groups. Error bars show standard deviation. An independent one-tailed t-test comparing combo with ICB in timepoint 2 resulted in a p value of 0.0481.*

4.2   Mass Cytometry on Spleen

4.2.1   Timepoint 1

Clusters found after running Phenograph on the spleen from timepoint 1 samples are shown in Figure 4.4. The clusters were further analysed with MEM to find cluster characteristic markers. Cluster cell numbers for each spleen sample was used to draw circles indicating the mean cluster size in each group. An extended table with means and standard deviations for every cluster in every group is presented in Table 10.3. An additional heatmap of median marker values for each cluster if presented in Figure 10.1. Finally, a two-way ANOVA with the independent variables bemcentinib treatment and ICB treatment was performed on the dependent variable cluster size. Cluster size indicates the number of cells in a given cluster. An extended table containing a summary of each ANOVA performed is presented in Table 10.4.

*Figure 4.4: **Spleen timepoint 1 MEM heatmap and cluster statistics.** Clusters are shown as rows and markers as columns. Circles on the right side correspond to cell number in the treatment groups after equal subsampling. Statistical significance from ANOVAs performed with two independent variables (Bemcentinib treatment and ICB-treatment) on each cluster size is shown on the right. P-values adjusted with Bemjamini-Holberg are shown as ns (p > 0.05), * (0.05 > p), ** (0.01 > p), or *** (0.001 > p). Main cell phenotypes have been characterised at the far right.*

The ICB treatment shows a statistically significant decrease in a CD103$^-$ T helper cells subset (cluster 2), an increase in CD103$^+$ T helper cells subset (cluster 21) and cytotoxic T cells (cluster 8), but no significant change is found in NK cells. Two B cell subsets (cluster 6 and 14) were found to increase when treated with ICB and DCs (cluster 14) were found to slightly decrease with bemcentinib. No statistically significant change was found for TAM1 cells in either treatment. For type 2 (cluster 16), however, a statistically significant main effect was found for ICB showing an increase. Lastly, ICB was found to increase the number of cells in a MDSCs subset (cluster 7).

4.2.2   Timepoint 2

Clusters found after running Phenograph on the spleen samples from timepoint 2 are shown in Figure 4.5. The clusters were further analysed with MEM to find cluster characteristic markers. Cluster cell numbers for each spleen sample was used to draw circles indicating the mean cluster size in each group. An extended table with means and standard deviations for every cluster in every group is presented in Table 10.5. An additional heatmap of median marker values for each cluster if presented in Figure 10.2. Finally, a two-way ANOVA with the independent variables bemcentinib treatment and ICB treatment was performed on the dependent variable cluster size. Cluster size indicates the number of cells in a given cluster. An extended table containing a summary of each ANOVA performed is presented in Table 10.6.

*Figure 4.5: **Spleen timepoint 2 MEM heatmap and cluster statistics**. Each row is a cluster and each column is a marker. Circles on the right side correspond to cell number in the treatment groups after equal subsampling. Thus, it represents the proportional distribution of cells. The statistical results from a two-way ANOVA comparing the two treatments is shown on the right. P-values adjusted with Bemjamini-Holberg are indicated by ns (p > 0.05), * (0.05 > p), ** (0.01 > p), *** (0.001 > p). Main cell phenotypes have been characterised at the far right.*

Similar to timepoint 1, ICB treatment shows a statistically significant increase in a CD103+ T helper cell subset (cluster 11). An increase of the combo group is also shown in the second T helper cell subset (cluster 6), but it was not found statistically significant. Unadjusted p-values were just at the limit of significance for both ICB and bemcentinib (see Table 10.3).

No statistically significant change is found for cytotoxic T cells (cluster 8) and NK cells (cluster 13). For a small subset of CD24+ B cells (cluster 1) the number of cells were reduced by treatment of ICB. Both treatments were found to affect the number of DCs, however, the effects were opposite. While bemcentinib decreases the number of DCs, ICB treatment increases it (cluster 18). Since no statistically significant interaction was found between

bemcentinib and ICB treatment and the effects seem to cancel each other out during combination (see Table 10.5). For the TAM1 (cluster 17) cells no significant change was found in either treatment. For type 2 however, bemcentinib (cluster 7) treatment was found lead to a reduction. No statistically significant effect on MDSCs was found in either treatment (cluster 3, 19, 21), however, it is worth reporting that cluster 3, with an unadjusted p-value of 0.01 for an interaction effect between ICB and bemcentinib, shows a 25% reduction in the combination group compared to the control group, and a 50% reduction compared to the ICB treated group. Lastly, an unidentified phenotype $CD11b^+CD24^+F4/80^+AXL^+CD11c^+$ population (cluster 20) was found to be decrease by with ICB-treatment.

4.2.3   Axl staining and density

To visualise the distribution of AXL in the immune landscape, cells were plotted using calculated tSNE parameters. The clusters from Phenograph are overlaid in Figure 4.6 and Figure 4.7 for timepoint 1 and 2 respectively. tSNEs showing AXL expression for timepoint 1 and 2 are shown in Figure 4.8 and tSNEs showing density are in Figure 4.9.
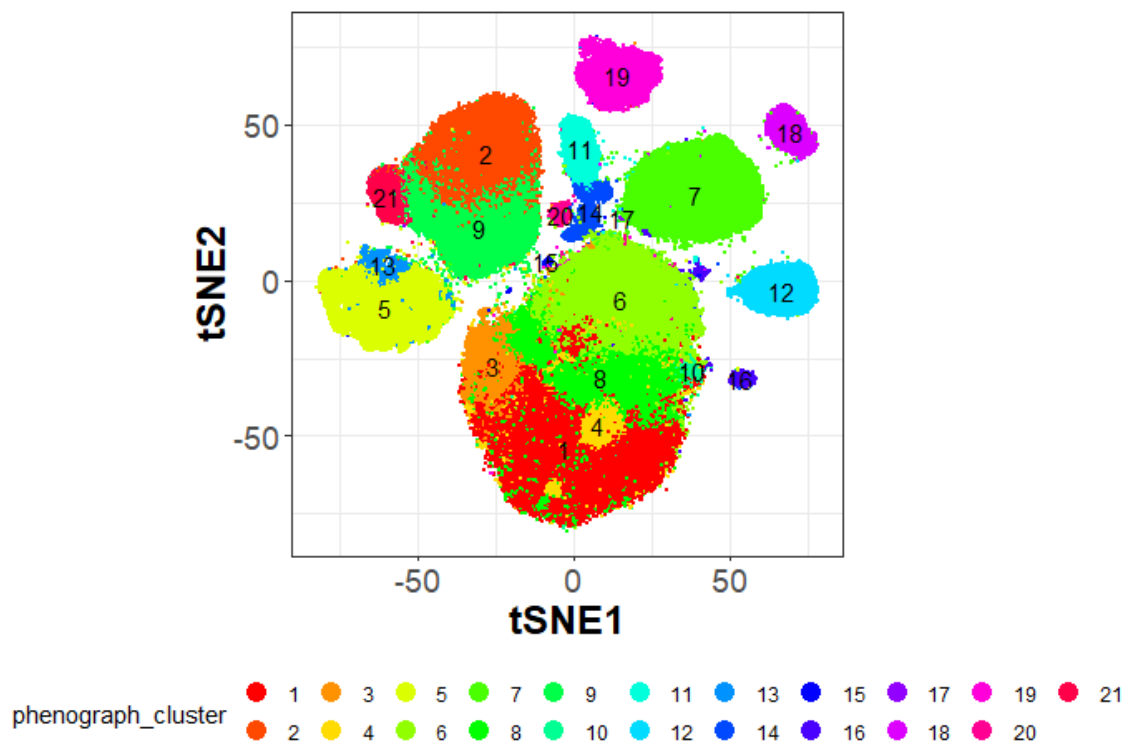
*Figure 4.6:**Spleen timepoint 1 Phenograph clusters overlaid on viSNE.**
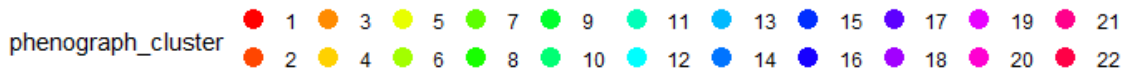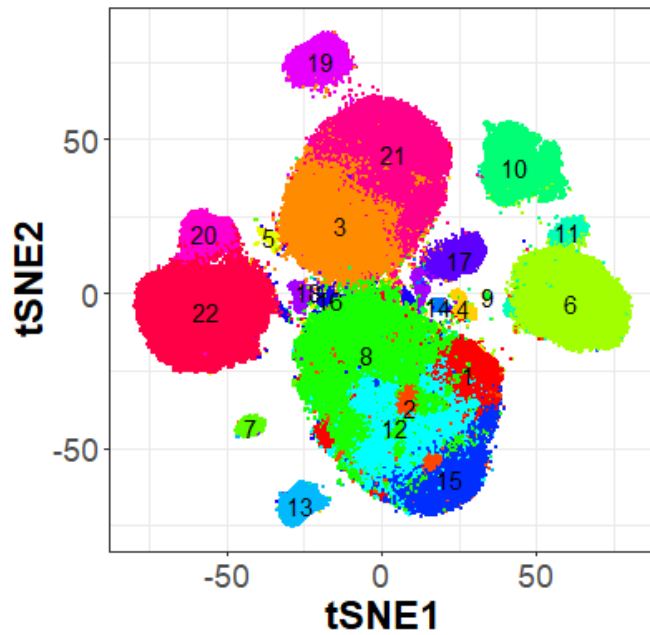
Figure 4.7: *Spleen timepoint 2 Phenograph clusters overlaid on viSNE.*
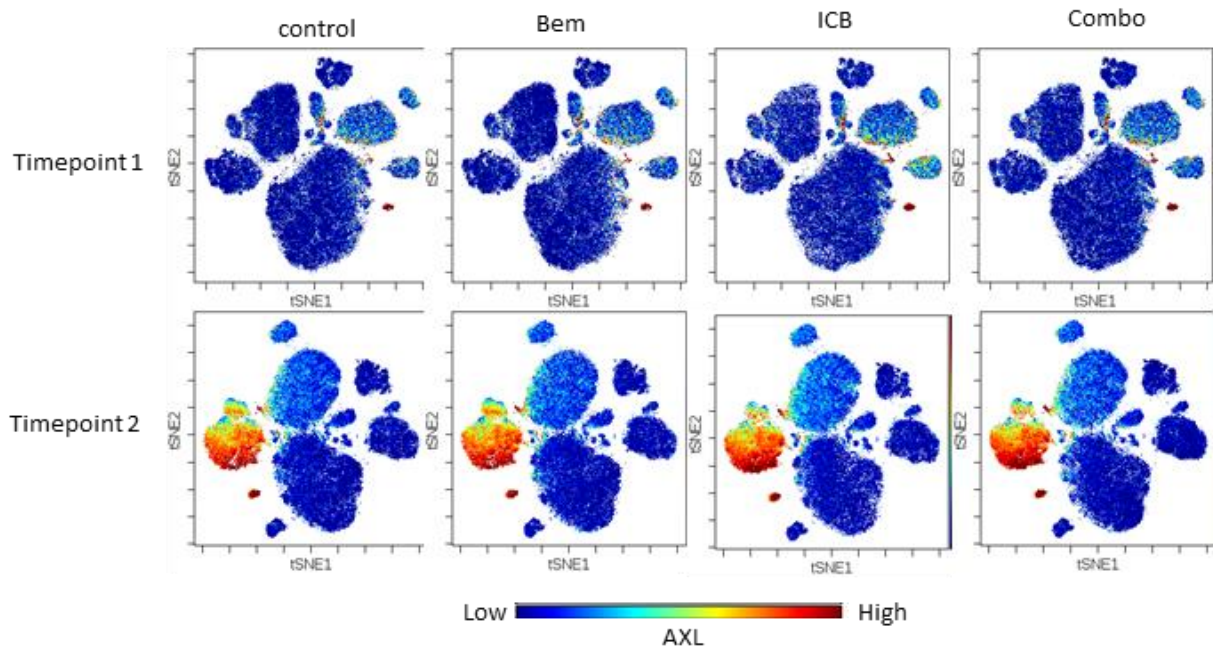
Figure 4.8: *viSNE of spleen treatment groups and timepoints coloured by AXL* intensity with binned pixels. Each dot represents a single cell. The colour scale is relative to each timepoint.

In timepoint 1 in Figure 4.8 almost no AXL staining is detected, only a small island of TAM2 cells in the lower right quadrant. In timepoint 2, however, a new island of AXL-expressing cells has appeared. The same TAM2 island can still be seen in now the lower right quadrant. The large AXL expressing island is partitioned in two clusters, number 20 and 22. These clusters

have not been phenotyped, but are characterised by AXL$^+$ MER$^+$ CD24$^+$ CD11b$^+$ CD83$^+$ PD-1$^+$ CD25$^+$. The upper partition stain positive for CD11c and PD-L1 in addition, while the lower part stains positive for CTLA-4 and CD114.

In Figure 4.9 density differences in the AXL-island are apparent depending on the treatment. Notably, the bemcentinib treatment seem to increase the density, while ICB treatment reduces it.
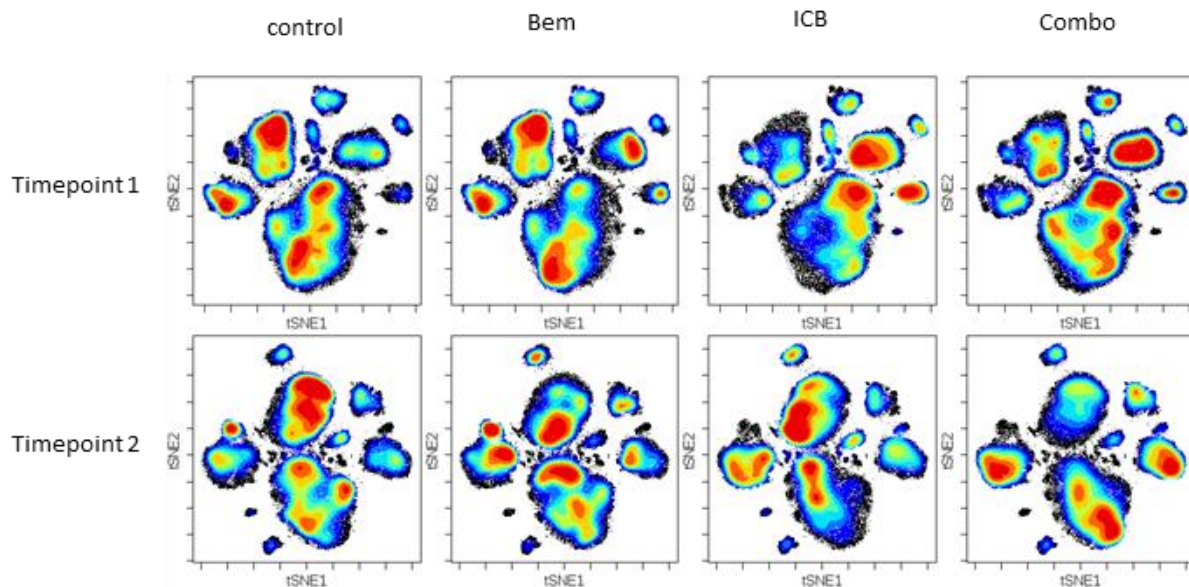
*Figure 4.9: **Spleen viSNE density plot.***

4.3 Mass Cytometry on Tumour

4.3.1 Timepoint 1

Clusters found after running Phenograph on the tumour samples from timepoint 1 are shown in Figure 4.10. The clusters were further analysed with MEM to find cluster characteristic markers. Cluster cell numbers for each spleen sample was used to draw circles indicating the mean cluster size in each group. An extended table with means and standard deviations for every cluster in every group is presented in Table 10.7. An additional heatmap of median marker values for each cluster if presented in Figure 10.3. Finally, a two-way ANOVA with the independent variables bemcentinib treatment and ICB treatment was performed on the dependent variable cluster size. Cluster size indicates the number of cells in a given cluster. An extended table containing a summary of each ANOVA performed is presented in Table 10.8.
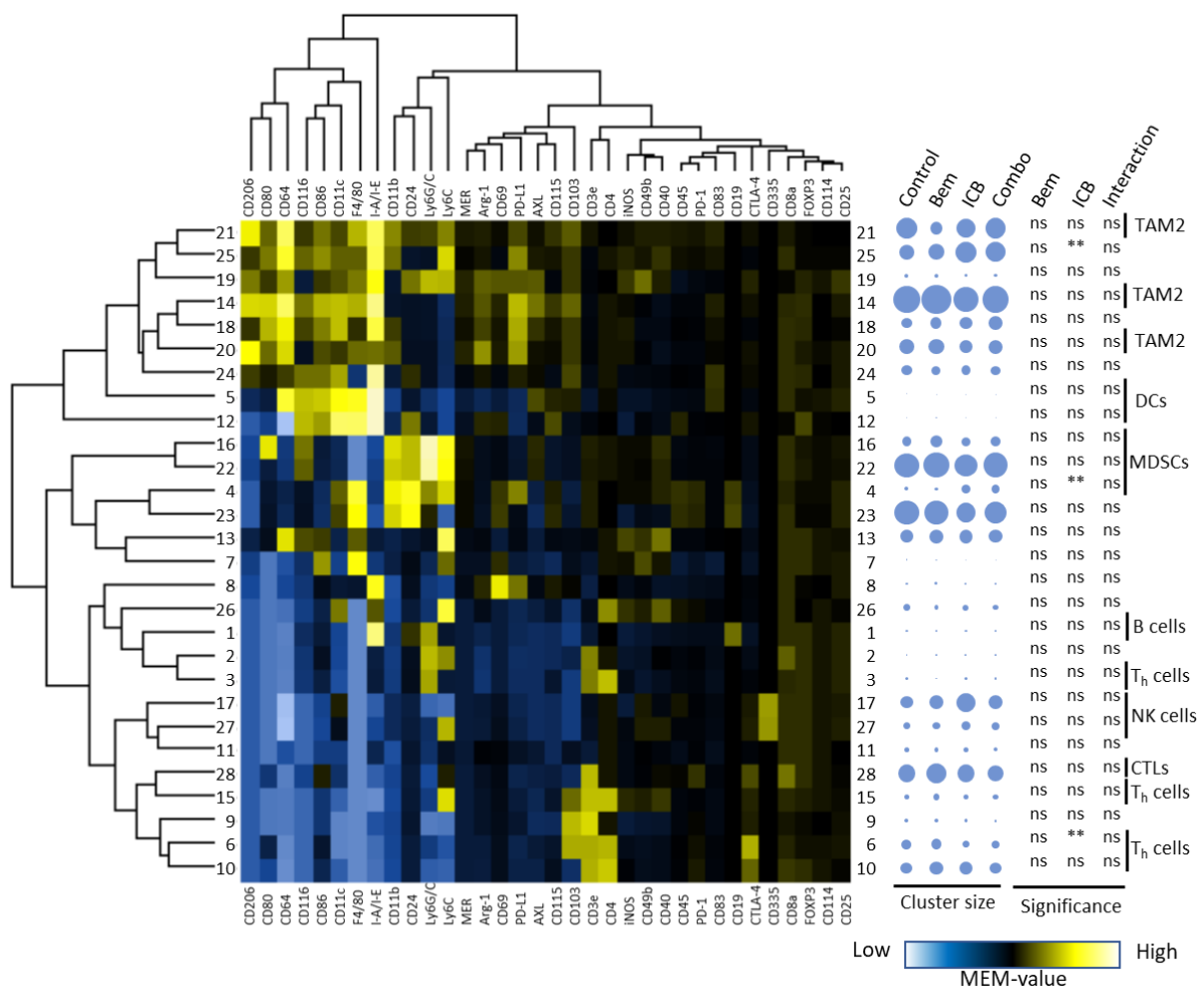
*Figure 4.10: **Tumour timepoint 1. MEM heatmap.** Each row is a cluster and each column is a marker. Circles on the right side correspond to cell number in the treatment groups after equal subsampling. Thus, it represents the proportional distribution of cells. The statistical results from a two-way ANOVA comparing the two treatments is shown on the right. P-values adjusted with Bemjamini-Holberg are indicated by ns (p > 0.05), * (0.05 > p), ** (0.01 > p), *** (0.001 > p). Main cell phenotypes have been characterised at the far right.*

A statistically significant main effect of ICB is found to decrease the number of cells in a CD103^{+} T helper cell subset (cluster 6). No statistically significant effects were found on CTLs (cluster 28), NK cells, B cells, and DCs. Phenograph failed to find any distinct TAM1 subset and thus any effect on this population in this run has not been studied. The TAM2 population was highly heterogenous and Phenograph partitioned the population into three different subsets presumably based on AXL, Arginase, and CD206 expression (data not shown). A statistically significant main effect of ICB is found to increase the number of cells in a MDSC subset (cluster 4). Lastly, a statistically significant main effect of ICB is found to increase the number of cells in a CD11b^{+}Ly6C^{+}cell subset (cluster 25).

4.3.2   Timepoint 2

Clusters found after running Phenograph on the tumour samples from timepoint 2 are shown in Figure 4.11. The clusters were further analysed with MEM to find cluster characteristic markers. Cluster cell numbers for each spleen sample was used to draw circles indicating the mean cluster size in each group. An extended table with means and standard deviations for every cluster in every group is presented in Table 10.9. An additional heatmap of median marker values for each cluster if presented in Figure 10.4.Finally, a two-way ANOVA with the independent variables bemcentinib treatment and ICB treatment was performed on the dependent variable cluster size. Cluster size indicates the number of cells in a given cluster. An extended table containing a summary of each ANOVA performed is presented in Table 10.10.
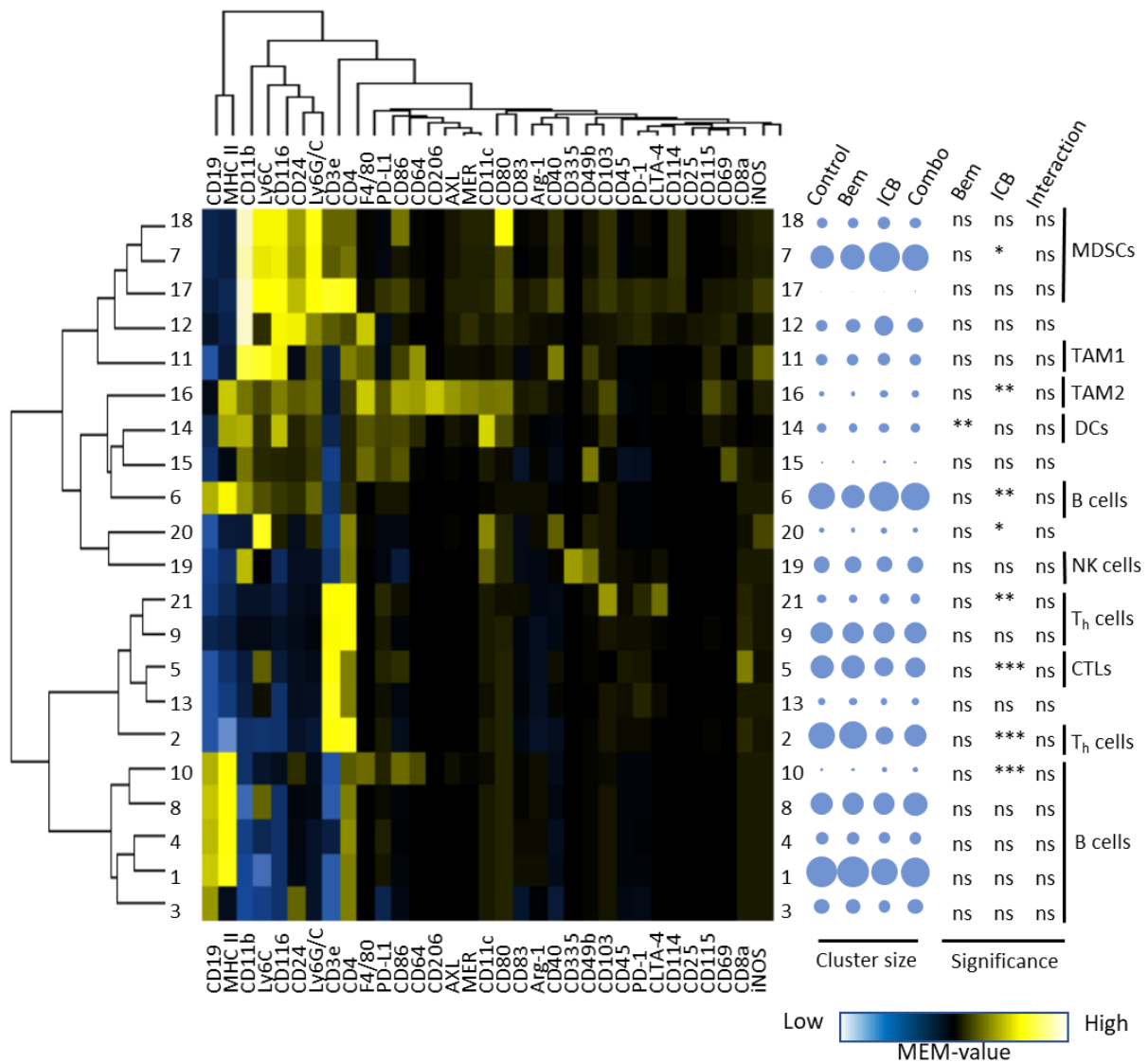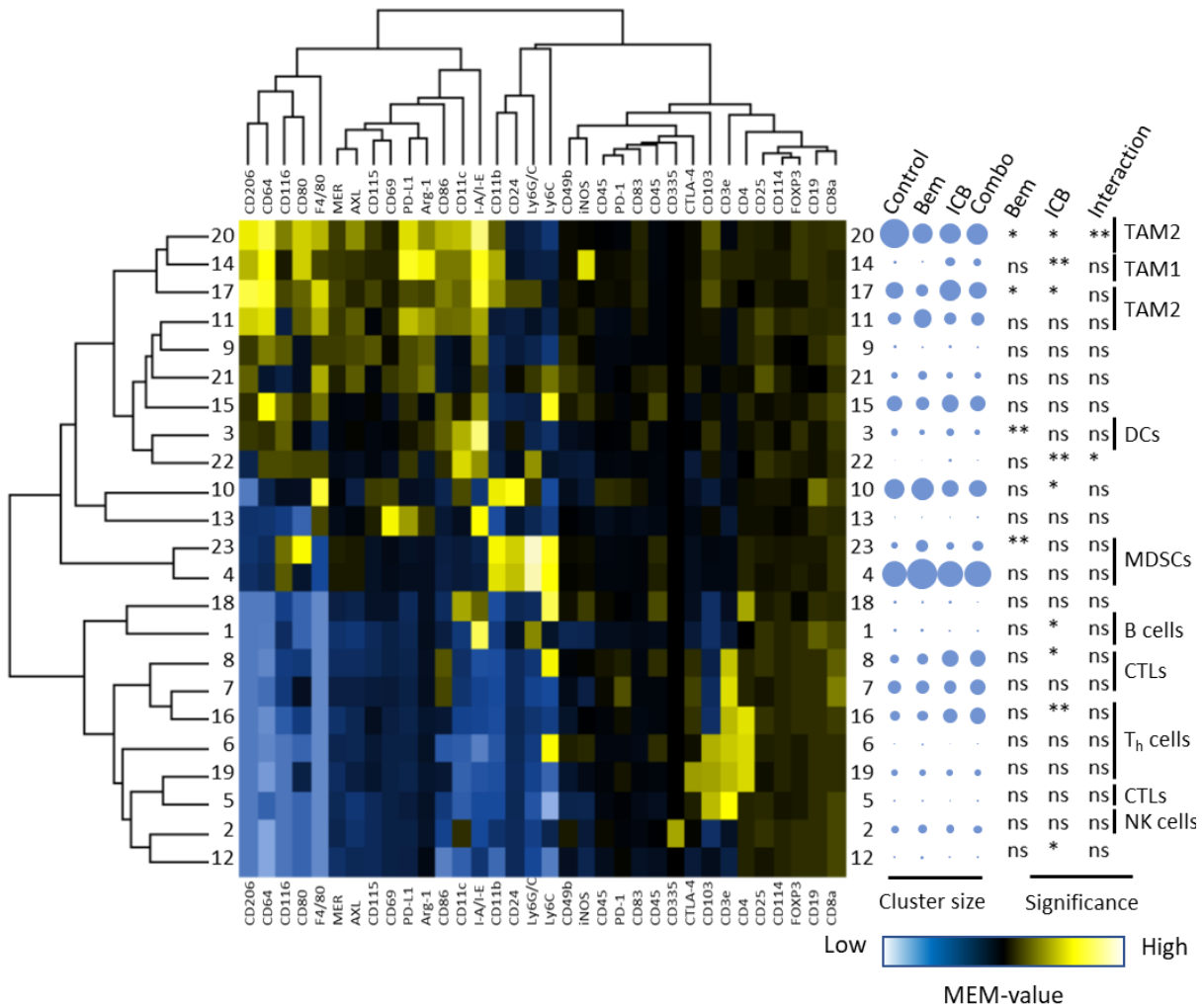

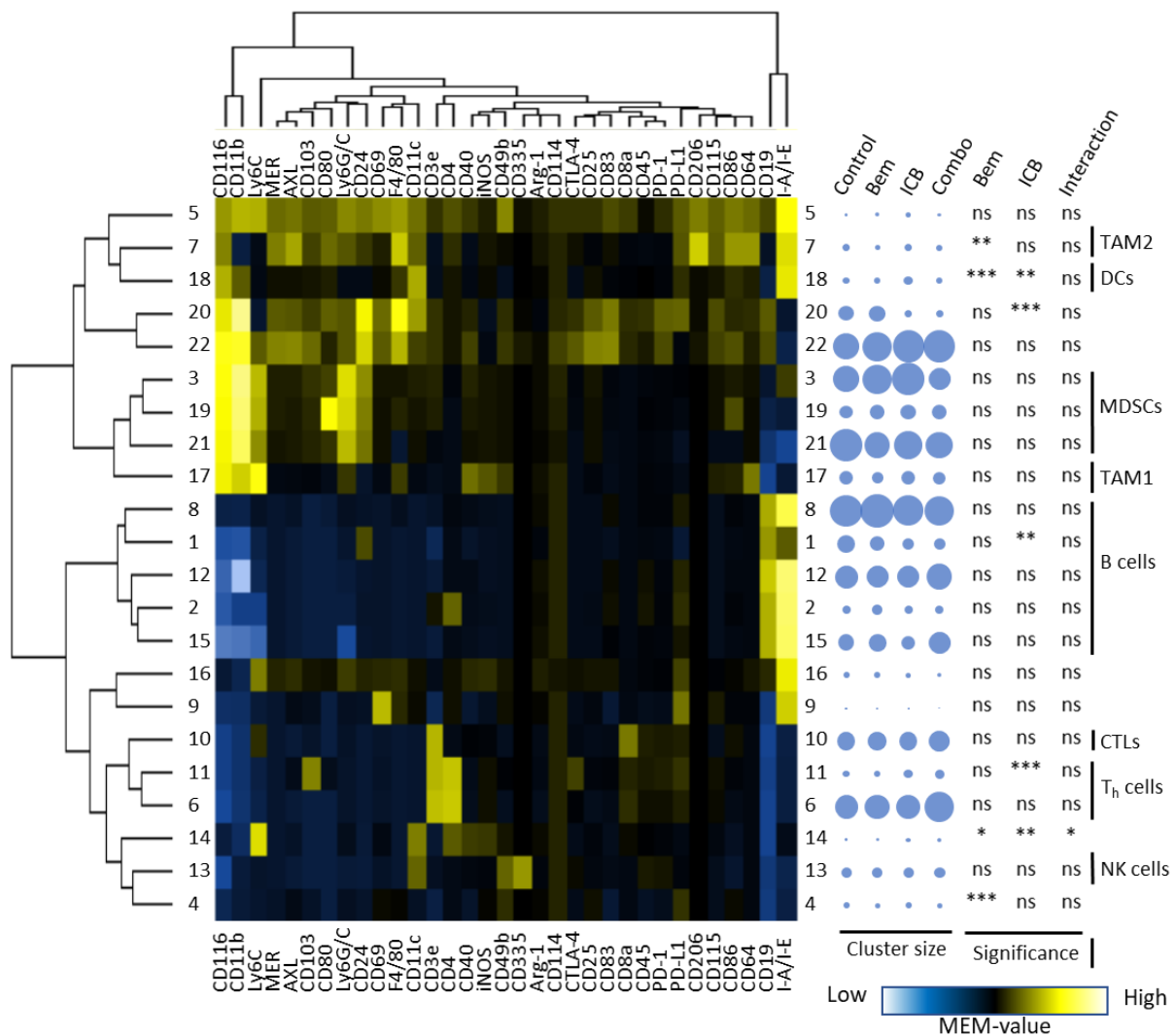*Figure 4.11: **Tumour timepoint 2 MEM heatmap .** Each row is a cluster and each column is a marker. Circles on the right side correspond to cell number in the treatment groups after equal subsampling. Thus, it represents the proportional distribution of cells. The statistical results from a two-way ANOVA comparing the two treatments is shown on the right. P-values adjusted*

A statistically significant effect of ICB was to increase the number of cells in a CD103$^-$ T helper cell subset (cluster 16) and in a Ly6C$^+$CTL subset (cluster 8). No statistically significant effects were found on NK cells. A statistically significant main effect of bemcentinib was, however, found to decrease the number of B cells and DCs. A statistically significant main effect of ICB was found to increase the number of TAM1s. Both bemcentinib and ICB have statistically significant effects that decrease the number of cells in a subtype of TAM2 (cluster 20). The interaction effect between bemcentinib and ICB is also significant. Due to the significant interaction direct interpretation is difficult and plotting the means is necessary for complete understanding. As shown in Figure 4.12 despite both bemcentinib and ICB alone show reduction of the TAM2 subset, the combination of the two does not result in any further reduction.
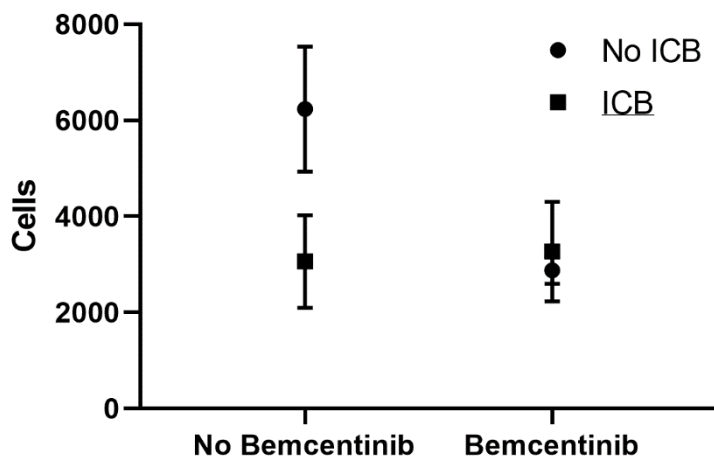
*Figure 4.12: **Size of cluster 20 (tumour timepoint 2) in different groups** plotted with means and standard deviation. Despite both bemcentinib and ICB show an effect on their own, the combination gives no added effect.*

For another TAM2 subset (cluster 17), both bemcentinib and ICB have statistically significant effects that decrease and increase the number of cells in a subtype of TAM2 (cluster 20). The interaction effect between bemcentinib and ICB is, however not significant. A cancellation is therefore expected. As shown in Figure 4.13, such a cancellation is indeed the case.
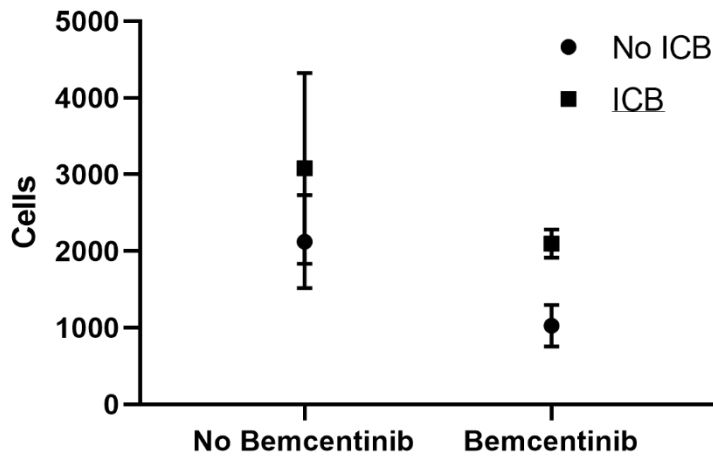
*Figure 4.13: **Size of cluster 17 (tumour timepoint 2) in different groups** plotted with means and standard deviation. Despite both bemcentinib and ICB show an effect on their own, the combination leads to cancellation of the effect.*

Lastly, a statistically significant effect of bemcentinib is found to increase the number of a CD80$^+$ subpopulation of MDSCs (cluster 23).

4.3.3   Axl staining and density

To visualise the distribution of AXL in the immune landscape, cells were plotted using calculated tSNE parameters. The clusters from Phenograph are overlaid in Figure 4.14 and Figure 4.15 for timepoint 1 and 2 respectively. tSNEs showing AXL expression for timepoint 1 and 2 are shown in Figure 4.17.
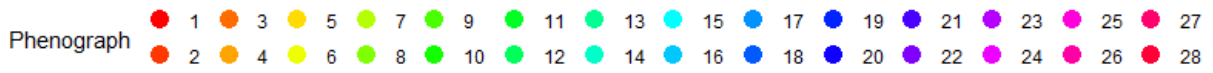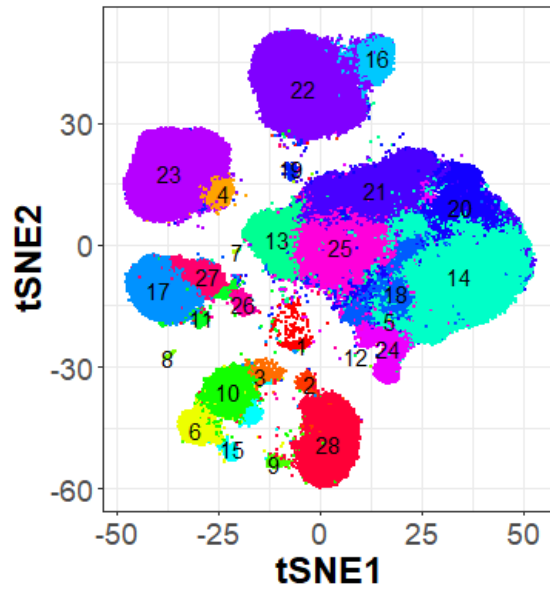
Figure 4.14: Tumour timepoint 1 Phenograph clusters overlaid on viSNE.
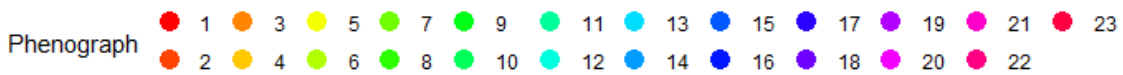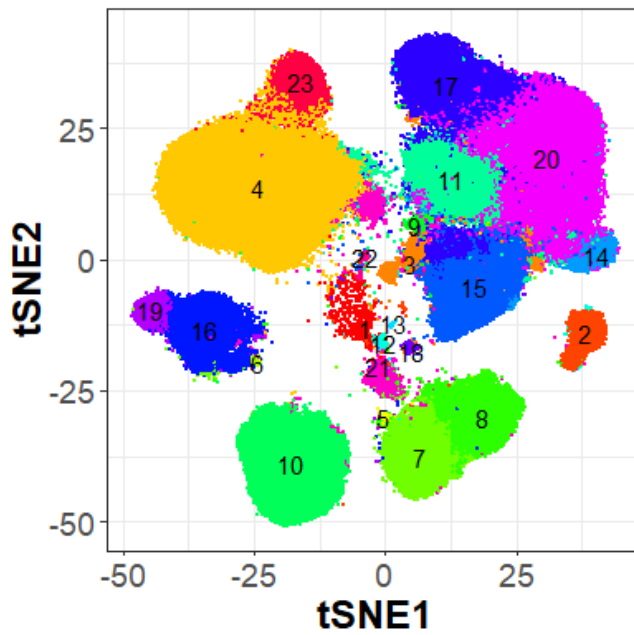
Figure 4.15: Tumour timepoint 2 Phenograph clusters overlaid on viSNE..
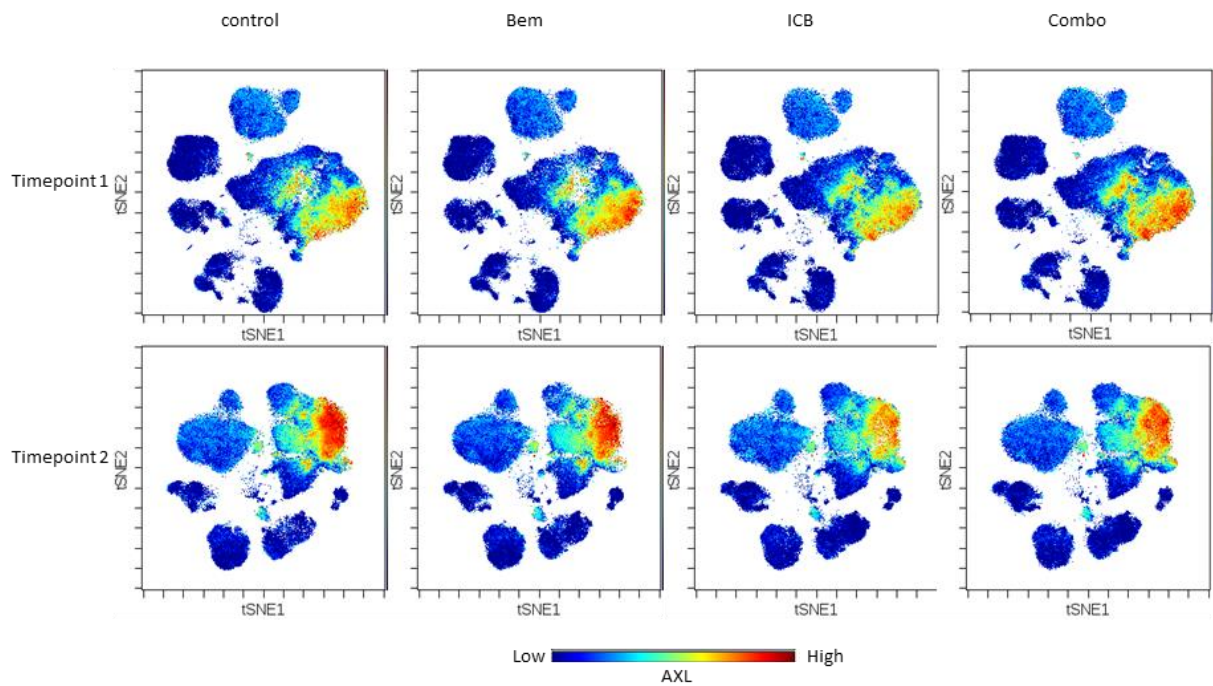
*Figure 4.16:**viSNE of tumour treatment groups and timepoints coloured by AXL** intensity with binned pixels. . Each dot represents a single cell. The colour scale is relative to each timepoint.*

In Figure 4.16 and Figure 4.17, it is clear that the distribution of AXL+ cells changes with treatment.
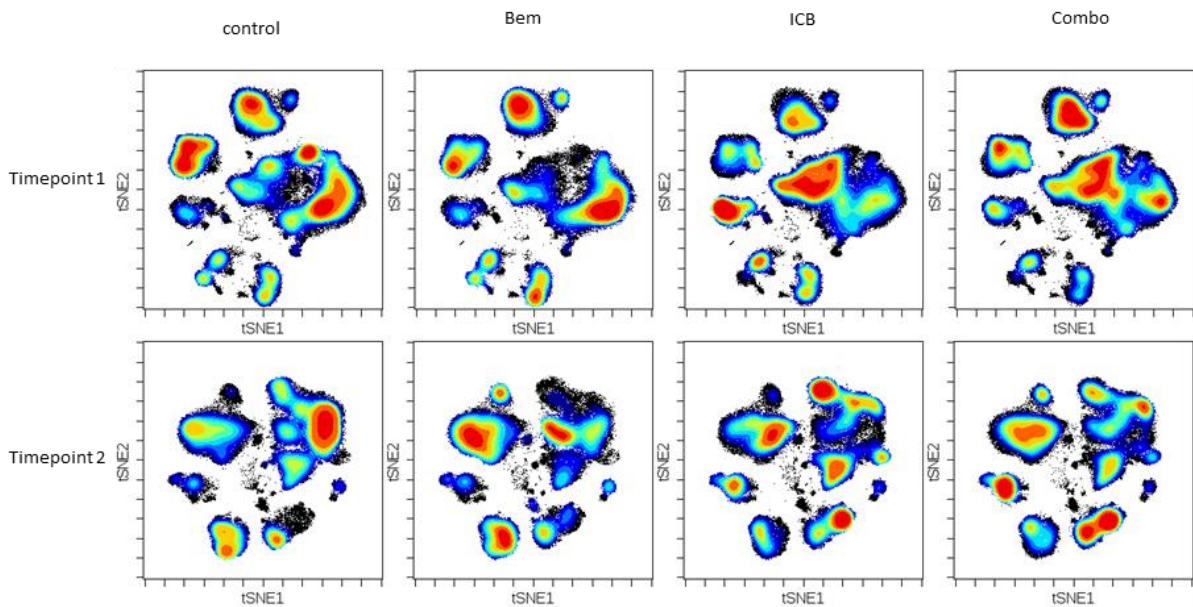
*Figure 4.17: **Tumour viSNE density plot.***

5   Discussion

5.1   Spleen and Tumour Weight

In section 4.1.1 we found that ICB has a statistically significant effect on tumour volume, while bemcentinib treatment did not. This is in contrast to the trials reported by Davidsen et al. in section 1.3.3 where a tumour volume of 500 mm^3 was used as an endpoint and a significant effect of combination of ICB with bemcentinib was found [35]. As shown in Figure 1.6, the difference between the ICB and combo treatment seems to be more prevalent in the later stages of tumour development and not the early stages, which have been analysed here. It is therefore likely that the observed effect of bemcentinib-ICB combination on tumour growth is more prominent in the later stages of tumour development, which is congruent with the expected timecourse of immune-mediated anti-tumour effects.

Cancer is a systemic disease and affects several organs distal to the tumour. Given the high correlation of spleen and tumour weight, as shown in Figure 4.2, 4T1 tumour development plays a role in the observed splenomegaly. Earlier, 4T1 induced splenomegaly has been associated with anaemia and an increase of Gr-1(Ly6G/C)$^+$CD11b$^+$ cells [77-79]. Interestingly, these markers are the same as used to phenotype myeloid derived suppressor cells (MDSCs) which promote tumour growth via suppression of the tumour immune response. However, MDSCs share these markers with some granulocyte subsets, and a functional study would be needed for proper classification [80]. In addition, these cells have also been classified as inflammatory monocytes with the potential migrate to other tissues to aid in wound healing [81]. This link indicates splenomegaly as a negative prognostic marker. The fact that there is a statistically significant difference between spleen, as shown in Figure 4.3, but not tumour volume might indicate that one of the benefits of combination therapy can be observed in the spleen.

5.2   Mass Cytometry Analyses

As shown in Figure 4.3, the spleens vary across the groups, thus, cluster sizes presented in the heatplots (Figure 4.4, Figure 4.5, Figure 4.10, and Figure 4.11) represent distribution among the clusters and not absolute cell counts. Thus, an observed reduction in cluster size from the control group to a treatment group might not indicate a change in the total cell count of a

given cell type in an organ, but rather an increase of other cell types resulting in a reduced ratio.

5.2.1 Spleen Clusters

Among the spleen samples, ICB was found to have varying effects depending on the timepoint. In timepoint 1 ICB was found to decrease the portion of a CD103⁻ T helper cells subset and increase cytotoxic T cells (cluster 8). In timepoint 2, however, ICB alone showed no statistically significant increase in a similar subset. An increase in the combination group was, however, observed. Although not statistically significant, the unadjusted p-values for effect of both ICB and bemcentinib were just at the limit of statistical significance. This interesting effect found only in combination warrants further study.

Bemcentinib showed both in timepoint 1 and 2 that it can decrease the amount of a CD80/83/86 low DC subset in the spleen. A lack of these "activation markers" could indicate a phenotype similar to suppressive tolerogenic DCs [82].However, ICB displays an ability to increase the DC proportion, and in combination these effects seem to cancel out. Thus, the observed reduction of DCs when treated with bemcentinib alone disappears when combined with ICB.

ICB was found to increase both TAM2 and MDSCs; two potent immune suppressive cells. Increase of TAM2 and MDSCs was only found to be statistically significant in timepoint 1 and thus might only play a role in the early parts of treatment. Bemcentinib, however, was found to decrease the amount of TAM2 in timepoint 2.

An MDSC subset (cluster 3) timepoint 2 was found to show an almost statistically significant effect (unadjusted p value 0.01, see Table 10.6) from an interaction between ICB and bemcentinib. Neither treatment showed a reduction when used alone, in fact both bemcentinib and ICB show a slight increase (not statistically significant), but when combined a reduction of 25% reduction compared to the control group, and a 50% reduction compared to the ICB treated group was seen.

Finally, an unidentified AXL⁺ population (cluster 20 and 22), only found in the spleen at timepoint 2 in all treatment groups, was found to be directly linked to tumour development. Cluster 20 differed from cluster 22 in higher expression of PD-L1, and lack of expression of CTLA-4 and CD103. Cluster 20 was also found to decrease with ICB-treatment.

5.2.2 Tumour Clusters

Among the tumour samples, ICB was found to affect the T_h in both timepoints, but in different types of subset. In timepoint 1 ICB was shown to reduce the amount of CD103$^+$ T_h cells, while in timepoint 2 a CD103$^-$ subset was increased. Earlier it has been shown that tumour infiltrating CD103$^+$ T_{regs} have potent suppressive capabilities [83]. However, to verify this cluster T regulatory cells, a functioning T_{reg} marker, such as FOXP3 is needed. ICB also showed an increase the number of Ly6C$^+$ CTLs. Ly6C has earlier been shown to be a marker of memory CTLs [84]. No TAM1 were classified in timepoint 1 due to Phenograph not recognising TAM1 as a single population. In timepoint 2, however, a TAM1 population was classified and ICB was found to increase the number of TAM1 cells. In both timepoints three different TAM2 subsets were found, one of which was characterised by high AXL and CD11c (cluster 21 in timepoint1 and 20 timepoint 2). The other two clusters did not have any clear distinction, being based on varying amounts of Arginase, CD206 and CD11c (data not shown). In timepoint 1 the bemcentinib treatment showed a reduction of the AXL$^+$ TAM2 of almost 70% compared to the control. This effect was, however, not statistically significant and similar effects was not seen in the combination group. In timepoint 2, however, both bemcentinib and ICB showed a statistically significant reduction in the amount of AXL$^+$ TAM2 cells. As shown in Figure 4.12, even though both treatments independently reduced the number of AXL$^+$ TAM2 cells, no added effect was seen with the combination. There might however be an added functional effect from the inhibition of AXL. In timepoint 2, one of the other TAM2 populations (cluster 17) was shown to be increased with ICB treatment and reduced by bemcentinib. In combination, these treatments seem to cancer each other out and result in the same amount of these cells as in the control.

Lastly, in timepoint 2, bemcentinib was shown to increase the amount of CD80$^+$ MDSCs (cluster 23).

5.3 Sources of Error

5.3.1 Sample Origin

Starting with the mice, a problem is that the tumours develop at different rates in different mice, despite being the same strain. As mentioned in the methods, this was one of the reasons of having an E group. This way, outliers with slower or faster growing tumours could be

removed from the experiment. Moving on to the tissue dissociation, it is not certain that the single cell suspension is representative of the tissue. Some cell types, such as dendritic cells and fibroblasts, might be more strongly attached to the extra cellular matrix than epithelial cells and lymphocytes. The suspension was also fixed before freezing. Unproper mixing during fixation might fix cells together causing some cells to appear as single cells clouds while having doubled the intercalator content. Further, some cell types might be more affected by freezing and possibly fragmented more easily.

5.3.2 Staining

Cisplatin, which is used to stain dead cells, might also stain cells performing endocytosis, such as macrophages and tumour cells and cells undergoing cell division. Some granulocytes have also been shown to bind the X8 polymers from Fluidigm leading to unspecific staining [85]. NK cells and some granulocytes also have FC-receptors that can bind the constant portion of antibodies. The Fc-block should, however, have counteracted this. As mentioned in the methodological considerations, the staining from the barcoding solution is highly dependent on the cell type and cell count. Thus, debarcoding with wrong parameters might change the cell type distribution depending on sample. Some say that mass cytometry eliminates autofluorescence [86]. In theory this might be true, but in practice the cells are always contaminated with some heavy metal. Especially barium and lead are prominent sources of background noise. Because of the sensitivity of the instrument, heavy metals in the glass of glass bottles and fumes from striker flints might contaminate the sample [87].

As shown in Figure 4.8, different cell phenotypes emerge at different timepoints. The E-group, which was used for titration and testing of antibodies, was also subject to this transformation. This variation between the timepoints (and between the tissues) indicate that a better approach might have been to combine samples from both timepoint and tissues and titrate them all at once or titrate the timepoints and tissues independently.

5.3.3 Data Analysis

Moving on to the data analysis, the pre-gating to select for single immune cells is also biased. Firstly, a subjectively determined arcsinh argument is used to transform the data. This transformation changes the data distribution of the channel intensities and could potentially create fictious populations and remove real populations. During gating, each gate has to be

made specifically for each data set. Therefore, it is drawn subjectively by the user, based on density estimations. No clear rules exist for how to place each gate, however, recommendations for some parameters are available [88]. As shown in Figure 3.4, doublets can still occur after the gaussian gating. This might be due to improper mixing during fixation, leading to cells getting fixed to each other. Before clustering was performed the sample was subsampled. The randomness in subsampling might have resulted in an unrepresentative sample. The unsupervised clustering provided by Phenograph presents very little bias, except for the manually chosen k parameter. It has also been shown to handle noise well and to find rare cell populations [72]. Phenograph has also been shown to be quite resilient and similar clusters are found despite variation in k [86]. The ability to find rare populations can however be a two-sided sword and result in clustering of doublets, or debris stained cells.

6 Concluding Remarks

We have developed a mass cytometry panel that can be used to map multiple myeloid and lymphoid populations.

AXL positive populations develop in both the spleen and tumour during tumour development of BALB/c mice implanted with 4T1 breast cancer cell line. Bemcentinib alone has been shown to reduce the amount of TAM2 cells in both spleen and tumour. In the tumour specifically, bemcentinib treatment counteracts an ICB (anti-PD-1 and anti-CTLA-4)-dependent increase of TAM2 cells.

A population of MDSCs found in the spleen was shown to decrease only in combination of bemcentinib and ICB. Despite a p-value of 0.01, the result was not deemed statistically significant after correction for multiple testing.

A new population of $CD24^+AXL^+$ cells in the spleen has been directly linked to tumour development. A $CD11c^+$ subset of this population was found to be reduced by ICB treatment.

7 Future Perspectives

In each mass cytometry run a control sample was included to be able to compare all samples across runs. We did unfortunately not have enough time to use this data. The data acquired during this experiment amounts to approximately 50 000 000 events and only about 300 000 events (~0.6%) were used in calculation of the statistics. Using the controls, all the data sets can be merged and cell types potentially originating from the spleen can be found in the tumour. The application of single cell trajectory inference methods, such as wanderlust and slingshot, might in this case be very interesting. In addition, with more computational power, larger samples can be clustered and even rarer populations and cells in between states can be found. In the future, the same panel can be used as is or as a template for similar studies studying both the myeloid and the lymphoid cells of the immune system.

8   References

9

1.   Norwegian Institute of Public Health. *Causes of death, Norway*. 22.Oct.2018; Available from: http://statistikkbank.fhi.no/dar/.
2.   World Health Organisation. *Cancer*. Available from: http://www.who.int/news-room/fact-sheets/detail/cancer.
3.   Kreftregisteret. *Kreftregisterets statistikkbank*. 1,nov,2018]; Available from: https://sb.kreftregisteret.no/insidens/.
4.   Oslo Economics, *Kreft i Norge — kostnader for pasientene, helsetjenesten og samfunnet*

En undersøkelse basert på data fra norske helseregistre. 2016.
5.   Gonzalez-Angulo, A.M., F. Morales-Vasquez, and G.N. Hortobagyi, *Overview of resistance to systemic therapy in patients with breast cancer.* Adv Exp Med Biol, 2007. **608**: p. 1-22.
6.   Tomasetti, C., B. Vogelstein, and G. Parmigiani, *Half or more of the somatic mutations in cancers of self-renewing tissues originate prior to tumor initiation.* Proceedings of the National Academy of Sciences, 2013. **110**(6): p. 1999-2004.
7.   Venter, J.C., et al., *The Sequence of the Human Genome.* Science, 2001. **291**(5507): p. 1304-1351.
8.   Wu, S., et al., *History of Severe Sunburn and Risk of Skin Cancer Among Women and Men in 2 Prospective Cohort Studies.* American Journal of Epidemiology, 2016. **183**(9): p. 824-833.
9.   National Center for Chronic Disease Prevention and Health Promotion (US) Office on Smoking and Health, *The Health Consequences of Smoking—50 Years of Progress: A Report of the Surgeon General*. 2014, Centers for Disease Control and Prevention (US): Atlanta (GA).
10.   Institute, N.C., *NCI Dictionary of Cancer Terms.*
11.   Hanahan, D. and R.A. Weinberg, *The Hallmarks of Cancer.* Cell, 2000. **100**(1): p. 57-70.
12.   Hanahan, D. and Robert A. Weinberg, *Hallmarks of Cancer: The Next Generation.* Cell, 2011. **144**(5): p. 646-674.
13.   Thiery, J.P. and J.P. Sleeman, *Complex networks orchestrate epithelial-mesenchymal transitions.* Nat Rev Mol Cell Biol, 2006. **7**(2): p. 131-142.
14.   Nieto, M.A., *Epithelial Plasticity: A Common Theme in Embryonic and Cancer Cells.* Science, 2013. **342**(6159).
15.   Zheng, X., et al., *Epithelial-to-mesenchymal transition is dispensable for metastasis but induces chemoresistance in pancreatic cancer.* Nature, 2015. **527**(7579): p. 525-530.
16.   Fischer, K.R., et al., *Epithelial-to-mesenchymal transition is not required for lung metastasis but contributes to chemoresistance.* Nature, 2015. **527**(7579): p. 472-476.
17.   Thiery, J.P., et al., *Epithelial-Mesenchymal Transitions in Development and Disease.* Cell, 2009. **139**(5): p. 871-890.
18.   Yilmaz, M. and G. Christofori, *EMT, the cytoskeleton, and cancer cell invasion.* Cancer and Metastasis Reviews, 2009. **28**(1): p. 15-33.
19.   Terry, S., et al., *New insights into the role of EMT in tumor immune escape.* Molecular Oncology, 2017. **11**(7): p. 824-846.
20.   Klymkowsky, M.W. and P. Savagner, *Epithelial-Mesenchymal Transition: A Cancer Researcher's Conceptual Friend and Foe.* The American Journal of Pathology, 2009. **174**(5): p. 1588-1593.
21.   Thiery, J.P., *Epithelial-mesenchymal transitions in tumour progression.* Nat Rev Cancer, 2002. **2**(6): p. 442-454.
22.   Gjerdrum, C., et al., *Axl is an essential epithelial-to-mesenchymal transition-induced regulator of breast cancer metastasis and patient survival.* Biological Sciences - Cell Biology, 2009. **107**(3): p. 1124-1129.

23.   Liu, L., et al., *Novel Mechanism of Lapatinib Resistance in HER2-Positive Breast Tumor Cells: Activation of AXL.* Cancer Research, 2009. **69**(17): p. 6871.
24.   Vuoriluoto, K., et al., *Vimentin regulates EMT induction by Slug and oncogenic H-Ras and migration by governing Axl expression in breast cancer.* Oncogene, 2011. **30**(12): p. 1436-1448.
25.   Graham, D.K., et al., *The TAM family: phosphatidylserine-sensing receptor tyrosine kinases gone awry in cancer.* Nat Rev Cancer, 2014. **14**(12): p. 769-785.
26.   Kirane, A., et al., *Warfarin Blocks Gas6-Mediated Axl Activation Required for Pancreatic Cancer Epithelial Plasticity and Metastasis.* Cancer Research, 2015. **75**(18): p. 3699.
27.   Holland, S.J., et al., *R428, a Selective Small Molecule Inhibitor of Axl Kinase, Blocks Tumor Spread and Prolongs Survival in Models of Metastatic Breast Cancer.* Cancer Research, 2010. **70**(4): p. 1544.
28.   Leach, D.R., M.F. Krummel, and J.P. Allison, *Enhancement of Antitumor Immunity by CTLA-4 Blockade.* Science, 1996. **271**(5256): p. 1734.
29.   Pardoll, D.M., *The blockade of immune checkpoints in cancer immunotherapy.* Nature Reviews Cancer, 2012. **12**: p. 252.
30.   Ager, A., et al., *Homing to solid cancers: a vascular checkpoint in adoptive cell therapy using CAR T-cells.* Biochemical Society Transactions, 2016. **44**(2): p. 377.
31.   Chen, Daniel S. and I. Mellman, *Oncology Meets Immunology: The Cancer-Immunity Cycle.* Immunity, 2013. **39**(1): p. 1-10.
32.   Ishida, Y., et al., *Induced expression of PD-1, a novel member of the immunoglobulin gene superfamily, upon programmed cell death.* The EMBO journal, 1992. **11**(11): p. 3887-3895.
33.   Chiu, K.-C., et al., *Polarization of tumor-associated macrophages and Gas6/Axl signaling in oral squamous cell carcinoma.* Oral Oncology, 2015. **51**(7): p. 683-689.
34.   Sica, A., P. Allavena, and A. Mantovani, *Cancer related inflammation: The macrophage connection.* Cancer Letters, 2008. **267**(2): p. 204-215.
35.   Davidsen, K., et al., *Bemcentinib (BGB324) - a selective small molecule inhibitor of the receptor tyrosine kinase AXL, targets tumour immune suppression and enhances immune checkpoint inhibitor efficacy*, in *AACR Annual Meeting*. 2018: Chicago.
36.   Lowry, L.E. and W.A. Zehring, *Potentiation of Natural Killer Cells for Cancer Immunotherapy: A Review of Literature.* Frontiers in immunology, 2017. **8**: p. 1061-1061.
37.   Naume, B., et al., *Nasjonalt handlingsprogram med retningslinjer for diagnostikk, behandling og oppfølging av pasienter med brystkreft*, Helsedirektoratet, Editor. 2018, Helsedirektoratet.
38.   Hodi, F.S., et al., *Combined nivolumab and ipilimumab versus ipilimumab alone in patients with advanced melanoma: 2-year overall survival outcomes in a multicentre, randomised, controlled, phase 2 trial.* The Lancet Oncology, 2016. **17**(11): p. 1558-1568.
39.   Borghaei, H., et al., *Nivolumab versus Docetaxel in Advanced Nonsquamous Non–Small-Cell Lung Cancer.* New England Journal of Medicine, 2015. **373**(17): p. 1627-1639.
40.   Chae, Y.K., et al., *Current landscape and future of dual anti-CTLA4 and PD-1/PD-L1 blockade immunotherapy in cancer; lessons learned from clinical trials with melanoma and non-small cell lung cancer (NSCLC).* Journal for ImmunoTherapy of Cancer, 2018. **6**(1): p. 39.
41.   Vonderheide, R.H., S.M. Domchek, and A.S. Clark, *Immunotherapy for Breast Cancer: What Are We Missing?* Clinical cancer research : an official journal of the American Association for Cancer Research, 2017. **23**(11): p. 2640-2646.
42.   Yule, M., et al., *A Ph II study of the selective AXL inhibitor BGB324 in combination with pembrolizumab in patients with previously treated, locally advanced and unresectable or metastatic triple negative breast cancer (TNBC) or triple negative inflammatory breast cancer (TN-IBC)*, in *San Antonio Breast Cancer Symposium* 2017 San Antoni.
43.   Fluidigm, *Helios Technical Overview.*
44.   Fluidigm, *Helios, a CyTOF System USER GUIDE* 2017.
45.   Ornatsky, O.I., et al., *Development of analytical methods for multiplex bio-assay with inductively coupled plasma mass spectrometry.* Journal of analytical atomic spectrometry, 2008. **23**(4): p. 463-469.

46.   Bandura, D.R., et al., *Mass cytometry: technique for real time single cell multitarget immunoassay based on inductively coupled plasma time-of-flight mass spectrometry.* Anal Chem, 2009. **81**(16): p. 6813-22.

47.   Ornatsky, O., et al., *Highly multiparametric analysis by mass cytometry.* J Immunol Methods, 2010. **361**(1-2): p. 1-20.

48.   Tanner, S.D., et al., *An introduction to mass cytometry: fundamentals and applications.* Cancer Immunol Immunother, 2013. **62**(5): p. 955-65.

49.   Olsen, L.R., et al., *The anatomy of single cell mass cytometry data.* Cytometry Part A, 2018. **0**(0).

50.   Fluidigm. *Helios, a CyTOF System*. 2018 [cited 2018; Available from: https://www.fluidigm.com/products/helios.

51.   Fluidigm, *Derivation of Quantitative Data from CyTOF® Using Dual Counts and Di Calibration.*

52.   Han, G., et al., *Atomic mass tag of bismuth-209 for increasing the immunoassay multiplexing capacity of mass cytometry.* Cytometry A, 2017. **91**(12): p. 1150-1163.

53.   Mei Henrik, E., D. Leipold Michael, and T. Maecker Holden, *Platinum-conjugated antibodies for application in mass cytometry.* Cytometry Part A, 2015. **89**(3): p. 292-300.

54.   Lou, X., et al., *Polymer-based elemental tags for sensitive bioassays.* Angew Chem Int Ed Engl, 2007. **46**(32): p. 6111-4.

55.   Ornatsky, O.I., et al., *Study of Cell Antigens and Intracellular DNA by Identification of Element-Containing Labels and Metallointercalators Using Inductively Coupled Plasma Mass Spectrometry.* Analytical Chemistry, 2008. **80**(7): p. 2539-2547.

56.   Catena, R., et al., *Enhanced multiplexing in mass cytometry using osmium and ruthenium tetroxide species.* Cytometry Part A, 2016. **89**(5): p. 491-497.

57.   Behbehani Gregory, K., et al., *Single-cell mass cytometry adapted to measurements of the cell cycle.* Cytometry Part A, 2012. **81A**(7): p. 552-566.

58.   Frei, A.P., et al., *Highly multiplexed simultaneous detection of RNAs and proteins in single cells.* Nat Methods, 2016. **13**(3): p. 269-75.

59.   Mavropoulos, A., et al., *Simultaneous Detection of Protein and mRNA in Jurkat and KG-1a Cells by Mass Cytometry.* Cytometry Part A, 2017. **91**(12): p. 1200-1208.

60.   McCarthy, R.L., et al., *Rapid monoisotopic cisplatin based barcoding for multiplexed mass cytometry.* Sci Rep, 2017. **7**(1): p. 3779.

61.   Zunder, E.R., et al., *Palladium-based mass tag cell barcoding with a doublet-filtering scheme and single-cell deconvolution algorithm.* Nat Protoc, 2015. **10**(2): p. 316-33.

62.   Fienberg Harris, G., et al., *A platinum-based covalent viability reagent for single-cell mass cytometry.* Cytometry Part A, 2012. **81A**(6): p. 467-475.

63.   Lai, L., et al., *A CD45-based barcoding approach to multiplex mass-cytometry (CyTOF).* Cytometry Part A, 2015. **87**(4): p. 369-374.

64.   Bjornson, Z.B., G.P. Nolan, and W.J. Fantl, *Single-cell mass cytometry for analysis of immune system functional states.* Current Opinion in Immunology, 2013. **25**(4): p. 484-494.

65.   Jones, L.M., et al., *Complementary MS Methods Assist Conformational Characterization of Antibodies with Altered S–S Bonding Networks.* Journal of The American Society for Mass Spectrometry, 2013. **24**(6): p. 835-845.

66.   Perfetto, S.P., P.K. Chattopadhyay, and M. Roederer, *Seventeen-colour flow cytometry: unravelling the immune system.* Nat Rev Immunol, 2004. **4**(8): p. 648-655.

67.   Finck, R., et al., *Normalization of mass cytometry data with bead standards.* Cytometry A, 2013. **83**(5): p. 483-94.

68.   Fluidigm, *Normalization of Mass Cytometry Data using EQ™ Four Element Calibration Beads.* 2015.

69.   C. Bruce Bagwell MD, P.D., Veriety Software House,, *A new analytic approach for live singlet identification: sweeping away unwanted events*.

70.   Maaten;, L.v.d., *Visualizing Data using t-SNE.* Journal of Machine Learning Reasearch, 2008. **9**: p. 2579-2605.

71. Amir el, A.D., et al., *viSNE enables visualization of high dimensional single-cell data and reveals phenotypic heterogeneity of leukemia.* Nat Biotechnol, 2013. **31**(6): p. 545-52.

72. Levine, Jacob H., et al., *Data-Driven Phenotypic Dissection of AML Reveals Progenitor-like Cells that Correlate with Prognosis.* Cell, 2015. **162**(1): p. 184-197.

73. Diggins, K.E., et al., *Characterizing cell subsets using marker enrichment modeling.* Nature Methods, 2017. **14**: p. 275.

74. Ellis B, H.P., Hahne F, Le Meur N, Gopalakrishnan N, Spidlen J, Jiang M, Finak G *flowCore: Basic structures for flow cytometry data.*

R package version 1.47.9. 2018.

75. Chen, H., et al., *Cytofkit: A Bioconductor Package for an Integrated Mass Cytometry Data Analysis Pipeline.* PLOS Computational Biology, 2016. **12**(9): p. e1005112.

76. Diggins Kirsten, E., et al., *Generating Quantitative Cell Identity Labels with Marker Enrichment Modeling (MEM).* Current Protocols in Cytometry, 2018. **83**(1): p. 10.21.1-10.21.28.

77. DuPré, S.A., D. Redelman, and K.W. Hunter, Jr., *The mouse mammary carcinoma 4T1: characterization of the cellular landscape of primary tumours and metastatic tumour foci.* International journal of experimental pathology, 2007. **88**(5): p. 351-360.

78. DuPre, S.A. and K.W. Hunter, Jr., *Murine mammary carcinoma 4T1 induces a leukemoid reaction with splenomegaly: association with tumor-derived growth factors.* Exp Mol Pathol, 2007. **82**(1): p. 12-24.

79. Liu, M., et al., *Macrophages Support Splenic Erythropoiesis in 4T1 Tumor-Bearing Mice.* PLOS ONE, 2015. **10**(3): p. e0121921.

80. Damuzzo, V., et al., *Complexity and Challenges in Defining Myeloid-Derived Suppressor Cells.* Cytometry. Part B, Clinical Cytometry, 2015. **88**(2): p. 77-91.

81. Swirski, F.K., et al., *Identification of splenic reservoir monocytes and their deployment to inflammatory sites.* Science (New York, N.Y.), 2009. **325**(5940): p. 612-616.

82. Domogalla, M.P., et al., *Tolerance through Education: How Tolerogenic Dendritic Cells Shape Immunity.* Frontiers in immunology, 2017. **8**: p. 1764-1764.

83. Anz, D., et al., *CD103 is a hallmark of tumor-infiltrating regulatory T cells.* International Journal of Cancer, 2011. **129**(10): p. 2417-2426.

84. Walunas, T.L., et al., *Ly-6C is a marker of memory CD8+ T cells.* J Immunol, 1995. **155**(4): p. 1873-83.

85. Rahman, A.H., L. Tordesillas, and M.C. Berin, *Heparin reduces nonspecific eosinophil staining artifacts in mass cytometry experiments.* Cytometry Part A, 2016. **89**(6): p. 601-607.

86. M., W.L. and R.M. D., *Comparison of clustering methods for high-dimensional single-cell flow and mass cytometry data.* Cytometry Part A, 2016. **89**(12): p. 1084-1096.

87. Leipold, M.D., E.W. Newell, and H.T. Maecker, *Multiparameter Phenotyping of Human PBMCs Using Mass Cytometry.* Methods in molecular biology (Clifton, N.J.), 2015. **1343**: p. 81-95.

88. Fluidigm, *Recommendations for Use of Gaussian Discrimination Parameters.*

10 Attachments

10.1 Titrated Antibody Panel

Table 10.1: Final titrated antibody panel used during staining of mouse spleen and tumour tissue.

Mass tag	Marker	Titration 1/X	Concentration
142Nd	CD11c	100	NA
143Nd	CD69	100	NA
144Nd	CD115	100	NA
145Nd	CD4	400	NA
146Nd	CD8a	100	NA
147Sm	CD45	600	NA
148Nd	PD-1	100	0.5 mg/ml
149Sm	CD83	100	0.5 mg/ml
150Nd	CD24	400	NA
151Eu	CD64	200	NA
152Sm	CD3e	400	NA
153Eu	PD-L1	200	NA
154Sm	CD11b	600	NA
155Gd	G-CSF-R/CD114	100	0.5 mg/ml
156Gd	CD103	100	0.5 mg/ml
158Gd	FoxP3	100	NA
159Tb	F4/80	400	NA
160Gd	Arginase-1	100	0.5 mg/ml
161Dy	iNOS	100	NA
162Dy	Ly6C	800	NA
163Dy	CD40	200	0.5 mg/ml
164Dy	CD49b	100	NA
165Ho	CD25	100	0.5 mg/ml
166Er	CD19	200	NA
167Er	CD335 (NKp46)	400	NA
168Er	CTLA4	100	0.5 mg/ml
169Tm	CD206	800	NA

170Er	MerTK	100	0.5 mg/ml		
171Yb	CD80 (B7.1)	400	NA		
172Yb	CD86 (B7.2)	100	NA		
173Yb	GM-CSF-R/CD116	200	0.5 mg/ml		
174Yb	Ly6G/C	1600	NA		
176Yb	Axl - MAB854	100	0.5 mg/ml		
176Yb	Axl - MAB8541	100	0.5 mg/ml		
209Bi	MHCII	400	NA		

10.2 Spleen and Tumour Statistics

Table 10.2:Calculated means and standard deviations for spleen weight, tumour weight and tumour volume.

Type	Timepoint	Group	Mean	SD	n
Spleen weight	1	A	0.17	0.025	5
Spleen weight	1	B	0.18	0.032	5
Spleen weight	1	C	0.26	0.023	5
Spleen weight	1	D	0.26	0.023	5
Spleen weight	2	A	0.60	0.103	5
Spleen weight	2	B	0.45	0.067	5
Spleen weight	2	C	0.41	0.070	5
Spleen weight	2	D	0.33	0.057	5
Tumour volume	1	A	152.10	27.522	5
Tumour volume	1	B	136.96	19.046	5
Tumour volume	1	C	155.96	31.317	5
Tumour volume	1	D	130.88	35.976	5
Tumour volume	2	A	316.18	81.079	5
Tumour volume	2	B	389.53	41.464	5
Tumour volume	2	C	227.12	128.934	5
Tumour volume	2	D	199.50	70.534	5
Tumour weight	1	A	0.19	0.029	5
Tumour weight	1	B	0.20	0.015	5
Tumour weight	1	C	0.21	0.052	5
Tumour weight	1	D	0.22	0.004	5

Tumour weight	2	A	0.45	0.059	5
Tumour weight	2	B	0.45	0.040	5
Tumour weight	2	C	0.27	0.106	5
Tumour weight	2	D	0.28	0.094	5

10.3 Spleen Timepoint 1 Statistics

10.3.1 Cluster Medians Heatmap
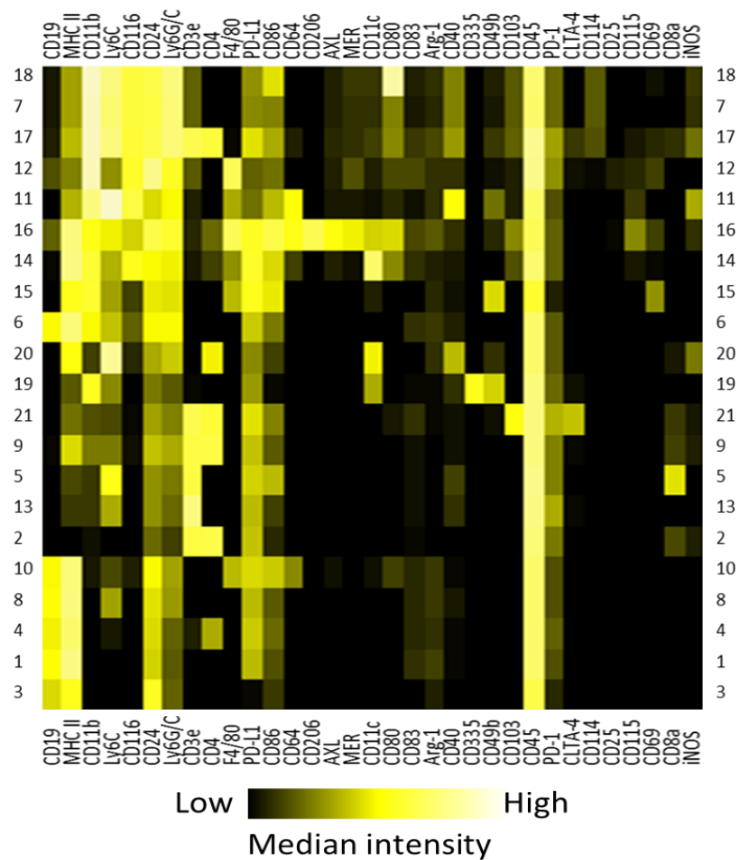
*Figure 10.1: **Heatmap of median intensities for spleen in timepoint 1.** Row numbers indicate cluster. Intensities have been transformed with an arsinh argument of 2.*

10.3.2 Cluster Means and Standard Deviation

Table 10.3: Calculated means and standard deviations for each group in each cluster. Group A was treated with vehicle only, group B was treated with bemcentinib only, group C was treated with immunotherapy only (anti-CTLA-4 and anti-PD-1 combination), and group D was treated with a combination of immunotherapy and bemcentinib.

Group	Cluster	mean	SD	n
A	1	3276.00	490.55	5
B	1	3342.60	385.75	5

C	1	2460.00	643.68	5
D	1	2998.60	232.83	5
A	2	2505.80	222.57	5
B	2	2643.60	187.62	5
C	2	1102.20	342.72	5
D	2	1592.20	157.23	5
A	3	822.20	251.58	5
B	3	804.60	215.31	5
C	3	508.80	240.17	5
D	3	814.40	148.37	5
A	4	567.80	165.45	5
B	4	557.00	114.90	5
C	4	461.20	90.13	5
D	4	532.60	97.55	5
A	5	1897.80	111.05	5
B	5	1910.40	156.69	5
C	5	1230.40	205.47	5
D	5	1419.40	115.27	5
A	6	2384.40	290.83	5
B	6	1876.20	244.20	5
C	6	3125.20	642.15	5
D	6	2703.00	364.67	5
A	7	1876.40	414.05	5
B	7	2093.00	585.02	5
C	7	3190.20	740.14	5
D	7	2449.60	306.33	5
A	8	1746.20	229.89	5
B	8	1645.60	136.29	5
C	8	1642.00	466.39	5
D	8	1922.80	222.99	5
A	9	1651.60	180.52	5
B	9	1601.60	274.50	5
C	9	1606.20	132.25	5

D	9	1671.00	102.00	5
A	10	50.00	15.30	5
B	10	48.80	13.99	5
C	10	89.80	13.10	5
D	10	112.00	29.85	5
A	11	451.20	80.52	5
B	11	485.20	119.40	5
C	11	580.60	73.96	5
D	11	519.40	93.16	5
A	12	477.80	259.24	5
B	12	704.40	365.49	5
C	12	1334.80	788.63	5
D	12	795.20	231.21	5
A	13	193.40	13.79	5
B	13	201.60	27.67	5
C	13	156.20	47.73	5
D	13	156.60	21.43	5
A	14	307.00	50.16	5
B	14	259.60	39.55	5
C	14	363.80	15.67	5
D	14	282.20	13.41	5
A	15	17.40	4.77	5
B	15	21.80	6.72	5
C	15	34.00	10.98	5
D	15	20.60	6.31	5
A	16	79.80	18.62	5
B	16	79.60	15.39	5
C	16	241.40	88.00	5
D	16	150.60	36.74	5
A	17	6.40	3.51	5
B	17	4.40	2.70	5
C	17	3.00	3.16	5
D	17	6.80	4.49	5

A	18	384.40	155.58	5
B	18	409.80	80.17	5
C	18	524.20	117.05	5
D	18	460.00	31.31	5
A	19	926.40	116.09	5
B	19	960.00	140.23	5
C	19	868.80	117.69	5
D	19	943.60	103.80	5
A	20	105.00	19.53	5
B	20	89.20	18.99	5
C	20	135.20	13.44	5
D	20	107.40	16.26	5
A	21	273.00	29.09	5
B	21	261.00	43.59	5
C	21	342.00	41.56	5
D	21	342.00	18.30	5

10.3.3 ANOVA results

Table 10.4: Reported results form a factorial analysis of variance to compare the main effects of bemcentinib treatment (BGB) and immune chekcpoint blockade (ICB, anti-PD-1 and anti-CLTA-4 combination) and the interaction effect between ICB and BGB on the number of cells in each cluster.

Cluster	Response	Df	Sum Sq	Mean Sq	F value	Pr(>F)	Benjamini-Hochberg (5% FDR)
1	BGB	1	457833.8	457833.8	2.13	0.16	0.32
1	BGB:ICB	1	278480	278480	1.30	0.27	0.43
1	ICB	1	1682000	1682000	7.84	0.01	0.06
1	Residuals	16	3431900.4	214493.775	NA	NA	
2	BGB	1	492666.05	492666.05	8.68	0.01	0.05
2	BGB:ICB	1	155056.05	155056.05	2.73	0.12	0.27
2	ICB	1	7533781.25	7533781.25	132.80	0.00	0.00
2	Residuals	16	907653.6	56728.35	NA	NA	
3	BGB	1	103680	103680	2.19	0.16	0.32
3	BGB:ICB	1	130572.8	130572.8	2.76	0.12	0.27
3	ICB	1	115216.2	115216.2	2.43	0.14	0.31
3	Residuals	16	757388	47336.75	NA	NA	
4	BGB	1	4590.45	4590.45	0.32	0.58	0.71
4	BGB:ICB	1	8446.05	8446.05	0.58	0.46	0.64
4	ICB	1	21451.25	21451.25	1.47	0.24	0.41
4	Residuals	16	232866.8	14554.175	NA	NA	

5	BGB	1	50803.2	50803.2	2.20	0.16	0.32
5	BGB:ICB	1	38896.2	38896.2	1.68	0.21	0.38
5	ICB	1	1677363.2	1677363.2	72.62	0.00	0.00
5	Residuals	16	369554.4	23097.15	NA	NA	
6	BGB	1	1082055.2	1082055.2	6.28	0.02	0.09
6	BGB:ICB	1	9245	9245	0.05	0.82	0.85
6	ICB	1	3071712.2	3071712.2	17.82	0.00	0.01
6	Residuals	16	2758202.8	172387.675	NA	NA	
7	BGB	1	343220	343220	1.19	0.29	0.45
7	BGB:ICB	1	1145289.8	1145289.8	3.97	0.06	0.18
7	ICB	1	3487795.2	3487795.2	12.08	0.00	0.02
7	Residuals	16	4621285.2	288830.325	NA	NA	
8	BGB	1	40590.05	40590.05	0.48	0.50	0.64
8	BGB:ICB	1	181832.45	181832.45	2.15	0.16	0.32
8	ICB	1	37411.25	37411.25	0.44	0.52	0.65
8	Residuals	16	1354676.8	84667.3	NA	NA	
9	BGB	1	273.8	273.8	0.01	0.93	0.93
9	BGB:ICB	1	16473.8	16473.8	0.49	0.50	0.64
9	ICB	1	720	720	0.02	0.89	0.90
9	Residuals	16	543337.2	33958.575	NA	NA	
10	BGB	1	551.25	551.25	1.48	0.24	0.41
10	BGB:ICB	1	684.45	684.45	1.83	0.19	0.37
10	ICB	1	13261.25	13261.25	35.54	0.00	0.00
10	Residuals	16	5969.6	373.1	NA	NA	
11	BGB	1	924.8	924.8	0.11	0.75	0.81
11	BGB:ICB	1	11328.8	11328.8	1.30	0.27	0.43
11	ICB	1	33456.2	33456.2	3.84	0.07	0.19
11	Residuals	16	139556	8722.25	NA	NA	
12	BGB	1	122461.25	122461.25	0.56	0.47	0.64
12	BGB:ICB	1	733828.05	733828.05	3.35	0.09	0.22
12	ICB	1	1122906.05	1122906.05	5.13	0.04	0.13
12	Residuals	16	3504709.6	219044.35	NA	NA	
13	BGB	1	92.45	92.45	0.10	0.76	0.81
13	BGB:ICB	1	76.05	76.05	0.08	0.78	0.82
13	ICB	1	8446.05	8446.05	9.15	0.01	0.05
13	Residuals	16	14772.4	923.275	NA	NA	
14	BGB	1	20801.25	20801.25	18.46	0.00	0.01
14	BGB:ICB	1	1462.05	1462.05	1.30	0.27	0.43
14	ICB	1	7880.45	7880.45	7.00	0.02	0.08
14	Residuals	16	18024.8	1126.55	NA	NA	
15	BGB	1	101.25	101.25	1.77	0.20	0.37
15	BGB:ICB	1	396.05	396.05	6.94	0.02	0.08
15	ICB	1	296.45	296.45	5.19	0.04	0.13
15	Residuals	16	913.2	57.075	NA	NA	
16	BGB	1	10351.25	10351.25	4.28	0.06	0.18
16	BGB:ICB	1	10260.45	10260.45	4.24	0.06	0.18

16	ICB	1	67628.45	67628.45	27.95	0.00	0.00
16	Residuals	16	38710.4	2419.4	NA	NA	
17	BGB	1	4.05	4.05	0.33	0.58	0.71
17	BGB:ICB	1	42.05	42.05	3.38	0.08	0.22
17	ICB	1	1.25	1.25	0.10	0.76	0.81
17	Residuals	16	199.2	12.45	NA	NA	
18	BGB	1	1881.8	1881.8	0.17	0.69	0.79
18	BGB:ICB	1	10035.2	10035.2	0.89	0.36	0.53
18	ICB	1	45125	45125	3.98	0.06	0.18
18	Residuals	16	181252.8	11328.3	NA	NA	
19	BGB	1	14688.2	14688.2	1.02	0.33	0.49
19	BGB:ICB	1	2121.8	2121.8	0.15	0.71	0.79
19	ICB	1	6845	6845	0.47	0.50	0.64
19	Residuals	16	231077.2	14442.325	NA	NA	
20	BGB	1	2376.2	2376.2	8.01	0.01	0.06
20	BGB:ICB	1	180	180	0.61	0.45	0.64
20	ICB	1	2928.2	2928.2	9.87	0.01	0.04
20	Residuals	16	4748.8	296.8	NA	NA	
21	BGB	1	180	180	0.15	0.70	0.79
21	BGB:ICB	1	180	180	0.15	0.70	0.79
21	ICB	1	28125	28125	23.39	0.00	0.00
21	Residuals	16	19236	1202.25	NA	NA	

10.4 Spleen Timepoint 2 Statistics

10.4.1 Cluster Medians Heatmap

Figure 10.2: ***Heatmap of median intensities for spleen in timepoint 2.*** *Row numbers indicate cluster. Intensities have been transformed with an arsinh argument of 2.*

10.4.2 Cluster Means and Standard Deviation

Table 10.5: Calculated means and standard deviations for each group in each cluster. Group A was treated with vehicle only, group B was treated with bemcentinib only, group C was treated with immunotherapy only (anti-CTLA-4 and anti-PD-1 combination), and group D was treated with a combination of immunotherapy and bemcentinib.

Group	Variable	mean	SD	n
A	1	969.80	166.04	5
B	1	694.60	303.38	5
C	1	441.80	155.19	5
D	1	432.20	100.75	5
A	2	216.80	44.63	5
B	2	360.00	67.42	5
C	2	218.00	92.94	5
D	2	204.20	37.86	5

A	3	2107.60	302.98	5
B	3	2642.20	858.85	5
C	3	3209.00	1364.49	5
D	3	1520.20	488.72	5
A	4	131.20	22.31	5
B	4	79.00	8.31	5
C	4	126.60	34.38	5
D	4	72.60	9.86	5
A	5	43.20	12.52	5
B	5	57.20	21.44	5
C	5	84.00	41.18	5
D	5	49.40	43.79	5
A	6	1652.80	309.54	5
B	6	1860.40	377.07	5
C	6	1845.00	828.76	5
D	6	2689.40	574.66	5
A	7	184.00	36.66	5
B	7	93.40	34.96	5
C	7	193.20	63.48	5
D	7	116.40	16.15	5
A	8	3170.60	371.33	5
B	8	3342.80	411.97	5
C	8	2841.60	689.60	5
D	8	2626.60	340.92	5
A	9	18.00	5.15	5
B	9	14.80	2.95	5
C	9	18.20	8.35	5
D	9	8.80	2.68	5
A	10	1004.00	108.22	5
B	10	1105.80	193.64	5
C	10	995.00	370.53	5
D	10	1343.20	257.11	5
A	11	140.80	27.44	5

B	11	134.20	15.85	5
C	11	242.20	58.84	5
D	11	256.20	37.33	5
A	12	1632.60	250.35	5
B	12	1499.60	387.79	5
C	12	1493.00	656.88	5
D	12	1978.40	332.05	5
A	13	334.00	137.26	5
B	13	316.80	63.44	5
C	13	351.40	89.78	5
D	13	381.80	74.34	5
A	14	36.20	6.76	5
B	14	36.20	4.09	5
C	14	65.20	8.87	5
D	14	43.40	10.01	5
A	15	814.80	346.24	5
B	15	959.00	315.68	5
C	15	569.20	289.31	5
D	15	1515.20	1139.31	5
A	16	127.40	52.83	5
B	16	115.60	20.34	5
C	16	94.40	44.31	5
D	16	55.20	14.17	5
A	17	524.40	61.58	5
B	17	392.00	81.96	5
C	17	586.20	152.74	5
D	17	467.80	69.03	5
A	18	154.60	23.08	5
B	18	114.20	15.25	5
C	18	258.80	45.14	5
D	18	147.20	26.70	5
A	19	538.00	174.30	5
B	19	669.40	117.96	5

C	19	709.20	218.95	5	
D	19	610.00	161.06	5	
A	20	694.80	352.57	5	
B	20	801.00	220.60	5	
C	20	158.80	61.18	5	
D	20	184.80	94.23	5	
A	21	3357.00	1025.62	5	
B	21	2036.60	415.78	5	
C	21	2396.80	761.80	5	
D	21	2217.40	489.31	5	
A	22	2147.40	1163.65	5	
B	22	2675.20	778.74	5	
C	22	3102.40	710.82	5	
D	22	3079.60	1011.51	5	

10.4.3 ANOVA results

Table 10.6: Reported results form a factorial analysis of variance to compare the main effects of bemcentinib treatment (BGB) and immune chekcpoint blockade (ICB, anti-PD-1 and anti-CLTA-4 combination) and the interaction effect between ICB and BGB on the number of cells in each cluster.

Cluster	Response	Df	Sum Sq	Mean Sq	F value	Pr(>F)	Benjamini-Hochberg (5% FDR)
1	BGB	1	101388.8	101388.8	2.64	0.12	0.29
1	BGB:ICB	1	88179.2	88179.2	2.29	0.15	0.30
1	ICB	1	780915.2	780915.2	20.30	0.00	0.00
1	Residuals	16	615367.6	38460.475	NA	NA	
2	BGB	1	20930.45	20930.45	5.04	0.04	0.13
2	BGB:ICB	1	30811.25	30811.25	7.42	0.02	0.07
2	ICB	1	29876.45	29876.45	7.20	0.02	0.07
2	Residuals	16	66437.6	4152.35	NA	NA	
3	BGB	1	1665222.05	1665222.05	2.27	0.15	0.30
3	BGB:ICB	1	6179384.45	6179384.45	8.44	0.01	0.06
3	ICB	1	530.45	530.45	0.00	0.98	0.98
3	Residuals	16	11720368.8	732523.05	NA	NA	
4	BGB	1	14098.05	14098.05	30.55	0.00	0.00
4	BGB:ICB	1	4.05	4.05	0.01	0.93	0.94
4	ICB	1	151.25	151.25	0.33	0.57	0.68
4	Residuals	16	7383.2	461.45	NA	NA	
5	BGB	1	530.45	530.45	0.50	0.49	0.65
5	BGB:ICB	1	2952.45	2952.45	2.79	0.11	0.29
5	ICB	1	1361.25	1361.25	1.29	0.27	0.45

5	Residuals	16	16918.8	1057.425	NA	NA	
6	BGB	1	1383380	1383380	4.41	0.05	0.16
6	BGB:ICB	1	506892.8	506892.8	1.62	0.22	0.40
6	ICB	1	1303561.8	1303561.8	4.15	0.06	0.18
6	Residuals	16	5020325.2	313770.325	NA	NA	
7	BGB	1	35028.45	35028.45	20.43	0.00	0.00
7	BGB:ICB	1	238.05	238.05	0.14	0.71	0.80
7	ICB	1	1296.05	1296.05	0.76	0.40	0.56
7	Residuals	16	27429.2	1714.325	NA	NA	
8	BGB	1	2289.8	2289.8	0.01	0.92	0.94
8	BGB:ICB	1	187404.8	187404.8	0.83	0.37	0.55
8	ICB	1	1365553.8	1365553.8	6.07	0.03	0.09
8	Residuals	16	3597506.4	224844.15	NA	NA	
9	BGB	1	198.45	198.45	7.08	0.02	0.07
9	BGB:ICB	1	48.05	48.05	1.71	0.21	0.38
9	ICB	1	42.05	42.05	1.50	0.24	0.41
9	Residuals	16	448.4	28.025	NA	NA	
10	BGB	1	253125	253125	4.01	0.06	0.18
10	BGB:ICB	1	75891.2	75891.2	1.20	0.29	0.47
10	ICB	1	65208.2	65208.2	1.03	0.32	0.51
10	Residuals	16	1010423.6	63151.475	NA	NA	
11	BGB	1	68.45	68.45	0.05	0.83	0.91
11	BGB:ICB	1	530.45	530.45	0.36	0.56	0.68
11	ICB	1	62384.45	62384.45	42.58	0.00	0.00
11	Residuals	16	23441.2	1465.075	NA	NA	
12	BGB	1	155232.2	155232.2	0.82	0.38	0.55
12	BGB:ICB	1	478023.2	478023.2	2.53	0.13	0.30
12	ICB	1	143820.8	143820.8	0.76	0.40	0.56
12	Residuals	16	3019209.6	188700.6	NA	NA	
13	BGB	1	217.8	217.8	0.02	0.88	0.92
13	BGB:ICB	1	2832.2	2832.2	0.31	0.58	0.68
13	ICB	1	8487.2	8487.2	0.93	0.35	0.54
13	Residuals	16	145808.8	9113.05	NA	NA	
14	BGB	1	594.05	594.05	9.84	0.01	0.04
14	BGB:ICB	1	594.05	594.05	9.84	0.01	0.04
14	ICB	1	1638.05	1638.05	27.14	0.00	0.00
14	Residuals	16	965.6	60.35	NA	NA	
15	BGB	1	1485670.05	1485670.05	3.71	0.07	0.20
15	BGB:ICB	1	803604.05	803604.05	2.01	0.18	0.33
15	ICB	1	120590.45	120590.45	0.30	0.59	0.68
15	Residuals	16	6405002.4	400312.65	NA	NA	
16	BGB	1	3251.25	3251.25	2.42	0.14	0.30
16	BGB:ICB	1	938.45	938.45	0.70	0.42	0.57
16	ICB	1	10904.45	10904.45	8.12	0.01	0.06
16	Residuals	16	21474.4	1342.15	NA	NA	
17	BGB	1	78625.8	78625.8	8.15	0.01	0.06

17	BGB:ICB	1	245	245	0.03	0.88	0.92
17	ICB	1	23667.2	23667.2	2.45	0.14	0.30
17	Residuals	16	154420.8	9651.3	NA	NA	
18	BGB	1	28880	28880	32.86	0.00	0.00
18	BGB:ICB	1	6336.8	6336.8	7.21	0.02	0.07
18	ICB	1	23529.8	23529.8	26.77	0.00	0.00
18	Residuals	16	14061.6	878.85	NA	NA	
19	BGB	1	1296.05	1296.05	0.04	0.84	0.91
19	BGB:ICB	1	66470.45	66470.45	2.25	0.15	0.30
19	ICB	1	15624.05	15624.05	0.53	0.48	0.64
19	Residuals	16	472698	29543.625	NA	NA	
20	BGB	1	21846.05	21846.05	0.47	0.50	0.65
20	BGB:ICB	1	8040.05	8040.05	0.17	0.68	0.78
20	ICB	1	1659456.05	1659456.05	35.77	0.00	0.00
20	Residuals	16	742368.4	46398.025	NA	NA	
21	BGB	1	2811750.05	2811750.05	5.50	0.03	0.11
21	BGB:ICB	1	1627351.25	1627351.25	3.18	0.09	0.25
21	ICB	1	759330.45	759330.45	1.49	0.24	0.41
21	Residuals	16	8178159.2	511134.95	NA	NA	
22	BGB	1	318781	318781	0.37	0.55	0.68
22	BGB:ICB	1	378950	378950	0.43	0.52	0.66
22	ICB	1	2309960	2309960	2.65	0.12	0.29
22	Residuals	16	13955712	872232	NA	NA	

10.5 Tumour Timepoint 1 Statistics

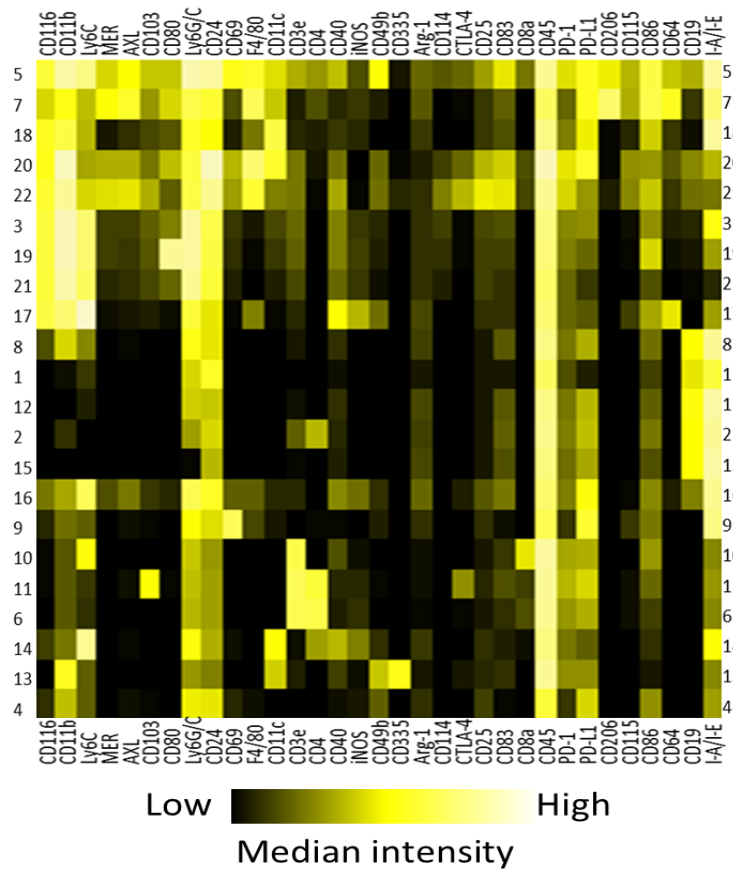### 10.5.1 Cluster Medians Heatmap
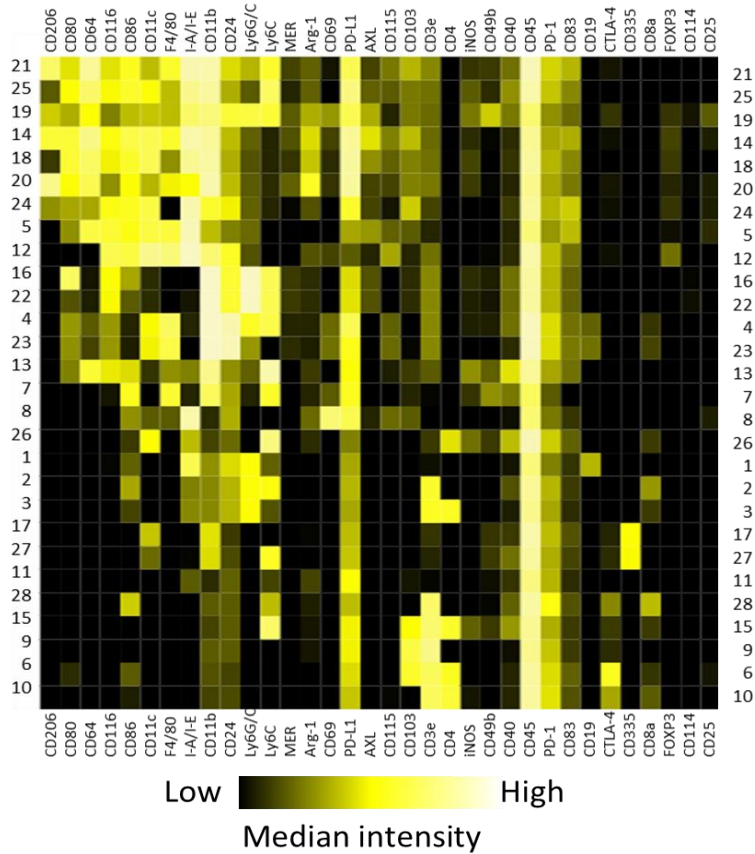
*Figure 10.3: **Heatmap of median intensities for tumour in timepoint 1.** Row numbers indicate cluster. Intensities have been transformed with an arsinh argument of 2.*

10.5.2 Cluster Means and Standard Deviation

Table 10.7: Calculated means and standard deviations for each group in each cluster. Group A was treated with vehicle only, group B was treated with bemcentinib only, group C was treated with immunotherapy only (anti-CTLA-4 and anti-PD-1 combination), and group D was treated with a combination of immunotherapy and bemcentinib.

Group	Cluster	mean	SD	n
A	1	29.2	7.854934755	5
B	1	22	4.183300133	5
C	1	25.8	9.884331035	5
D	1	27.4	5.176871642	5
A	2	13.4	5.176871642	5
B	2	10.6	2.880972058	5
C	2	21.6	14.2583309	5
D	2	19.2	4.711687596	5

A	3	27	6.595452979	5
B	3	15	4.636809248	5
C	3	31.4	18.31119876	5
D	3	25.8	6.534523701	5
A	4	88.6	31.580057	5
B	4	57	38.27531842	5
C	4	449.4	295.594824	5
D	4	403.8	132.0632424	5
A	5	3.4	1.673320053	5
B	5	2.2	2.48997992	5
C	5	1.6	2.073644135	5
D	5	1.4	0.547722558	5
A	6	567	120.359877	5
B	6	664.8	248.1414919	5
C	6	267.6	49.3791454	5
D	6	300.4	54.55089367	5
A	7	18.2	17.69745744	5
B	7	12.4	7.300684899	5
C	7	2.4	2.701851217	5
D	7	3.8	4.147288271	5
A	8	38.6	11.86591758	5
B	8	52	22.3159136	5
C	8	23.4	14.38054241	5
D	8	41.4	16.13381542	5
A	9	86.6	30.18774586	5
B	9	107.4	35.54293179	5
C	9	82	44.42409256	5
D	9	48.4	15.85244461	5
A	10	800.6	49.83272017	5
B	10	974.2	172.6649936	5
C	10	945.4	341.5820546	5
D	10	797.4	156.5464787	5
A	11	114.8	29.81107177	5

B	11	130	12.46996391	5
C	11	126.2	25.44995088	5
D	11	97.8	32.59140991	5
A	12	1.4	1.516575089	5
B	12	13.2	21.13527856	5
C	12	1.4	2.19089023	5
D	12	3.6	6.426507605	5
A	13	991.4	258.9368649	5
B	13	1052	189.2604026	5
C	13	1060.2	341.6272823	5
D	13	1002.4	238.3931627	5
A	14	4297.2	757.3686025	5
B	14	4802.4	1086.921248	5
C	14	3684.2	1146.471631	5
D	14	3976.4	576.2094237	5
A	15	159.2	46.90628956	5
B	15	246.6	209.2864066	5
C	15	184.6	30.07158127	5
D	15	173.8	21.99318076	5
A	16	489.4	188.7930083	5
B	16	731	488.0507146	5
C	16	433.4	204.9885363	5
D	16	556	100.2546757	5
A	17	890	264.8612844	5
B	17	986.8	264.0316269	5
C	17	2026.2	1428.962456	5
D	17	1150.4	285.1811705	5
A	18	592.6	189.969208	5
B	18	688	240.9802897	5
C	18	857.8	214.9318497	5
D	18	970.4	101.9131984	5
A	19	85	45.97281806	5
B	19	77.6	35.65529414	5

C	19	55.8	23.73183516	5
D	19	66.2	25.84956479	5
A	20	1322.8	222.9017721	5
B	20	1315.8	358.7724906	5
C	20	914.6	415.3797058	5
D	20	1112.4	377.8502349	5
A	21	2437	1118.764274	5
B	21	887	294.6633673	5
C	21	2226.8	800.0135624	5
D	21	2362.8	290.2786592	5
A	22	3299.8	1181.197782	5
B	22	3572.8	1873.746968	5
C	22	2774.8	874.3879002	5
D	22	3491.6	994.8795404	5
A	23	3379.2	404.2984046	5
B	23	2999.6	1223.244579	5
C	23	2173.8	201.1285658	5
D	23	2552	766.32728	5
A	24	609.6	131.2680464	5
B	24	454.6	75.49039674	5
C	24	541.4	57.98534298	5
D	24	500.6	66.74428815	5
A	25	1287	264.1401143	5
B	25	1379.2	360.8153267	5
C	25	2457.2	854.2451053	5
D	25	2231	267.1638074	5
A	26	214.8	126.6143752	5
B	26	111.6	47.52157405	5
C	26	199.2	24.56013029	5
D	26	182.4	37.37378761	5
A	27	288.4	83.60801397	5
B	27	309.8	83.49670652	5
C	27	513.4	266.2870631	5

D	27	353	90.27181177	5
A	28	1676.8	538.1400375	5
B	28	2133.4	946.8501993	5
C	28	1727.4	601.3695203	5
D	28	1357.2	360.0523573	5

10.5.3 ANOVA results

Table 10.8: Reported results form a factorial analysis of variance to compare the main effects of bemcentinib treatment (BGB) and immune chekcpoint blockade (ICB, anti-PD-1 and anti-CLTA-4 combination) and the interaction effect between ICB and BGB on the number of cells in each cluster.

Cluster	Response	Df	Sum Sq	Mean Sq	F value	Pr(>F)	Bemjamini-Hochberg (5% FDR)
1	BGB	1	39.2	39.2	0.77	0.39	0.69
1	BGB:ICB	1	96.8	96.8	1.90	0.19	0.50S
1	ICB	1	5	5	0.10	0.76	0.90
1	Residuals	16	814.8	50.925	NA	NA	
2	BGB	1	33.8	33.8	0.52	0.48	0.76
2	BGB:ICB	1	0.2	0.2	0.00	0.96	0.98
2	ICB	1	352.8	352.8	5.42	0.03	0.31
2	Residuals	16	1042.4	65.15	NA	NA	
3	BGB	1	387.2	387.2	3.50	0.08	0.36
3	BGB:ICB	1	51.2	51.2	0.46	0.51	0.77
3	ICB	1	288.8	288.8	2.61	0.13	0.44
3	Residuals	16	1772	110.75	NA	NA	
4	BGB	1	7449.8	7449.8	0.28	0.61	0.81
4	BGB:ICB	1	245	245	0.01	0.93	0.97
4	ICB	1	625872.2	625872.2	23.34	0.00	0.01
4	Residuals	16	429117.2	26819.825	NA	NA	
5	BGB	1	2.45	2.45	0.72	0.41	0.69
5	BGB:ICB	1	1.25	1.25	0.37	0.55	0.80
5	ICB	1	8.45	8.45	2.49	0.13	0.45
5	Residuals	16	54.4	3.4	NA	NA	
6	BGB	1	21320.45	21320.45	1.05	0.32	0.67
6	BGB:ICB	1	5281.25	5281.25	0.26	0.62	0.81

6	ICB	1	550788.05	550788.05	27.04	0.00	0.01
6	Residuals	16	325899.2	20368.7	NA	NA	
7	BGB	1	24.2	24.2	0.25	0.63	0.81
7	BGB:ICB	1	64.8	64.8	0.66	0.43	0.70
7	ICB	1	744.2	744.2	7.61	0.01	0.23
7	Residuals	16	1564	97.75	NA	NA	
8	BGB	1	1232.45	1232.45	4.46	0.05	0.36
8	BGB:ICB	1	26.45	26.45	0.10	0.76	0.90
8	ICB	1	832.05	832.05	3.01	0.10	0.38
8	Residuals	16	4423.6	276.475	NA	NA	
9	BGB	1	204.8	204.8	0.19	0.67	0.83
9	BGB:ICB	1	3699.2	3699.2	3.36	0.09	0.36
9	ICB	1	5056.2	5056.2	4.60	0.05	0.36
9	Residuals	16	17597.6	1099.85	NA	NA	
10	BGB	1	819.2	819.2	0.02	0.89	0.97
10	BGB:ICB	1	129283.2	129283.2	2.98	0.10	0.38
10	ICB	1	1280	1280	0.03	0.87	0.97
10	Residuals	16	693926.4	43370.4	NA	NA	
11	BGB	1	217.8	217.8	0.32	0.58	0.81
11	BGB:ICB	1	2376.2	2376.2	3.45	0.08	0.36
11	ICB	1	540.8	540.8	0.79	0.39	0.69
11	Residuals	16	11016.4	688.525	NA	NA	
12	BGB	1	245	245	1.98	0.18	0.50
12	BGB:ICB	1	115.2	115.2	0.93	0.35	0.67
12	ICB	1	115.2	115.2	0.93	0.35	0.67
12	Residuals	16	1980.4	123.775	NA	NA	
13	BGB	1	9.8	9.8	0.00	0.99	1.00
13	BGB:ICB	1	17523.2	17523.2	0.25	0.62	0.81
13	ICB	1	460.8	460.8	0.01	0.94	0.97
13	Residuals	16	1105633.2	69102.075	NA	NA	
14	BGB	1	794808.45	794808.45	0.93	0.35	0.67
14	BGB:ICB	1	56711.25	56711.25	0.07	0.80	0.91
14	ICB	1	2588401.25	2588401.25	3.04	0.10	0.38

14	Residuals	16	13605678	850354.875	NA	NA	
15	BGB	1	7334.45	7334.45	0.62	0.44	0.72
15	BGB:ICB	1	12054.05	12054.05	1.02	0.33	0.67
15	ICB	1	2808.45	2808.45	0.24	0.63	0.81
15	Residuals	16	189556	11847.25	NA	NA	
16	BGB	1	165802.05	165802.05	2.03	0.17	0.50
16	BGB:ICB	1	17701.25	17701.25	0.22	0.65	0.81
16	ICB	1	66701.25	66701.25	0.82	0.38	0.69
16	Residuals	16	1303630.4	81476.9	NA	NA	
17	BGB	1	758551.25	758551.25	1.34	0.26	0.60
17	BGB:ICB	1	1182438.45	1182438.45	2.09	0.17	0.50
17	ICB	1	2111850.05	2111850.05	3.73	0.07	0.36
17	Residuals	16	9052504.8	565781.55	NA	NA	
18	BGB	1	54080	54080	1.44	0.25	0.58
18	BGB:ICB	1	369.8	369.8	0.01	0.92	0.97
18	ICB	1	374832.2	374832.2	9.95	0.01	0.13
18	Residuals	16	602967.2	37685.45	NA	NA	
19	BGB	1	11.25	11.25	0.01	0.92	0.97
19	BGB:ICB	1	396.05	396.05	0.34	0.57	0.81
19	ICB	1	2060.45	2060.45	1.79	0.20	0.50
19	Residuals	16	18464.8	1154.05	NA	NA	
20	BGB	1	45505.8	45505.8	0.37	0.55	0.80
20	BGB:ICB	1	52428.8	52428.8	0.42	0.52	0.79
20	ICB	1	467568.2	467568.2	3.79	0.07	0.36
20	Residuals	16	1974856	123428.5	NA	NA	
21	BGB	1	2499245	2499245	4.85	0.04	0.36
21	BGB:ICB	1	3553245	3553245	6.89	0.02	0.26
21	ICB	1	2002179.2	2002179.2	3.88	0.07	0.36
21	Residuals	16	8250973.6	515685.85	NA	NA	
22	BGB	1	1224630.05	1224630.05	0.74	0.40	0.69
22	BGB:ICB	1	246198.05	246198.05	0.15	0.71	0.86
22	ICB	1	459348.05	459348.05	0.28	0.61	0.81
22	Residuals	16	26641981.6	1665123.85	NA	NA	

23	BGB	1	2.45	2.45	0.00	1.00	1.00
23	BGB:ICB	1	717826.05	717826.05	1.26	0.28	0.62
23	ICB	1	3415511.25	3415511.25	5.97	0.03	0.28
23	Residuals	16	9149978.8	571873.675	NA	NA	
24	BGB	1	47922.05	47922.05	6.23	0.02	0.28
24	BGB:ICB	1	16302.05	16302.05	2.12	0.16	0.50
24	ICB	1	616.05	616.05	0.08	0.78	0.90
24	Residuals	16	122988.8	7686.8	NA	NA	
25	BGB	1	22445	22445	0.09	0.77	0.90
25	BGB:ICB	1	126723.2	126723.2	0.51	0.49	0.76
25	ICB	1	5110605	5110605	20.42	0.00	0.01
25	Residuals	16	4004275.6	250267.225	NA	NA	
26	BGB	1	18000	18000	3.55	0.08	0.36
26	BGB:ICB	1	9331.2	9331.2	1.84	0.19	0.50
26	ICB	1	3808.8	3808.8	0.75	0.40	0.69
26	Residuals	16	81158	5072.375	NA	NA	
27	BGB	1	24151.25	24151.25	1.04	0.32	0.67
27	BGB:ICB	1	41314.05	41314.05	1.78	0.20	0.50
27	ICB	1	89914.05	89914.05	3.87	0.07	0.36
27	Residuals	16	372079.2	23254.95	NA	NA	
28	BGB	1	9331.2	9331.2	0.02	0.88	0.97
28	BGB:ICB	1	854497.8	854497.8	2.04	0.17	0.50
28	ICB	1	658119.2	658119.2	1.57	0.23	0.55
28	Residuals	16	6709612	419350.75	NA	NA	

10.6 Tumour Timepoint 2 Statistics

10.6.1 Cluster Medians Heatmap
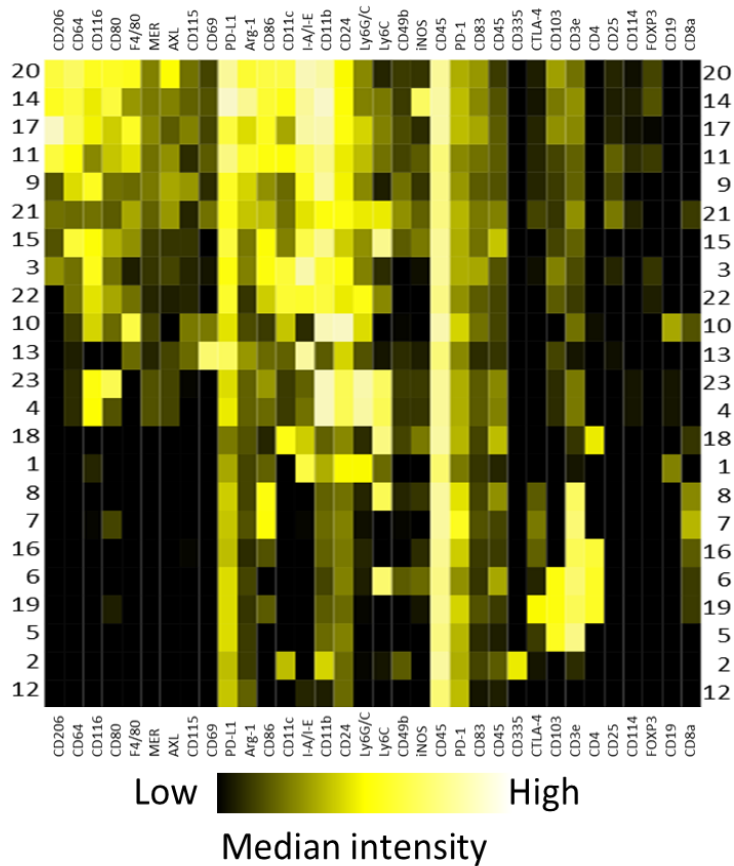
Figure 10.4: **Heatmap of median intensities for tumour in timepoint 2.** *Row numbers indicate cluster. Intensities have been transformed with an arsinh argument of 2.*

10.6.2 Cluster Means and Standard Deviation

Table 10.9: Calculated means and standard deviations for each group in each cluster. Group A was treated with vehicle only, group B was treated with bemcentinib only, group C was treated with immunotherapy only (anti-CTLA-4 and anti-PD-1 combination), and group D was treated with a combination of immunotherapy and bemcentinib.

Group	Cluster	mean	SD	n
A	1	79.80	28.87	5
B	1	61.00	8.60	5
C	1	46.20	22.34	5
D	1	37.60	7.70	5
A	2	446.80	126.94	5
B	2	572.60	285.51	5
C	2	473.60	222.46	5
D	2	450.00	127.19	5

A	3	396.60	70.61	5
B	3	209.00	18.65	5
C	3	358.40	85.26	5
D	3	230.00	55.33	5
A	4	4630.00	1061.04	5
B	4	6537.40	912.06	5
C	4	4894.60	979.31	5
D	4	4873.40	1302.49	5
A	5	25.80	8.58	5
B	5	55.20	34.13	5
C	5	18.60	5.32	5
D	5	35.60	17.04	5
A	6	30.00	30.01	5
B	6	35.80	21.02	5
C	6	22.80	13.52	5
D	6	27.60	15.13	5
A	7	1348.40	686.64	5
B	7	1314.00	288.02	5
C	7	1203.00	763.03	5
D	7	1624.80	306.89	5
A	8	504.00	124.83	5
B	8	858.80	379.84	5
C	8	2014.80	1325.63	5
D	8	1996.40	1098.45	5
A	9	72.20	25.78	5
B	9	36.80	25.61	5
C	9	72.80	40.88	5
D	9	42.80	7.22	5
A	10	2989.20	953.32	5
B	10	3481.80	729.96	5
C	10	1990.80	517.27	5
D	10	2127.00	469.42	5
A	11	1240.20	1071.74	5

B	11	2439.00	1627.58	5
C	11	1080.80	84.05	5
D	11	1265.40	358.56	5
A	12	45.40	15.45	5
B	12	81.60	21.22	5
C	12	38.20	19.54	5
D	12	33.60	10.38	5
A	13	12.20	3.11	5
B	13	10.40	4.34	5
C	13	14.80	7.40	5
D	13	18.80	14.94	5
A	14	83.20	63.48	5
B	14	55.60	17.70	5
C	14	623.80	255.07	5
D	14	443.20	307.02	5
A	15	1744.20	590.61	5
B	15	1385.00	254.75	5
C	15	2150.20	431.97	5
D	15	1712.00	513.53	5
A	16	767.00	128.12	5
B	16	833.40	174.71	5
C	16	1482.00	778.64	5
D	16	1981.40	564.37	5
A	17	2124.20	606.13	5
B	17	1028.00	269.96	5
C	17	3079.60	1242.39	5
D	17	2098.80	183.90	5
A	18	78.20	29.83	5
B	18	45.60	16.98	5
C	18	46.80	14.18	5
D	18	30.40	15.11	5
A	19	294.60	78.75	5
B	19	320.20	47.87	5

C	19	327.40	138.92	5
D	19	367.20	91.14	5
A	20	6233.40	1301.29	5
B	20	2877.00	279.37	5
C	20	3060.00	965.07	5
D	20	3266.80	1037.66	5
A	21	310.20	296.56	5
B	21	531.20	208.10	5
C	21	343.80	97.71	5
D	21	353.40	120.14	5
A	22	6.00	1.87	5
B	22	8.40	2.07	5
C	22	49.80	22.69	5
D	22	20.00	8.63	5
A	23	347.40	184.04	5
B	23	1031.20	174.32	5
C	23	416.20	170.75	5
D	23	772.80	261.35	5

10.6.3 ANOVA results

Table 10.10: Reported results form a factorial analysis of variance to compare the main effects of bemcentinib treatment (BGB) and immune chekcpoint blockade (ICB, anti-PD-1 and anti-CLTA-4 combination) and the interaction effect between ICB and BGB on the number of cells in each cluster.

Cluster	Response	Df	Sum Sq	Mean Sq	F value	Pr(>F)	Bemjamini-Hochberg (5% FDR)
1	BGB	1	938.45	938.45	2.56	0.13	0.32
1	BGB:ICB	1	130.05	130.05	0.35	0.56	0.70
1	ICB	1	4061.25	4061.25	11.08	0.00	0.03
1	Residuals	16	5862.8	366.425	NA	NA	
2	BGB	1	13056.05	13056.05	0.32	0.58	0.70
2	BGB:ICB	1	27900.45	27900.45	0.68	0.42	0.60
2	ICB	1	11472.05	11472.05	0.28	0.60	0.72
2	Residuals	16	653169.2	40823.075	NA	NA	
3	BGB	1	124820	124820	31.87	0.00	0.00

3	BGB:ICB	1	4380.8	4380.8	1.12	0.31	0.53
3	ICB	1	369.8	369.8	0.09	0.76	0.85
3	Residuals	16	62658.4	3916.15	NA	NA	
4	BGB	1	4447188.05	4447188.05	3.86	0.07	0.19
4	BGB:ICB	1	4649372.45	4649372.45	4.03	0.06	0.19
4	ICB	1	2447900.45	2447900.45	2.12	0.16	0.35
4	Residuals	16	18452775.6	1153298.48	NA	NA	
5	BGB	1	2691.2	2691.2	6.91	0.02	0.07
5	BGB:ICB	1	192.2	192.2	0.49	0.49	0.64
5	ICB	1	897.8	897.8	2.31	0.15	0.34
5	Residuals	16	6228	389.25	NA	NA	
6	BGB	1	140.45	140.45	0.32	0.58	0.70
6	BGB:ICB	1	1.25	1.25	0.00	0.96	0.96
6	ICB	1	296.45	296.45	0.68	0.42	0.60
6	Residuals	16	7014.8	438.425	NA	NA	
7	BGB	1	187598.45	187598.45	0.61	0.45	0.61
7	BGB:ICB	1	260148.05	260148.05	0.85	0.37	0.58
7	ICB	1	34196.45	34196.45	0.11	0.74	0.84
7	Residuals	16	4923274	307704.625	NA	NA	
8	BGB	1	141456.2	141456.2	0.18	0.68	0.78
8	BGB:ICB	1	174097.8	174097.8	0.22	0.64	0.75
8	ICB	1	8767528.2	8767528.2	11.23	0.00	0.03
8	Residuals	16	12494964.8	780935.3	NA	NA	
9	BGB	1	5346.45	5346.45	7.03	0.02	0.07
9	BGB:ICB	1	36.45	36.45	0.05	0.83	0.88
9	ICB	1	54.45	54.45	0.07	0.79	0.85
9	Residuals	16	12175.2	760.95	NA	NA	
10	BGB	1	494236.8	494236.8	1.02	0.33	0.55

10	BGB:ICB	1	158776.2	158776.2	0.33	0.57	0.70
10	ICB	1	6921937.8	6921937.8	14.35	0.00	0.02
10	Residuals	16	7718292.4	482393.275	NA	NA	
11	BGB	1	2392244.45	2392244.45	2.43	0.14	0.33
11	BGB:ICB	1	1285752.05	1285752.05	1.31	0.27	0.49
11	ICB	1	2221111.25	2221111.25	2.26	0.15	0.34
11	Residuals	16	15733040.8	983315.05	NA	NA	
12	BGB	1	1248.2	1248.2	4.24	0.06	0.18
12	BGB:ICB	1	2080.8	2080.8	7.06	0.02	0.07
12	ICB	1	3808.8	3808.8	12.93	0.00	0.02
12	Residuals	16	4714.4	294.65	NA	NA	
13	BGB	1	6.05	6.05	0.08	0.78	0.85
13	BGB:ICB	1	42.05	42.05	0.55	0.47	0.62
13	ICB	1	151.25	151.25	1.97	0.18	0.37
13	Residuals	16	1225.6	76.6	NA	NA	
14	BGB	1	54184.05	54184.05	1.32	0.27	0.49
14	BGB:ICB	1	29261.25	29261.25	0.72	0.41	0.60
14	ICB	1	1076944.05	1076944.05	26.32	0.00	0.00
14	Residuals	16	654661.6	40916.35	NA	NA	
15	BGB	1	794808.45	794808.45	3.68	0.07	0.20
15	BGB:ICB	1	7801.25	7801.25	0.04	0.85	0.88
15	ICB	1	671611.25	671611.25	3.11	0.10	0.25
15	Residuals	16	3456119.6	216007.475	NA	NA	
16	BGB	1	400162.05	400162.05	1.65	0.22	0.43
16	BGB:ICB	1	234361.25	234361.25	0.96	0.34	0.56
16	ICB	1	4338461.25	4338461.25	17.86	0.00	0.01

16	Residuals	16	3886898.4	242931.15	NA	NA	
17	BGB	1	5392411.25	5392411.25	10.69	0.00	0.03
17	BGB:ICB	1	16646.45	16646.45	0.03	0.86	0.88
17	ICB	1	5131858.05	5131858.05	10.17	0.01	0.03
17	Residuals	16	8070484.8	504405.3	NA	NA	
18	BGB	1	3001.25	3001.25	7.47	0.01	0.06
18	BGB:ICB	1	328.05	328.05	0.82	0.38	0.58
18	ICB	1	2714.45	2714.45	6.75	0.02	0.07
18	Residuals	16	6430	401.875	NA	NA	
19	BGB	1	5346.45	5346.45	0.59	0.45	0.61
19	BGB:ICB	1	252.05	252.05	0.03	0.87	0.88
19	ICB	1	7960.05	7960.05	0.88	0.36	0.58
19	Residuals	16	144394	9024.625	NA	NA	
20	BGB	1	12399975.2	12399975.2	13.12	0.00	0.02
20	BGB:ICB	1	15870492.8	15870492.8	16.80	0.00	0.01
20	ICB	1	9685536.2	9685536.2	10.25	0.01	0.03
20	Residuals	16	15118030	944876.875	NA	NA	
21	BGB	1	66470.45	66470.45	1.71	0.21	0.42
21	BGB:ICB	1	55862.45	55862.45	1.44	0.25	0.47
21	ICB	1	25992.05	25992.05	0.67	0.43	0.60
21	Residuals	16	620935.6	38808.475	NA	NA	
22	BGB	1	938.45	938.45	6.29	0.02	0.08
22	BGB:ICB	1	1296.05	1296.05	8.68	0.01	0.04
22	ICB	1	3836.45	3836.45	25.70	0.00	0.00
22	Residuals	16	2388	149.25	NA	NA	
23	BGB	1	1353040.2	1353040.2	33.47	0.00	0.00
23	BGB:ICB	1	133824.8	133824.8	3.31	0.09	0.23
23	ICB	1	44935.2	44935.2	1.11	0.31	0.53
23	Residuals	16	646867.6	40429.225	NA	NA	